

FOLATE RECEPTOR-SPECIFIC, REDOX-RESPONSIVE MESOPOROUS SILICA
NANOPARTICLES FOR THE SIMULTANEOUS DELIVERY OF CISPLATIN AND
GEMCITABINE TO TREAT CANCER

by

Eric Douglas Fink

A thesis submitted to the faculty of
The University of North Carolina at Charlotte
in partial fulfillment of the requirements
for the degree of Master of Science in
Chemistry

Charlotte

2016

Approved by:

Dr. Juan Vivero-Escoto

Dr. Daniel Rabinovich

Dr. Kirill Afonin

Dr. Ahmed El-Ghannam

©2016
Eric Douglas Fink
ALL RIGHTS RESERVED

ABSTRACT

ERIC DOUGLAS FINK. Folate receptor-specific, redox-responsive mesoporous silica nanoparticles for the simultaneous delivery of cisplatin and gemcitabine to treat cancer. (Under the direction of DR. JUAN VIVERO-ESCOTO)

Nanoparticles are an innovative platform for cancer treatment that reduces systemic toxicity and allows for active targeting of tumor sites to enhance the therapeutic efficacy. Mesoporous silica nanoparticles (MSNs) have emerged as an attractive drug delivery system due to their high surface area, vast functionalization potential, and biocompatibility. The main goal of this project is to develop a target-specific stimuli-responsive MSN based drug delivery system for the simultaneous delivery of cisplatin and gemcitabine. Both drugs were chemically attached to the MSNs via stimuli-responsive linkers that respond to the high reducing environment and low pH characteristic of cancer cells. The MSN materials fabricated in this work were successfully synthesized and characterized with a wide variety of spectroscopic and microscopic techniques. The loading of cisplatin and gemcitabine and their release profile under high reducing conditions were determined using atomic absorption (AA) and UV-vis spectroscopy, respectively. *In vitro* toxicity studies were performed on human cervical cancer (HeLa) cells in the presence of different ratios of cisplatin/gemcitabine drugs to determine the best ratio to kill HeLa cells. Based on this data, MSN materials carrying individual drugs and the corresponding combinatorial nanoparticles were fabricated and their *in vitro* cytotoxicity evaluated in HeLa and pancreatic cancer cells (AsPC1 and BxPC-3). The next step in this project was to further modify with folic acid to enhance its targeting ability toward cancer cells overexpressing folate receptors.

DEDICATION

I would like to dedicate the work of this project to my family, who provided continuous moral and financial support. Thank you for believing in me.

ACKNOWLEDGEMENTS

First and foremost, I would like to acknowledge Dr. Juan Vivero-Escoto. Without his tutelage and research interests, I would have never been so fortunate as to research a field that interests me. Furthermore, he allowed me to gain professional experience that will prove beneficial when seeking employment.

I would also like to acknowledge the continued support as shown to me by the Heilborn family, who encouraged me even from afar. Thank you for the thoughts and prayers sent, they were well appreciated.

Furthermore, I would like to thank the members of my committee – Dr. Dan Rabinovich, Dr. Kirill Afonin, and Dr. Ahmed El-Ghannam – for their guidance throughout the project.

I would like to thank all members of the Vivero Research Group, especially those who assisted in this research. Those members primarily include Sebin Yang, Ricky Son, and Mubin Tarannum. I would like to thank our former post-doctorate Dr. Merlis Alvarez-Berrios for her contribution to the preliminary studies with cisplatin and the increase of cellular uptake using the folic acid moiety.

A special thanks goes to Zach Lyles for his continued encouragement and support both inside and outside of the laboratory.

I thank Dr. Michael Murphy and Dr. Clifford Carlin for the use of the atomic absorption spectrometer and for the extensive repairs of the instrument.

Finally, I would like to thank the UNCC Chemistry Department for the opportunity to perform this research, as well as the NIH for their combined funding throughout the program.

TABLE OF CONTENTS

LIST OF ABBREVIATIONS	x
CHAPTER 1: INTRODUCTION.....	1
1.1 Cancer	1
1.2 Current Therapies	1
1.3 Chemotherapy	2
1.3.1 Cisplatin.....	3
1.3.2 Gemcitabine.....	5
1.3.3 Combination Therapy	6
1.4 Drug Delivery Systems	7
1.5 Mesoporous Silica Nanoparticles.....	10
1.5.1 MSNs as Drug Delivery Platforms.....	12
1.5.2 MSNs for the Delivery of Cisplatin and/or Gemcitabine	13
1.6 Research Objective	14
1.6.1 Design and Synthetic Strategy.....	15
1.6.2 Synthesis of the Stimuli-Responsive Linker, Gemcitabine, and Cisplatin.....	15
Prodrugs	
1.6.3 Synthesis of MSN Materials.....	17
1.6.4 Determination of <i>In Vitro</i> Synergy for Different Ratios of Cisplatin and.....	17
Gemcitabine Drugs	
1.6.5 Evaluation of <i>In Vitro</i> Cytotoxicity for MSN Materials.....	18
CHAPTER 2: EXPERIMENTAL.....	20
2.1 Materials and Methods.....	20
2.2 Synthesis and Characterization of Cisplatin and Gemcitabine Prodrugs.....	20
Redox-Responsive Linker, NH ₂ -PEG-FA, and NH ₂ -PEG-MeO	
2.2.1 Synthesis of Cisplatin Prodrug.....	21

2.2.2 Synthesis of Redox-Responsive Linker (RRL)	22
2.2.3 Synthesis of Gemcitabine Prodrug	25
2.2.4 Synthesis of Folic Acid-Polyethylene Glycol-Amine (NH ₂ -PEG-FA).....	26
2.2.5 Synthesis of Methoxy-Polyethylene Glycol-Amine (NH ₂ -PEG-MeO).....	29
2.3 Synthesis and Characterization of MSN Materials.....	30
2.3.1 Synthesis of Aminopropyl-Mesoporous Silica Nanoparticles (AP-MSNs).....	30
2.3.2 Synthesis of Cisplatin-MSNs (cisPt-MSN).....	31
2.3.3 Synthesis of Redox-Responsive-Linker-MSNs (RRL-MSN)	31
2.3.4 Synthesis of Gemcitabine-MSNs (Gem-MSN).....	32
2.3.5 Synthesis of Cisplatin-Redox-Responsive-Linker-MSNs (cisPt-RRL-MSN)...	32
2.3.6 Synthesis of Cisplatin-Gemcitabine-MSNs (cisPt-Gem-MSN)	32
2.3.7 Synthesis of Passively Loaded Gemcitabine to AP-MSNs (GemPas-MSN).....	33
2.3.8 Synthesis of Passively Loaded Gemcitabine to Cisplatin-MSNs..... (cisPt-GemPas-MSN)	33
2.3.9 Synthesis of FITC-cisPt-Gem-MSNs.....	34
2.3.10 Amine Activation of PEG Derivatives.....	34
2.3.11 Synthesis of MeO-PEG-FITC-cisPt-Gem-MSN	34
2.3.12 Synthesis of FA-PEG-FITC-cisPt-Gem-MSN.....	35
2.4 Release Profiles	35
2.4.1 Cisplatin Release Profile	35
2.4.2 Gemcitabine Release Profile	36
2.5 Cell Growth, Handling and Maintenance.....	36
2.6 Cytotoxicity Assay	36
2.6.1 Drug Cytotoxicity Assay.....	36
2.6.2 Drug Synergy Determination	37
2.7 Flow Cytometry.....	38

2.8 Confocal Microscopy.....	38
CHAPTER 3: RESULTS AND DISCUSSION.....	40
3.1. Synthesis and Characterization of Cisplatin Prodrug.....	40
3.2. Synthesis and Characterization of Gemcitabine Prodrug, and Redox-Responsive Linker (RRL).....	41
3.3. Synthesis and Characterization of NH ₂ -PEG-FA, NH ₂ -PEG-MeO.....	44
3.4 Characterization of MSN Materials.....	46
3.4.1 Synthesis and Characterization of AP-MSNs.....	46
3.4.2 Synthesis and Characterization of cisPt-MSNs.....	47
3.4.3 Synthesis and Characterization of RRL-MSNs.....	48
3.4.4 Synthesis and Characterization of Gem-MSNs.....	48
3.4.5 Synthesis and Characterization of cisPt-Gem-MSNs.....	49
3.4.6 Synthesis and Characterization of cisPt-GemPas-MSN.....	49
3.5 Determination of LD ₅₀ of Cisplatin and Gemcitabine Drugs in Human Cervical Cancer (HeLa) and Pancreatic Cancer (AsPC1 and BxPC-3) Cell Lines.....	50
3.6 Therapeutic Combination and Synergy Determination of Cisplatin and Gemcitabine in the HeLa Cell Line.....	52
3.7 Selection of Loading Ratio of Cisplatin and Gemcitabine to MSN Materials.....	53
3.8 Drug Release Profile.....	54
3.9 <i>In Vitro</i> Cytotoxicity of MSN-Based Combination Therapy.....	57
3.10 Targeting Moiety of FA-Functionalized MSNs.....	62
3.11 Flow Cytometry of FA-Functionalized Drug-Loaded MSNs.....	62
3.12 Confocal Microscopy.....	63
3.13 Cytotoxicity of FA-PEG-MSN Materials.....	65
CHAPTER 4: CONCLUSIONS AND FUTURE WORK.....	67
REFERENCES.....	71

APPENDIX A: FIGURES80

LIST OF ABBREVIATIONS

AAS	Atomic Absorption Spectroscopy
APTES	Aminopropyl Triethoxysilane
BET	Brunauer-Emmett-Teller (method to determine surface area)
BJH	Barrett-Joyner-Halenda (method to determine pore size and volume)
CI	Combination Index
cisPt	Cisplatin
CTAB	Cetyl trimethylammonium bromide
DAPI	4',6-diamidino-2-phenylindole
DCM	Dichloromethane
DIC	Differential Interference Contrast Microscopy
DIPEA	Diisopropylethylamine
DLS	Dynamic Light Scattering
DMF	Dimethyl Formamide
DMSO	Dimethyl Sulfoxide
DPBS	Dulbecco's Phosphate Buffer Solution
EDC	1-Ethyl-3-(3-dimethylaminopropyl)carbodiimide
ESI-MS	Electrospray Ionization – Mass Spectrometry
FA	Folic Acid
FBS	Fetal Bovine Serum
FDA	Food and Drug Administration
FTIR	Fourier Transform Infrared Spectroscopy
Gem	Gemcitabine
GSH	Glutathione

HPLC	High Performance Liquid Chromatography
MSN	Mesoporous Silica Nanoparticle
MTS	(3-(4,5-dimethylthiazol-2-yl)-5-(3-carboxymethoxyphenyl)-2-(4-sulfophenyl)-2H-tetrazolium)
NMR	Nuclear Magnetic Resonance
PBS	Phosphate Buffer Solution
PEG	Polyethylene Glycol
PEI	Polyethylenimine
PLA	Poly(lactic Acid)
PLGA	Poly(lactic-co-glycolic) Acid
RNR	Ribonucleotide Reductase
RRL	Redox-Responsive Linker
SEM	Scanning Electron Microscopy
TBTU	N,N,N',N'-Tetramethyl-O-(benzotriazol-1-yl)uronium tetrafluoroborate
TEOS	Tetraethyl orthosilicate
TGA	Thermogravimetric Analysis
THF	Tetrahydrofuran
UV-vis	Ultraviolet-Visible Spectroscopy

CHAPTER 1: INTRODUCTION

1.1 Cancer

Cancer is defined by the National Cancer Institute as “a genetic disease that is caused by changes to genes that control the way our cells function, especially how they grow and divide.”¹ This culmination of genetic alterations can be naturally inherited or induced by external influences called carcinogens, which can be found in materials that are used daily, such as parabens in sunblock or tobacco of any form.² The tumors that form from these mutated cells can be classified as either malignant or benign. Malignant tumors are those that can spread to other tissues or organs. Benign tumors are groups of mutated cells that have not yet metastasized and are considered non-cancerous. Furthermore, the genetic alteration often causes enhanced cell growth due to the deactivation of signals that regulate growth.³ This allows cancer to grow uninhibited, often more rapidly than normal tissue. This rapid growth also causes the stroma – the tissue surrounding the tumor, responsible for its structure – to form an abnormal or “leaky” vasculature, contrary to a healthy cell’s tight and well-ordered vasculature.⁴

1.2 Current Therapies

In 2016 it is estimated that more than 1.5 million people will be diagnosed with cancer and over half a million cancer related deaths will occur in the United States alone.⁵ Current treatments include surgical excision, radio- and chemotherapies. Surgical excision of the tumor is the preferred treatment as it is the quickest and has comparatively

limited side effects. However, for this treatment to be effective the tumor must be either near the surface or accessible to the surgeon as well as being contained within a certain area, *i.e.* the tumor has not metastasized. For those deep-tissue tumors that are inoperable, patients have two alternatives: radio- and/or chemotherapies. Radiation therapy treatment irradiates the section of the body in which the tumor is found with x-rays or γ -rays. Chemotherapy is the administration of one or more anticancer drugs into the body. Both approaches have shown to be effective in clinical applications, but the largest drawback is that they usually produce side effects such as nausea, memory loss, hair loss, or a significant decrease in the activity of the immune system, leaving the patient vulnerable to other illnesses such as contracting pneumonia.⁶ These side effects are usually associated to the lack of target specificity for these therapies.⁷ Because of that, these treatments cause mild to severe health issues for the patient post-treatment, decreasing their quality of life significantly.

1.3 Chemotherapy

Chemotherapy is chosen for its ability to shrink tumor size as well as to eliminate any cells that may have metastasized from the primary tumor. Chemotherapy involves the treatment of cancer through the use of one or more anticancer drugs. From its beginning, nearly 70 years ago, until the present day, a wide variety of chemotherapeutics have been discovered and utilized for cancer treatment. Each of these drugs have different mechanisms to kill cancer cells, and often are used in combination to form a drug “cocktail” in order to optimize the therapeutic effect. For example, alkylating agents and hormone therapy can be combined to maximize the therapeutic outcome. Alkylating agents, or alkylating-like agents such as cisplatin or oxaliplatin, are responsible for

targeting the DNA to stop cancer cells from division. Hormone therapies are target-specific and use inhibitors to block cancer cells from obtaining hormones, which they use to grow and reproduce, therefore starving the cancer cells.⁸

1.3.1 Cisplatin

Cisplatin, *cis*-[PtCl₂(NH₃)₂], has been used as an anticancer agent since 1971.⁹ The research revealed that cisplatin can form DNA adducts by cross-linking strands of DNA, suppressing division and growth. Cisplatin was approved by the U.S. FDA in December 1978 for testicular and bladder cancer treatment.¹⁰ Currently, cisplatin is approved as a first round treatment for cervical, ovarian, bladder and testicular cancer and approved for use in lung, gastric, head and neck cancers.¹¹ Cisplatin's antitumor toxicity was considered a milestone and its effectiveness as a chemotherapeutic remains high. Nevertheless, patients treated with cisplatin which experience a relapse of the tumor, often demonstrate a development of resistance of the tumor, acquired or perhaps inherent, to cisplatin making a second round treatment with the therapeutic less effective.¹²⁻¹⁴ Side effects of cisplatin include nausea, vomiting, hair-loss, and commonly dehydration, and are addressed by treating the patient with fluids for hydration concurrently with the chemotherapy agent.¹⁵

Platinum(II) complexes, such as cisplatin, undergo a fast ligand exchange rate which could lead to inactivation before localizing at the tumor.¹⁶ Since platinum(IV) has a slower exchange rate than Pt(II) and are more stable in physiological conditions, Pt(IV) alternatives have been the focus of research. Moreover, Pt(IV) complexes can be reduced to Pt(II) in the presence of a highly reducing environment, such as the one found in

cancer cells.¹⁷ The ability to design Pt(IV) molecules that can be reduced to Pt(II) complexes allows for the design of stable and more effective drug delivery systems.

Cisplatin travels through the cytoplasm and to the nucleus where one of the chloride ligands is replaced with an aqua ligand. The newly acquired aqua ligand is then substituted by the N-7 nitrogen on the guanine nucleobase. Once this has occurred the cisplatin is in close enough proximity to exchange another aqua ligand for a second N-7 nitrogen on a guanine nucleobase.¹⁶ This mechanism impacts the DNA strands either through inter- or intrastrand crosslinking (Figure 1), causing further DNA growth to be inhibited and apoptosis to occur. Intrastrand crosslinking has been shown to be the major product of this mechanism.¹⁶ Further research demonstrated that it was possible for cisplatin to be reduced from Pt(IV) to Pt(II) *in vivo* as well as in clinical trials, while still maintaining reactivity for apoptosis, or programmed cellular death.¹⁷⁻²⁰ Glutathione (GSH), one of the main natural reducing agents, has been found to be able to inactivate cisplatin by exchanging itself with the chlorine or ammonia ligand. A second glutathione molecule can then perform the same substitution to completely inactivate cisplatin.¹⁶

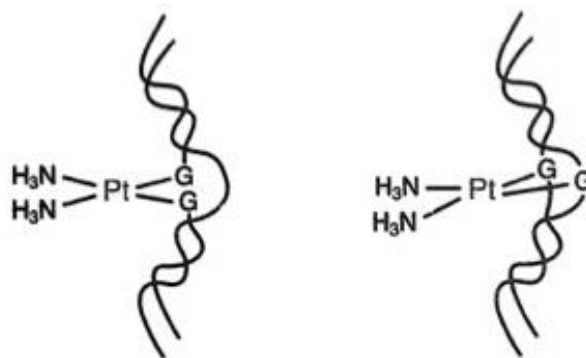


Figure 1: A representation of the intra- (left) or interstrand (right) crosslinking of cisplatin to DNA.¹⁶

1.3.2 Gemcitabine

Gemcitabine, 2,2'-difluorodeoxycytidine, was first identified as an anticancer therapeutic in 1988 by Heinemann et al.²¹ The U.S. FDA approved gemcitabine in 1996 for ovarian, breast, pancreatic, and non-small lung cancers.²² Gemcitabine acts as a nucleoside analog, mimicking deoxycytidine, with fluorine atoms at the 2' carbon of the sugar (Figure 2). Gemcitabine is usually used in treatments that involve multiple chemotherapeutics due to its high potency. A major concern with using gemcitabine is that it has an extremely short half-life, less than 1 h, once administered to the patient due to inactivating enzymes in plasma.²³⁻²⁶

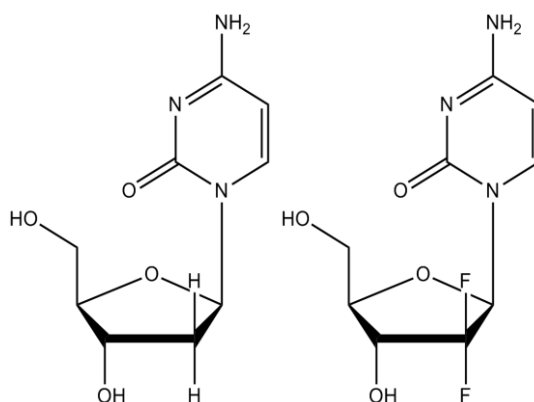


Figure 2: The molecular structure of deoxycytidine (left) and gemcitabine (right).

Gemcitabine is cytotoxic in both its di- or triphosphate backbone derivative, however is usually inactivated by cytidine deaminase before the derivatives can form. The gemcitabine diphosphate derivative is responsible for inhibiting ribonucleotide reductase (RNR) which is responsible for the catalysis of the reaction required for DNA synthesis and repair. Inhibition of RNR leads to a reduced concentration of DNA monomers available for growth, and with an abundant amount of gemcitabine present, the cell will not produce as much deoxycytidine to maintain the equilibrium of monomer

synthesis.²⁷ Once gemcitabine has added a third phosphate to its backbone, gemcitabine triphosphate, the cell recognizes it as a nucleobase and then competes with deoxycytidine for incorporation into DNA during growth. Under normal circumstances, another nucleobase would be added by the triphosphate backbone at the 2'-position of the molecule. However, due to the fluorines at the 2' position instead of hydrogen, the bond dissociation energy is much higher and therefore, there is no site of activation for another nucleobase, and so no more bases can be added to the strand once gemcitabine has been incorporated.²⁸ Furthermore, with a decreased concentration of deoxycytidine gemcitabine is able to phosphorylate faster, maintain a decreased metabolic clearance by the inactivating enzyme deoxycytidine monophosphate deaminase. Faster phosphorylation and decreased clearance allow for a higher degree of incorporation, causing cell apoptosis.²⁹

1.3.3 Combination Therapy

Combination therapy is a strategy which uses multiple therapeutics to enhance the efficacy of treatment, reduce the development of resistance, and limit the side-effects of treatment.³⁰ Currently, combination therapy has become standard clinical practice for a wide-variety of cancer types.³¹ An often used term in combination therapy is “synergy.” The idea of synergy is that the two or more drugs will work better together than if they were to be combined additively at any specific ratio. The ratio of the therapeutics must be tested across a wide range in order to determine the most synergistic combination. To mathematically determine synergy, the combination index (CI) must be calculated using Equation 1. If the two drugs together at any particular ratio is additive, then $CI = 1$. If the ratio is synergistic, the $CI < 1$. If the drugs are antagonistic, meaning they function worse

when they are combined than by themselves, the $CI > 1$. In Equation 1, $ID_{x,1}$ and $ID_{x,2}$ are the dosage of the individual drugs needed to achieve a certain percent viability (i.e. 50%) as determined by x . Furthermore D_1 and D_2 are the doses of drugs 1 and 2 needed to achieve $x\%$ viability when administered together.³²

$$CI = \frac{D_1}{ID_{x,1}} + \frac{D_2}{ID_{x,2}}$$

Equation 1: Combination Index Equation. CI – Combination Index; D_1 , D_2 – concentration of drug (1 and 2) to achieve a certain effect; $ID_{x,1}$, $ID_{x,2}$ – concentration of individual drug to achieve the same (x) effect.³²

Cisplatin and gemcitabine have shown promising results in clinical studies as a combined therapy. When used in tandem against the current method of treatment for advanced bladder cancer, cisplatin and gemcitabine demonstrated similar survival rates, but with less severe or life-threatening side effects, seeming to be a more beneficial treatment for the patient.³³ This was determined through the decrease in life-threatening toxicity and side effects; it is hypothesized that the synergy of the combined drugs can be attributed to their complimentary mechanism, as well as the targeting of DNA for inhibition of cell reproduction.

1.4 Drug Delivery Systems

Scientists have spent decades investigating alternative methods, to reduce the side-effects by increasing the targeting toward cancer tissue. Targeting therapy, which involves the use of nanocarriers to improve cellular uptake and increase drug concentration inside the cancer cell, is one example of these alternative treatments.³⁴ As seen in Figure 3, these nanoparticle-based therapies can be beneficial to the patient as well as improve efficacy of treatment.

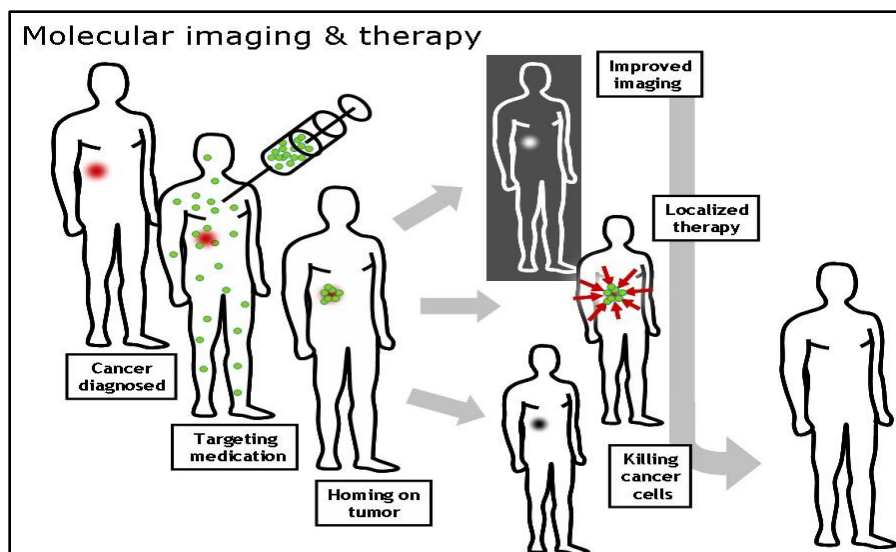


Figure 3: A schematic representation of the target specificity and multi-functionality of the nanoparticulate platform.³⁵

The nanoparticulate platform has been a popular and rising field in the past few decades, demonstrating their ability to overcome some major issues in current treatments and showing promise as a drug delivery system.³⁶ Nanoparticles serve as a delivery vehicle to transport the drugs safely to the tumor, preserving healthy cells and protecting its cargo from the harsh environment in the body. There are many different types of nanoparticle-based platforms. One way to divide them is by looking at the chemical nature of their framework. In this way, two main categories can be depicted: organic and inorganic delivery systems.

Organic nanoparticles are composed of organic matter such as polymers, liposomes, and dendrimers. Polymeric nanoparticles are usually biodegradable, composed of a variety of backbones, including, but not limited to poly(lactic-co-glycolic acid) (PLGA), polylactic acid (PLA), and chitosan. The size of these nanoparticles is easily controlled by the length of the polymer chain, and the functionality at the terminal site of the polymer can be used to functionalize the nanoparticles with a wide variety of

functional moieties.³⁷ Liposomes are also composed of biodegradable lipids that form a bilayer micelle in solution. This lipid bilayer contains a hydrophilic core surrounded by a hydrophobic membrane, allowing both hydrophobic drugs to be passively loaded into the particle.³⁸ One FDA approved liposomal-based nanocarrier currently used in clinic is DOXIL®, which is a doxorubicin loaded liposome for the treatment of ovarian cancer.³⁹ Dendrimers are another example of organic based nanoparticles. Dendrimers are unique in that the size and functionality of the nanoparticle is “grown.” These nanoparticles contain a chemical core, which is expanded upon by adding branching molecules. An example of this is the PAMAM dendrimer, which contains a diamine core that is reacted with further diamine derivatives to form the branches.⁴⁰ These branching molecules can be chosen to appropriate certain functional groups for conjugation. In addition, drugs can be passively loaded with hydrophobic molecules that will be protected by the generations of branching.⁴¹ Organic nanoparticles are generally injected intravenously because their organic composition cannot withstand the harsh conditions of the stomach for oral administration.

Inorganic nanoparticles are currently being explored as a promising alternative for drug delivery. Inorganic nanoparticles offer unique characteristics that are not found in organic nanoparticles such as optical, magnetic and photothermic properties.⁴² Some representative examples of inorganic nanoparticles are gold, iron oxide, and silica nanoparticles. Gold nanoparticles have unique optical properties that depend on the size and shape of the nanoparticle. Moreover, gold nanorods show outstanding features for photothermal therapy. Gold nanoparticles can also be easily functionalized with a wide variety of functional molecules. Iron oxide nanoparticles can be used as an MRI imaging

agent. The FDA has approved the use of superparamagnetic iron oxide nanoparticles, Feridex I.V.®, as a contrast imaging agent for magnetic resonance imaging (MRI).⁴³ Iron oxide nanoparticles also have magnetic and photothermal properties, which are being studied as an alternative treatment.⁴⁴ Silica nanoparticles are relatively non-toxic and highly stable. Silica nanoparticles also have a wide range of functionality and can be found in a variety of types, such as solid silica nanospheres, hollow silica nanoparticles, or mesoporous silica nanoparticles.⁴⁵ Mesoporous silica nanoparticles are the focus of this research and have been widely used as a drug delivery system due to their vast array of advantages.

1.5 Mesoporous Silica Nanoparticles

Vallet-Regi and co-workers first reported the use of MCM-41 type mesoporous silica nanoparticles (MSNs) as a platform for drug delivery in 2001.⁴⁶ MCM-41 mesoporous silica platform had originally shown promise as a drug delivery vehicle, however, due to its larger particle size in the microscale regime, its application for intravenous administration was prevented.⁴⁷ A critical breakthrough for its applications was achieved when researchers reported the synthesis of this material in the nano-size regimen. This material is generally called mesoporous silica nanoparticles (MSNs).⁴⁸

MSNs are typically synthesized using a surfactant-templated co-condensation approach. Template surfactants, such as cetyltrimethylammonium bromide (CTAB), are added to an aqueous mixture, forming micelles, which at the critical micellar concentration extend from spheres or ovoids into rod-shaped micelles.⁴⁹ Pore expanders, such as mesitylene, can also be added. These chemicals intercalate into the micelle to expand the volume providing larger pores. The silane precursor, usually tetraethyl

orthosilicate (TEOS), is then added to the solution. The silanes localize within the hydrophobic center of the micelle and migrates to the hydrophilic surface of the micelle.

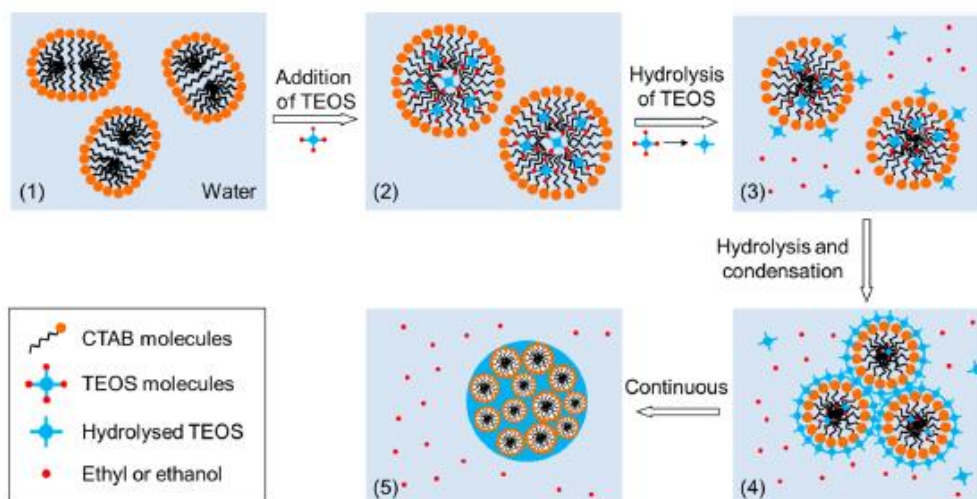


Figure 4: Surfactant-templated synthesis of MSN and formation of pores.⁵⁰

Slowly the silane precursor hydrolyzes to afford the framework of MSNs. Figure 4 shows a schematic illustrating the different steps for the formation of MSNs.⁵⁰ One of the outstanding advantages of this approach is the capability of introducing other silane precursors that carry different functional groups such as mercaptopropyl triethoxysilane (MPTES) and aminopropyl triethoxysilane (APTES). These groups end up on the interior surface of MSNs and can be used for further functionalization.

MSNs have shown several advantages such as high surface area, tunable surface properties, biocompatibility and cost efficient production.⁵¹ MSNs can also be modified with functional groups such as chromophores for imaging (*e.g.* fluorescein isothiocyanate (FITC)), polymers for improved biocompatibility and enhanced *in vivo* circulation time (*e.g.* polyethylene glycol (PEG)), therapeutic agents (*e.g.* cisplatin and gemcitabine), and targeting agents to increase target-specificity toward cancer cells (*e.g.* antibodies, aptamers and small targeting molecules). It is because of all these outstanding features

that MSNs have risen to be a promising candidate as a delivery platform for cancer treatment.

1.5.1 MSNs as Drug Delivery Platforms

MSNs offer several advantages as drug delivery systems that can overcome some of the main issues of chemotherapy.⁵² Firstly, the drugs are chemically attached to the nanoparticle, which allows control of their release under specific conditions such as a high reducing environment, changes in pH or enzymatic activity. This feature reduces the side-effects of the drugs while they are circulating in the blood and by avoiding their release in healthy tissues.⁵³ Furthermore, because the drugs are chemically attached to the nanoparticle, they can be protected from harsh conditions in the body or other factors that may inactivate them before reaching their targets.²⁷ This chemical control also allows for a sustained release of the drug, instead of the typical “burst” release that occurs in other drug delivery systems. Moreover, MSNs can also be grafted with a wide variety of polymers such as PEG, polyethylenimine (PEI) or poly(lactic-co-glycolic acid (PLGA), allowing the nanoparticle to escape recognition and phagocytosis by the immune system.⁵⁴ Finally, targeting agents can also be chemically attached to the MSN platform. These agents will render target-specificity toward cancer tissues.

The capability of developing stimuli-responsive drug delivery systems based on MSNs is an asset for this material and has been widely explored by scientists. These stimuli can be based on pH changes, redox environment, enzymatic activity, and light.⁵⁵ In particular, stimuli that are associated to specific conditions found in cancer cells are very attractive. Cancer tissues are slightly more acidic than normal tissues. pH-responsive MSN delivery systems have been developed using functional groups that can be modified

to release a drug or other moiety by the inclusion of a pH sensitive bond.⁵⁶ Redox responsive moieties are also useful functional groups due to the reducing environment of cancer cells. The disulfide bond is one of the most common redox-responsive moieties to develop drug delivery systems. The disulfide is usually broken inside of the cell by natural reducing agents such as glutathione and ascorbic acid.⁵⁷

1.5.2 MSNs for the Delivery of Cisplatin and/or Gemcitabine

A wide variety of approaches have been developed using MSNs as nanocarriers for delivering different types of platinum(IV) prodrugs, but the cisplatin(IV) prodrug has been the most popular anticancer drug.⁵⁸ Shi and co-workers have reported on MSN-based systems for the efficient delivery of cisplatin.⁵⁹⁻⁶¹ The authors selectively grafted a high density of carboxylic acid groups, which were used to complex to cisplatin, onto the surfaces of the MSNs. This approach increased the drug loading efficiency and greatly enhanced the growth inhibition effects against MCF-7, HeLa and A549 cancer cell lines. In a different study, a fluorescent mesoporous silica nanoparticle-based cisplatin(IV) prodrug delivery system was developed and tested *in vitro*.⁶² This platform took advantage of the reductive environment of cancer cells to release the active cisplatin. This delivery system not only demonstrated enhanced cellular uptake, but also showed significant drug effect. The use of combination therapy using MSNs as carriers to deliver cisplatin with other therapeutic agents has recently been explored.⁶³⁻⁶⁶ Di Pasqua, Balkus Jr. and co-workers demonstrated that the co-delivery of nitric oxide and cisplatin improved the treatment of non-small cell lung cancer cells.⁶⁴ All these results indicated that the cellular uptake and efficacy of cisplatin were improved using an MSN platform.

The MSN platform has already been used for the delivery of cisplatin or gemcitabine *in vitro* and *in vivo*. Cisplatin was chemically modified to achieve a redox responsive linking group that enabled it to be chemically attached to the MSN.⁶⁷ This research provided evidence that the cisplatin was able to be released from the MSN assuring that the platform allowed a more stable delivery and efficiency of treatment. While this research did not provide the maximum possible loading of cisplatin, the small amount loaded was able to outperform its free-release counterpart.

Gemcitabine has been used in MSNs as well, but in a wide variety of loading procedures. Nel *et al.*⁶⁸ was able to load gemcitabine into the MSN then coated the nanoparticle with a lipid bilayer. The group was able to achieve a 40 wt% passive loading using this method. The gemcitabine-MSN platform was used to treat pancreatic cancer *in vitro* and *in vivo*. Another group has been able to successfully modify gemcitabine with molecules of differing carbon lengths and chemically and actively loaded the gemcitabine to the MSN.⁶⁹ The *in vitro* analysis confirmed that the drug loaded MSN was able to outperform its free-release counterpart as well. The results of the active loading of the chemotherapeutic in these examples encouraged the work performed in this research, and active loading moieties were explored and utilized.

1.6 Research Objective

The main goal of this work is to synthesize a target-specific, stimuli-responsive mesoporous silica nanoparticle for the efficient co-delivery of cisplatin and gemcitabine. The MSN system consists of cisplatin and gemcitabine prodrugs chemically attached to the MSN through redox-responsive linkers. The MSN platform is further functionalized with folic acid as a targeting moiety. The therapeutic and synergistic effect of this

platform was tested *in vitro*. We hypothesized that, by combining both drugs in one MSN delivery system, the therapeutic effect will be dramatically increased. Furthermore, we envision that the addition of folic acid as a targeting agent, will enhance the target specificity toward cancer cells over-expressing folate receptors.

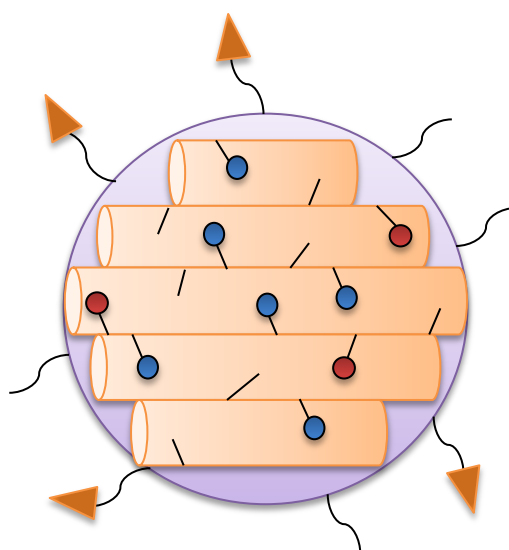


Figure 5: Goal of research: MSN loaded with cisplatin (red) and gemcitabine (blue) prodrugs attached to redox-responsive linkers and coated with a folic acid derivative of PEG (outer coating).

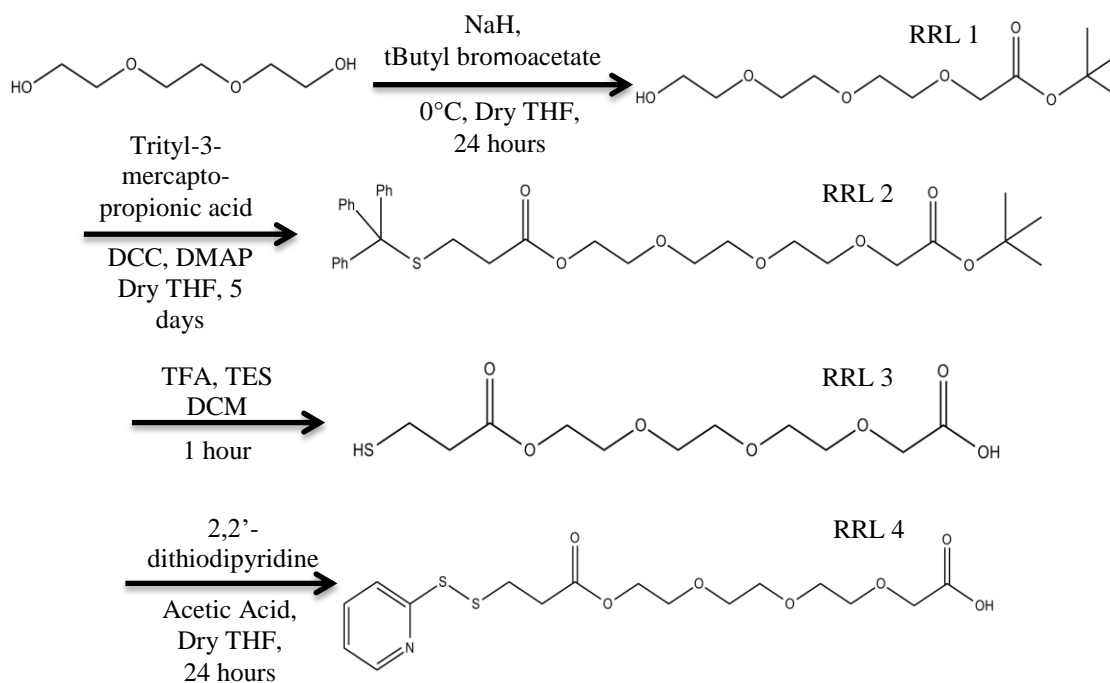
1.6.1 Design and Synthetic Strategy

To reach the goal of this work, the following specific aims were carried out: 1) To synthesize and characterize the stimuli-responsive linker, gemcitabine and cisplatin prodrugs; 2) To synthesize and characterize all MSN materials; 3) To determine *in vitro* synergy for different ratios of cisplatin and gemcitabine drugs; 4) To determine the *in vitro* cytotoxicity of MSN materials; and 5) To evaluate the targeting ability and therapeutic effect of the folic acid functionalized MSN platform.

1.6.2 Synthesis of the Stimuli-Responsive Linker, Gemcitabine, and Cisplatin Prodrugs.

The synthesis of the stimuli-responsive linker was performed using the synthetic approach depicted in Scheme 1. The final linker (RRL4) contains a carboxylic group to

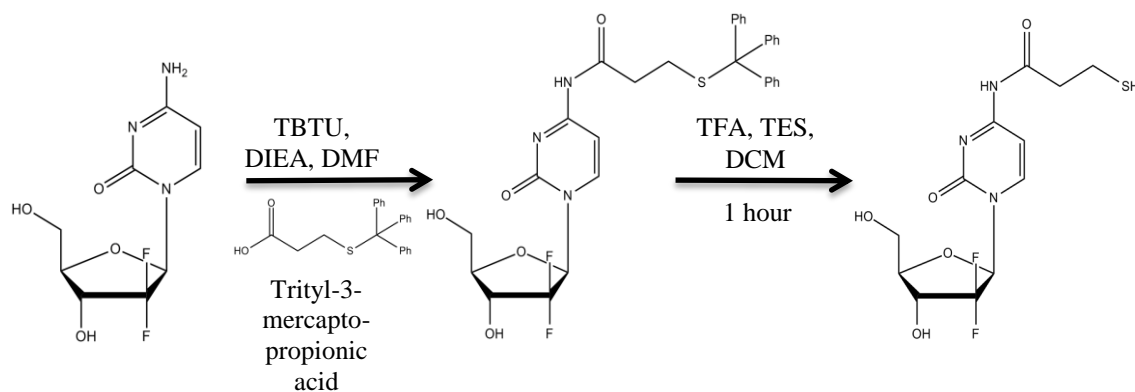
chemically attach to the MSNs. The linker also contains a disulfide bond on the other end, which was utilized to attach gemcitabine prodrug by performing a disulfide-thiol exchange reaction.⁷⁰



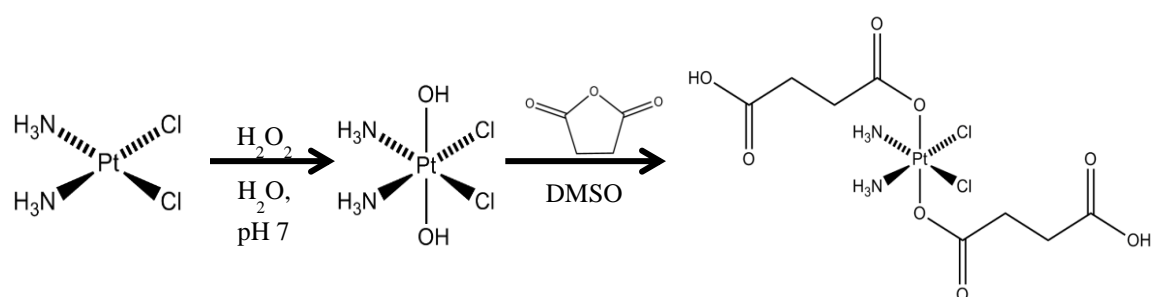
Scheme 1: Synthesis of stimuli-responsive linker responsible for the linkage of gemcitabine to the MSN.

The synthesis of gemcitabine prodrug was carried out using the synthetic method shown in Scheme 2. The gemcitabine contains an amide bond, which is pH sensitive and will be used to release the active drug once internalized into the cell.⁷¹

The synthesis of cisplatin prodrug was carried out using the synthetic pathway depicted in Scheme 3. Cisplatin was oxidized from the Pt(II) to Pt(IV) using hydrogen peroxide. The final molecule contains a carboxylic acid group for further reaction with the amine groups in MSNs.⁷²



Scheme 2: Synthesis of gemcitabine prodrug.



Scheme 3: Synthesis of cisplatin prodrug.

1.6.3 Synthesis of MSN Materials

The synthesis of the MSNs and AP-MSNs was performed using a surfactant-templated, co-condensation reaction.⁴⁶

1.6.4 Determination of *In Vitro* Synergy for Different Ratios of Cisplatin and Gemcitabine Drugs

Efficacy of the individual drugs was tested in order to determine the LD_{50} (lethal dose to achieve 50% viability) and the range at which further studies would be held. Cell trials for synergy determination were performed in a human cervical cancer cell line (HeLa). Determination of synergy was concluded through the incubation of the cells with

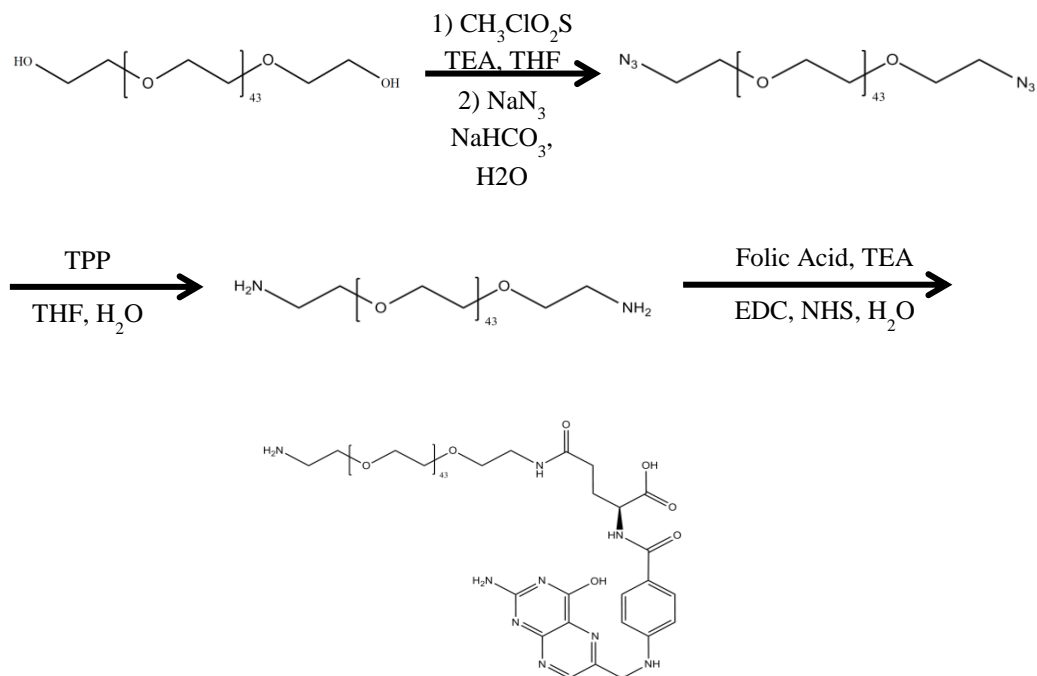
multiple ratios of cisplatin and gemcitabine. The CI was calculated and the optimal ratio to achieve the maximum synergy was determined.

1.6.5 Evaluation of *In Vitro* Cytotoxicity for MSN Materials.

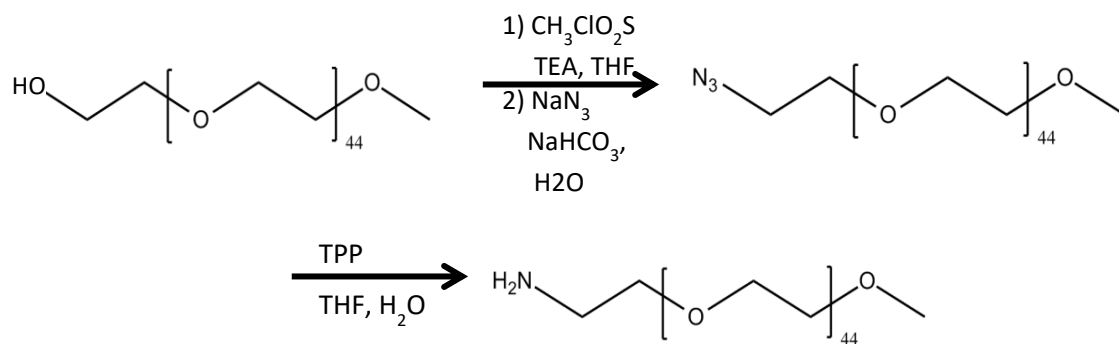
The cytotoxicity of the MSN materials was tested in human cervical cancer (HeLa) and pancreatic cancer (AsPC-1 and BxPC-3) cell lines. Concentrations of drug were normalized to gemcitabine to provide a comparison between cell lines. This normalization was also chosen because of the higher potency of gemcitabine.

1.6.6 Folate-Targeted MSN Platform

To functionalize the MSN platform with a folic acid-based targeting group; firstly the synthesis of the folic acid-PEG derivative was carried out using the synthetic approach described in Scheme 4. This FA-PEG targeting polymer was chemically attached to the MSN platform. The cytotoxicity and targeting ability of this MSN system was tested *in vitro*. Flow cytometry will be used to determine cellular uptake.



Scheme 4: Synthesis of Folic acid-PEG amine



Scheme 5: Synthesis of Methoxy-PEG-amine

CHAPTER 2: EXPERIMENTAL

2.1 Materials and Methods

All the reagents were purchased from Sigma Aldrich and used without further purification, with the exception of EDC from Oakwood Chemical and Gemcitabine, Hydrochloride salt from LC Laboratories. Thermogravimetric analysis (TGA) was performed on a Mettler Toledo TGA/SDTA851 instrument using a platinum sample pan and a method heating from 25°C to 800°C at a rate of 3 °C/min under a nitrogen atmosphere. Dynamic light scattering (DLS) and Zeta-potential measurements were performed on a Zetasizer Nano (by Malvern Instruments). The nitrogen sorption isotherms were performed using a NOVA 2200e Quantachrome surface area and pore size analyzer. UV-Vis analysis was performed using a Cary 300 UV-Vis Spectrophotometer. Atomic absorption spectrometry (AAS) was performed using a PerkinElmer HGA900 furnace, AAnalyst400 spectrometer, and an AS800 autosampler. (3-(4,5-dimethylthiazol-2-yl)-5-(3-caboxymethoxyphenyl)-2-(4-sulfophenyl)-2H-tetrazolium) (MTS, CellTiter 96®) was purchased from Promega. Cytotoxicity assays were evaluated using a Thermo Scientific™ Multiskan™ FC Microplate Photometer.

2.2 Synthesis and Characterization of Cisplatin and Gemcitabine Prodrugs, Redox-Responsive Linker, NH₂-PEG-FA, and NH₂-PEG-MeO

2.2.1 Synthesis of Cisplatin Prodrug

To synthesize the cisplatin prodrug, we followed a two-step approach based on previous reports (Scheme 3).¹⁶

2.2.1.1 Synthesis of Dihydroxycisplatin(IV)

To synthesize dihydroxycisplatin(IV), diamminedichloroplatinum(II) (cisplatin, 0.67 mmol, 200 mg) was added to nanopure water (9 mL, pH = 7) in a 25 mL 2-neck round-bottom flask covered with aluminum foil. To this solution, hydrogen peroxide (1.02 mL, 30%) was added. The solution was stirred at 70 °C for 5 h under a nitrogen atmosphere. Following this, the reaction cooled to room temperature and continued to stir overnight. The product was then washed one time with 10 mL cold nanopure water, followed by washing with 10 mL cold ethanol, and a final wash with 10 mL of ether. The product, a yellow solid, was centrifuged at 13,000 rpm for 8 minutes and the supernatant was discarded. The product was then dried *in vacuo* using a lyophilizer. Yield: 123.6 mg (34.7 wt%). FT-IR (cm⁻¹): 3513 (O-H), 3252 (N-H).

2.2.1.2 Synthesis of Cisplatin Prodrug

Dihydroxycisplatin(IV) (0.372 mmol, 123.6 mg) was weighed into a 20 mL scintillation vial covered with aluminum foil. Dimethyl sulfoxide (DMSO, 4 mL) was added to the scintillation vial along with succinic anhydride (1.489 mmol, 148.9 mg). The solution was heated and stirred overnight at 70 °C. After that the solution was dried in a lyophilizer. To obtain the cisplatin prodrug, the solid was washed one time with 10 mL cold acetone and the supernatant was discarded. The cisplatin prodrug solid was then

dried one more time using a lyophilizer. The final product is a white powder. Yield: 125.0 mg (62.9 wt%). ^1H NMR (300 MHz, DMSO- D_6 , ppm): δ 2.43-2.39 (m, 2H), 2.31-2.23 (m, 2H); ^{13}C NMR (300 MHz, DMSO- D_6 , ppm): δ 180.1 (COOPt), 174.3 (COOH), 30.9 (PtOOCCH₂), 29.1 (CH₂COOH); FT-IR (cm⁻¹): 3453 (O-H), 3252 (N-H), 2921 (C-H), 1701 (C=O), 1232 (C-C). ESI (m/z): 534.6 [M]⁺, Expected [M]⁺: 534.0.

2.2.2 Synthesis of Redox-Responsive Linker (RRL)

To synthesize the RRL a novel multi-step approach was developed in this work (Scheme 1).

2.2.2.1 Synthesis of Redox-Responsive Linker 1 (RRL1)

To synthesize RRL1, triethylene glycol (91.5 mmol, 12.5 mL) was dried overnight at 90 °C under vacuum in a 2-neck 250 mL round-bottom flask. The reagent was dissolved in dry tetrahydrofuran (THF, 55 mL) and placed in an ice bath. Sodium hydride (31.1 mmol, 745.8 mg) was added slowly to the solution. After 30 minutes of stirring, tert-butyl bromoacetate (18.9 mmol, 2.75 mL) was added dropwise. The product was stirred for 1 h in an ice bath. The reaction was then warmed to room temperature and stirred overnight. Following this, the product was then dried using a rotary evaporator. The product was then extracted with dichloromethane (DCM, 5x, 25 mL) and then washed with brine (3x, 75 mL). The organic phase was then treated with magnesium sulfate. The solution was then filtered and dried with rotary evaporation. Column chromatography was used to purify the product. Silica gel was used with a solvent mixture of methanol:ethyl acetate (7.5:92.5 %v/v). The desired product was identified using thin layer chromatography (TLC). The final product obtained after drying, is a clear/yellow-tinted oil. Yield: 1.815 g (7.5 wt%). ^1H NMR (300 MHz, CDCl₃, ppm): δ

3.88 (s, 2H), 3.61-3.52 (m, 12H), 1.33 (s, 9H). ^{13}C NMR (75 MHz, CDCl_3 , ppm): δ 169.67 (C=O), 81.63 ($\text{C}(\text{CH}_3)_3$), 72.59, 70.64, 70.58, 70.50, 70.26, 68.96 (OCH_2), 61.60 (HOCH_2), 28.09 ($\text{C}(\text{CH}_3)_3$). FT-IR (cm^{-1}): 3472 (O-H), 2871 (C-H), 1744 (C=O), 1227 (C-C), 1117 (C-O). ESI (m/z): 287.1 $[\text{M}+\text{Na}]^+$, Expected $[\text{M}]^+$: 264.3.

2.2.2.2 Synthesis of Redox-Responsive Linker 2 (RRL2)

To synthesize RRL2, RRL1 (6.87 mmol, 1.815 g) was added to a 250 mL round-bottom flask and dissolved in dry THF (30 mL). To this solution, $\text{N,N}'$ -dicyclohexylcarbodiimide (DCC, 7.56 mmol, 1.559 g), 4-dimethylaminopyridine (DMAP, 6.87 mmol, 0.839 g), and 3-(tritylthio)mercaptopropionic acid (4.46 mmol, 1.500 g) were added. The solution was stirred for 5 days at room temperature. The DCC urea byproduct, from the conjugation reaction, was filtered out using gravity filtration. Column chromatography was used to obtain the desired product. Silica gel was used with a solvent mixture of DCM:ethyl acetate (90%:10% v/v). The desired product was identified using TLC. The final product after drying was a clear/yellow-tinted oil. Yield: 1.037 g (25.4 wt%). ^1H NMR (300 MHz, CDCl_3 , ppm): δ 7.38-7.16 (m, 15H), 4.18 (s, 2H), 3.99 (s, 2H), 3.66-3.60 (m, 10H), 2.43 (t, 2H, $J=11.4$ Hz), 2.25 (t, 2H, $J=10.3$ Hz), 1.44 (s, 9H). ^{13}C NMR (75 MHz, CDCl_3 , ppm): δ 171.86 (COOCH_2), 169.58 (CH_2COO), 144.77, 129.67, 128.11, 126.79 (Ph), 81.49 ($\text{C}(\text{CH}_3)_3$), 70.58, 69.14, 67.10 (OCH_2), 63.75 ($\text{C}(\text{Ph}_3)$), 33.43 (CH_2SH), 28.15 ($\text{C}(\text{CH}_3)_3$), 26.96 ($\text{CH}_2\text{CH}_2\text{SH}$). FT-IR (cm^{-1}): 3057, 3030, 2928 (C-H), 1735 (C=O), 1594 (C=C), 1234 (C-C), 1122 (C-O). ESI (m/z): 616.8 $[\text{M}+\text{Na}]^+$, Expected $[\text{M}]^+$: 593.8.

2.2.2.3 Synthesis of Redox-Responsive Linker 3 (RRL3)

To synthesize RRL3, RRL2 (1.74 mmol, 1.037 g) was dissolved in DCM (10 mL) in a 50 mL round-bottom flask. To this solution, trifluoroacetic acid (TFA, 131 mmol, 10 mL) was added carefully. The solution turned yellow due to the formation of the trityl carbocation. Triethylsilane (TES, 6.26 mmol, 1 mL) was added and the solution turned clear again after the addition of a hydride to the trityl carbocation. The solution was stirred for 1 h at room temperature and then dried via rotary evaporation. The crude product was not purified due to the formation of dimers of RRL3 during the purification process.

2.2.2.4 Synthesis of Redox-Responsive Linker 4 (RRL4)

To synthesize RRL4, crude solution of RRL3 (0.252 mmol, 74.3 mg) was dissolved in a mixture of acetic acid (125.2 μ L, 2.19 mmol) and THF (20.0 mL). Dithiodipyridine (0.504 mmol, 0.111 g) was then added and the reaction was stirred for 24 h at room temperature. The solvent was removed via rotary evaporation and the product was purified using column chromatography. Silica gel was used with a solvent mixture of ethyl acetate:DCM (90:10 %v/v). The product was identified using TLC. The final product was collected after flushing the column with MeOH. The methanolic solution was removed using a rotary evaporator, and the product was dried under high vacuum overnight. The final product was a yellow/brown-tinted oil. Yield: 32.1 mg (31.4 wt%) ^1H NMR (300 MHz, CDCl_3 , ppm): δ 8.42 (d, 1H, J = 4.4 Hz), 7.64-7.63 (m, 2H), 7.06 (t, 1H, J = 8.3 Hz), 4.21 (t, 2H, J = 4.4 Hz), 3.86 (s, 2H), 3.72-3.46 (m, 10H), 2.99 (t, 2H, J = 7.4 Hz), 2.74 (t, 2H, J = 7.1 Hz). ^{13}C NMR (75 MHz, MeOD-d_4 , ppm): δ 167.89 (COOH), 155.64 (COO), 145.55, 133.29, 116.96, 115.99, ($\text{C}_5\text{H}_4\text{N}$), 66.45, 65.91, 65.07

(OCH₂), 60.17 (CH₂COOH), 29.86 (CH₂CH₂SH), 29.15 (CH₂SH). FT-IR (cm⁻¹): 3124 (O-H), 2936 (C-H), 1677, 1619 (C=C), 1203 (C-C), 1129 (C-O). ESI (m/z): 405.7 [M]⁺, 427.7 [M+Na]⁺, Expected [M]⁺: 405.0.

2.2.3 Synthesis of Gemcitabine Prodrug

To synthesize the gemcitabine prodrug a two-step synthetic approach was followed based on the literature (Scheme 2).⁷¹

2.2.3.1 Synthesis of (Tritylthio)mercapto-Gemcitabine

For the synthesis of (tritylthio)mercapto-gemcitabine, 3-(tritylthio)mercapto-propionic acid (142.7 μmol, 48.0 mg) was added to a 25 mL 2-neck round bottom flask covered with aluminum foil. Dry dimethylformamide (DMF, 2 mL) was added and the solution was stirred in an ice bath at 0 °C. N,N,N',N'-Tetramethyl-O-(benzotriazol-1-yl)uranium tetrafluoroborate (TBTU, 162.0 μmol, 52.0 mg) was added followed by N,N-diisopropylethylamine (DIPEA, 229.6 μmol, 40 μL) and the reaction stirred for 30 minutes under a nitrogen atmosphere. Gemcitabine hydrochloride salt (167 μmol, 50 mg) was added and the final solution stirred for 24 h. The crude product was washed with brine (20 mL, 180 g NaCl/500 mL) and the product was collected as a white solid via vacuum filtration. The solid was then stored at 0 °C. Yield: 35.1 mg (35.4 wt%). ¹H NMR (300 MHz, MeOD-d₄, ppm): δ 7.87 (d, 1H, J= 3.6 Hz), 7.39-7.23 (m, 16H), 6.25-6.21 (t, 1H, J= 8.4 Hz), 5.99-5.95 (d, 1H, J= 10.8 Hz), 4.57-4.55 (m, 1H), 4.28-4.23 (m, 2H), 4.00-3.80 (m, 1H) 2.45-2.42 (m, 2H), 2.22-2.15 (m, 2H). ¹³C NMR (75 MHz, MeOD-d₄, ppm): δ 172.34 (COOCH₂), 163.21 (N₂CO), 156.12 (CCN₂), 144.59 (NCCH), 141.46 (CF₂CH₂), 129.33, 127.53, 126.44 (Ph), 97.14 (CHCCH), 85.12 (CH₂CNO), 81.52 (CHCH₂), 68.78 (COH), 66.62 (C(Ph₃)), 58.70 (CH₂OH), 35.88 (CH₂SH), 26.38

(CH₂CH₂SH). FT-IR (cm⁻¹): 3245 (O-H), 2914 (C-H), 1722 (C=O), 1654, 1607 (C=C), 1559 (C=N), 1210 (C-C), 1124 (C-O). ESI (m/z): 566.5 [M-27]⁺, 616.7 [M+Na]⁺, Expected [M]⁺: 593.0.

2.2.3.2 Synthesis of Gemcitabine Prodrug

For the synthesis of gemcitabine prodrug, (tritylthio)mercapto-gemcitabine (118 μmol, 70.2 mg) was dissolved in DMF (2 mL) in a 25 mL round bottom flask and placed in an ice bath. TFA (26.2 mmol, 2 mL) was added and the solution turned yellow. TES (590 μmol, 95 μL) was then added and the solution turned clear again. The solution was allowed to react for 1 h. The product was dried via rotary evaporation and the product was washed with diethyl ether (5x, 5 mL). The product was collected as a white solid and stored at 0 °C. Yield: 34.0 mg (81.6 wt%). ¹H NMR (300 MHz, MeOD-d₄, ppm): δ 8.36 (d, 1H, J= 6.5 Hz), 7.51-7.45 (t, 1H, J= 7.6 Hz), 6.29-6.22 (t, 1H, J= 7.3 Hz), 4.30-4.24 (m, 1H), 3.97-3.94 (m, 2H), 3.81-3.78 (m, 1H) 2.79-2.74 (m, 4H). ¹³C NMR (75 MHz, MeOD-d₄, ppm): δ 172.54 (COOCH₂), 171.79 (N₂CO), 144.73 (CCN₂), 143.98 (NCCH), 129.09 (CF₂CH₂), 96.92 (CHCCH), 85.46 (CH₂CNO), 81.57 (CHCH₂), 62.04 (COH), 58.58 (CH₂OH), 37.83 (CH₂SH), 18.60 (CH₂CH₂SH). FT-IR (cm⁻¹): 3273 (O-H), 2931 (C-H), 1716 (C=O), 1651, 1609 (C=C), 1555 (C=N), 1238 (C-C), 1130 (C-O). ESI (m/z): 351.82 [M]⁺, Expected [M]⁺: 351.0.

2.2.4 Synthesis of Folic Acid-Polyethylene Glycol-Amine (NH₂-PEG-FA)

The synthesis of NH₂-PEG-FA was completed in a multistep approach using a procedure previously reported protocol.⁷³

2.2.4.1 Synthesis of Diazido-Polyethylene Glycol (Diazido-PEG)

For the synthesis of Diazido-PEG, polyethylene glycol (2.0 mmol, 4.0 g) was dried overnight at 90°C under high vacuum in a 250 mL 2-neck round-bottom flask. Dry THF (30 mL) was added followed by the addition of methanesulfonyl chloride (18.9 mmol, 1.46 mL). Moreover, a mixture of dry THF (12 mL) and trimethylamine (TEA, 17.2 mmol, 2.748 mL) was made and added dropwise to the reaction flask over 15 minutes. The solution was cooled in an ice bath while stirring for 2 h and then stirred overnight at room temperature. Nanopure water (30 mL) and sodium azide (24 mmol, 1.56 g) were then added, the solution turned clear. The reaction flask was cooled in an ice bath and sodium bicarbonate (1.0 M, 6 mL) was added. The solution was allowed to reflux for 48 h at 85 °C. The THF layer was then removed with a separatory funnel using DCM (4x, 50 mL) and brine (4x, 50 mL). The product (Diazido-PEG) was then dried via rotary evaporation and further dried overnight under high vacuum. Yield: 1.55 g (38.7 wt%). ¹H NMR (300 MHz, CDCl₃, ppm): δ 3.72-3.52 (m, 180H), 3.35-3.33 (t, 4H). ¹³C NMR (75 MHz, CDCl₃, ppm): δ 70.38 (OCH₂), 37.56 (CH₂N₃). FT-IR (cm⁻¹): 2883 (C-H), 2100 (Azide), 1240 (C-C), 1115 (C-O).

2.2.4.2 Synthesis of Diamino-Polyethylene Glycol (Diamino-PEG)

For the synthesis of Diamino-PEG, diazido-PEG (0.774 mmol, 1.5484 g) was dissolved in dry THF (15 mL). Triphenylphosphine (TPP, 4.645 mmol, 1.216 g) was added and the solution was stirred for 10 h at room temperature. Nanopure water (600 μL) was added and the final solution was stirred overnight at room temperature. THF was removed via rotary evaporation and nanopure water (20 mL) was added. The triphenylphosphine oxide byproduct was removed via gravity filtration and the solvent

was removed via rotary evaporation. The product (Diamino-PEG), a white solid, was dried under high vacuum overnight. Yield: 1.35 (87.0 wt%). ^1H NMR (300 MHz, CDCl_3 , ppm): 3.48-3.25 (m, 180H), 3.12-3.04 (m, 4H). ^{13}C NMR (75 MHz, MeOD-d_4 , ppm): δ 70.26 (OCH_2), 36.40 (CH_2NH_2). FT-IR (cm^{-1}): 2882 (C-H), 1240 (C-C), 1116 (C-O).

2.2.4.3 Synthesis of NH_2 -PEG-FA

For the synthesis of NH_2 -PEG-FA, folic acid (FA, 150 μmol , 66.21 mg) was added to a 25 mL round-bottom flask with nanopure water (8 mL). Triethylamine (330 μmol , 46.03 μL) was added and the solution was sonicated until FA was completely dissolved. 1-Ethyl-3-(3-dimethylaminopropyl)carbodiimide (EDC, 240 μmol , 37.25 mg) was added and the solution was stirred for 5 min at room temperature. After that, N-hydroxysuccinimide (NHS, 180 μmol , 20.71 mg) was added and the solution was stirred for 24 h at room temperature. Diamino-PEG (150 μmol , 300 mg) was dispersed in nanopure water (7 mL) and then added to the activated folic acid solution. The mixture was then stirred at room temperature for 48 h. The solution was then transferred to a dialysis cassette (2K MWCO) and dialyzed in nanopure water. The solution was changed two/three times per day for up to 5 days. The solution was then removed from the cassette and the water was eliminated via rotary evaporation. A yellow solid was obtained and further dried in a lyophilizer. Yield: 49.8 mg (13.6 wt%). ^1H NMR (300 MHz, DMSO-d_6 , ppm): δ 8.62 (s, 1H), 8.14-7.86 (d, 2H), 7.62-7.58 (d, 2H), 6.92-6.89 (t, 1H), 6.65-6.62 (d, 2H, $J=7.8$ Hz), 4.49-4.47 (d, 2H, $J=5.7$ Hz), 4.35-4.31 (m, 1H), 3.78-3.54 (m, 180H), 2.34-2.28 (t, 2H), 2.12-1.85 (m, 2H). ^{13}C NMR (75 MHz, D_2O , ppm): δ 181.87 (COOH), 179.31 (NCOCH_2), 169.38 (PhCO), 129.09, 115.12, 112.10 (Ph), 69.71 (OCH_2), 56.03 (CH_2CHN), 43.25 (CNH_2), 39.19 (CH_2NH), 33.94 (CH_2CH_2), 28.22

(CH₂). FT-IR (cm⁻¹): 3259 (O-H), 2883 (C-H), 1685 (C=O), 1607 (C=C), 1513 (C=N), 1240 (C-C), 1099 (C-O).

2.2.5 Synthesis of Methoxy-Polyethylene Glycol-Amine (NH₂-PEG-MeO)

The synthesis of NH₂-PEG-MeO was completed through a multistep approach.

2.2.5.1 Synthesis of Azido-Polyethylene Glycol Methyl Ether (Azido-PEG-MeO)

For the synthesis of Azido-PEG-MeO, polyethylene glycol methyl ether (PEG-MeO, 1 mmol, 2.0 g) was dried overnight at 90°C under vacuum. The reactant was dissolved in dry THF (10 mL), followed by the addition of methanesulfonyl chloride (19.4 mmol, 1.5 mL). The mixture was placed in an ice bath under a nitrogen atmosphere. DIPEA (17.2 mmol, 3.0 mL) was added dropwise to the solution over 30 minutes. The solution was stirred for 1 h in an ice bath, then removed and stirred overnight at room temperature. The formed solid was dissolved with cold water (10 mL) in an ice bath. Sodium bicarbonate (1.0 M, 2 mL) and sodium azide (23.1 mmol, 1.5 g) were subsequently added. The THF was removed via rotary evaporation and the aqueous phase was refluxed for 24 h at 100°C. The product was extracted with a separatory funnel using DCM (5x, 15 mL) and brine (5x, 15 mL). The excess water was removed using anhydrous magnesium sulfate. The DCM was removed via rotary evaporation and the product was dried under high vacuum overnight. Yield: 1.55 g (77.5 wt%). ¹H NMR (300 MHz, CDCl₃, ppm): δ 3.54-3.18 (m, 180H), 3.12-3.03 (m, 4H). ¹³C NMR (75 MHz, CDCl₃, ppm): δ 72.18 (OCH₂), 57.86 (OCH₃), 42.61 (CH₂N₃). FT-IR (cm⁻¹): 2883 (C-H), 2135 (Azide), 1240 (C-C), 1117 (C-O).

2.2.5.2 Synthesis of NH₂-PEG-MeO

For the synthesis of NH₂-PEG-MeO, Azido-PEG-MeO (0.776 mmol, 1.5501 g) was dissolved in dry THF (12 mL) under a nitrogen atmosphere. TPP (4.88 mmol, 1.28

g) was then added to the solution and the reaction stirred overnight at room temperature. Nanopure water (1.4 mL) was added and the solution was stirred overnight at room temperature. The THF was removed via rotary evaporation and nanopure water (21.0 mL) was added to the solution, forming a white solid (triphenylphosphine oxide). The biproduct was removed by gravity filtration and the water was removed via rotary evaporation. The product was dried overnight under high vacuum. Yield: 0.639 g (41.2 wt%). ^1H NMR (300 MHz, CDCl_3 , ppm): δ 3.49-3.19 (m, 180H), 3.12-2.98 (s, 4H), 1.20-1.11 (m, 4H). ^{13}C NMR (75 MHz, MeOD-d_4 , ppm): δ 71.27 (OCH_2), 57.82 (OCH_3), 42.64 (CH_2NH_2). FT-IR (cm^{-1}): 3411 (N-H), 2875 (C-H), 1249 (C-C), 1087 (C-O).

2.3 Synthesis and Characterization of MSN Materials

2.3.1 Synthesis of Aminopropyl-Mesoporous Silica Nanoparticles (AP-MSNs)

To synthesize of AP-MSNs, cetyltrimethylammonium bromide (0.548 mmol, 200 mg) was dissolved in nanopure water (100 mL) in a 250 mL round-bottom flask. Sodium hydroxide (2.0 M, 0.7 mL) and mesitylene (9.76 mmol, 1.4 mL) were then added to the solution. The mixture was stirred for 1 h at 80 °C. (3-aminopropyl)triethoxysilane (APTES, 0.600 mmol, 139.6 μL) and tetraethyl orthosilicate (TEOS, 4.48 mmol, 1.0 mL) were added subsequently to the solution. Then, the solution was stirred for another 2 h at 80 °C. The as-made AP-MSN material was washed in water (3x, 15 mL) and ethanol (3x, 15mL) and separated via centrifugation. The as-made MSNs then underwent an acid wash to remove CTAB by using a methanolic solution (10:1, mg MSN/mL MeOH) of hydrochloric acid (1:15, v/v HCl:MeOH). The nanoparticles were refluxed overnight at 60 °C. Following the acid wash, the nanoparticles were further washed with water and ethanol and separated via centrifugation. A second acid wash was performed to ensure

the complete elimination of the surfactant. The water/ethanol wash was repeated and the particles were finally redispersed in ethanol. The structural properties of the MSN material were characterized using a wide variety of techniques such as dynamic light scattering (DLS), thermogravimetric analysis (TGA), nitrogen sorption isotherms (BET and BJH), scanning electron microscopy (SEM), and transmission electron microscopy (TEM).

2.3.2 Synthesis of Cisplatin-MSNs (cisPt-MSN)

For the synthesis of cisPt-MSNs, AP-MSNs (500 mg) were dispersed in DMSO (15 mL) in a 50 mL round-bottom flask covered in aluminum foil. Triethylamine (196 μ mol, 27.4 μ L) was added to this solution. In a separate 25 mL round-bottom flask, cisplatin prodrug (234 μ mol, 125.3 mg) and EDC (1.29 mmol, 201 mg) were dissolved in DMSO (5 mL). This solution was added to the nanoparticle dispersion using a pipette and the reaction was stirred overnight at room temperature. The nanoparticles were then washed with DMSO (1x, 15mL), ethanol (2x, 15 mL), and stored in ethanol. The supernatants for each wash were collected for platinum content determination using atomic absorption spectroscopy (AAS). By subtracting the amount of platinum in the supernatant and washing solutions from the original amount added the loading efficiency was determined to be 62.1% and the amount of cisplatin loaded on the MSN was 9.6 wt%.

2.3.3 Synthesis of Redox-Responsive-Linker-MSNs (RRL-MSN)

For the synthesis of RRL-MSNs, AP-MSNs (150 mg) were dispersed in DMSO (7 mL) in a scintillation vial covered in aluminum foil. To this solution NHS (176 μ mol, 20.3 mg), EDC (218 μ mol, 33.9 mg), and RRL4 (125 μ mol, 49.3 mg) were added, and

the reaction was stirred for 48 h at room temperature. The nanoparticle suspension was washed with ethanol (3x, 15 mL) and the nanoparticles were redispersed and stored in ethanol.

2.3.4 Synthesis of Gemcitabine-MSNs (Gem-MSN)

For the synthesis of Gem-MSNs, RRL-MSNs (70 mg) were dispersed in DMSO (7 mL) in a scintillation vial covered in aluminum foil. Gemcitabine prodrug (19.8 μmol , 7.0 mg) was added to the vial, and the solution was stirred for 48 h at room temperature. The nanoparticle solution was washed in DMSO (3x, 15 mL) and the nanoparticles were stored in ethanol. The supernatant and washing solutions were used to determine the loading of gemcitabine using UV-Vis spectroscopy. Loading efficiency ($\lambda=270$ nm) was determined to be 45.7% and the amount of gemcitabine loaded onto the MSN was 4.57 wt%.

2.3.5 Synthesis of Cisplatin-Redox-Responsive-Linker-MSNs (cisPt-RRL-MSN)

For the synthesis of cisPt-RRL-MSNs, cisPt-MSNs (150 mg) were dispersed in DMSO (7 mL) in a scintillation vial covered in aluminum foil. To this solution NHS (242 μmol , 27.9 mg), EDC (251 μmol , 38.9 mg), and RRL4 (125 μmol , 49.0 mg) were added, and the reaction was stirred for 48 h at room temperature. The nanoparticle suspension was washed with ethanol (3x, 15 mL) and the nanoparticles were redispersed and stored in ethanol.

2.3.6 Synthesis of Cisplatin-Gemcitabine-MSNs (cisPt-Gem-MSN)

To synthesize cisPt-Gem-MSNs, cisPt-RRL-MSNs (50 mg) were dispersed in DMSO (7 mL) in a scintillation vial covered in aluminum foil. Gemcitabine prodrug (6.2 μmol , 2.2 mg) was added to the vial and the solution was stirred for 48 h at room

temperature. The nanoparticle solution was washed in DMSO (3x, 15 mL) and the nanoparticles were redispersed and stored in ethanol. The supernatant and washing solutions were collected to determine the loading of gemcitabine using UV-Vis spectroscopy. Loading efficiency ($\lambda=270$ nm) was determined to be 89.0% and the amount of gemcitabine loaded onto the MSN was 3.91 wt%.

2.3.7 Synthesis of Passively Loaded Gemcitabine to AP-MSNs (GemPas-MSN)

For the synthesis of GemPas-MSNs, AP-MSNs (45 mg) were dispersed in DMSO (5 mL) in a scintillation vial covered in aluminum foil. To this solution gemcitabine hydrochloride salt (7.3 μ mol, 2.2 mg) was added. The solution was stirred for 24 h at room temperature. The nanoparticle solution was washed with DMSO (3x, 15 mL) and redispersed and stored in ethanol. The supernatant and washing solutions were collected to determine the loading of gemcitabine using UV-Vis spectroscopy. Loading efficiency ($\lambda=270$ nm) was determined to be 60.5% and the amount of gemcitabine loaded onto the MSN was 2.96 wt%.

2.3.8 Synthesis of Passively Loaded Gemcitabine to Cisplatin-MSNs (cisPt-GemPas-MSN)

To synthesize cisPt-GemPas-MSNs, cisPt-MSNs (25 mg) were dispersed in DMSO (5 mL) in a scintillation vial covered in aluminum foil. To this solution gemcitabine hydrochloride salt (7.3 μ mol, 2.2 mg) was added. The solution was stirred for 24 h at room temperature. The nanoparticle solution was washed with DMSO (3x, 15 mL) and redispersed and stored in ethanol. The supernatant and washing solutions were collected to determine loading using UV-Vis spectroscopy. Loading efficiency ($\lambda=270$

nm) was determined to be 62.9% and the amount of gemcitabine loaded onto the MSN was 5.54 wt%.

2.3.9 Synthesis of FITC-cisPt-Gem-MSNs

To synthesize FITC-cisPt-Gem-MSNs, fluorescein isothiocyanate (FITC, 6.2 μmol , 2.4 mg) was dispersed in nanopure water (1.0 mL). To this solution, APTES (13.0 μmol , 3.1 μL) was added and the solution was allowed to stir at room temperature for 1.5 h. 50 mg of the cisPt-Gem-MSNs were then dispersed in 10 mL ethanol and the FITC solution was added. The solution was then refluxed at 60 °C overnight. The solution was washed with ethanol (3x) and redispersed and stored in ethanol.

2.3.10 Amine Activation of PEG derivatives

For the activation of MeO-PEG-NH₂ for further grafting to the MSNs, MeO-PEG-NH₂ (20.4 μmol , 50 mg) was dissolved in 1 mL of DMSO in a 5 mL scintillation vial. To this solution TEA (40.8 μmol , 5.7 μL) and triethoxysilylpropylisocyanate (TESPIC, 0.06 μmol , 15.2 μL) were added and the solution was allowed to stir at room temperature for 4 h. This process was repeated for FA-PEG-NH₂.

2.3.11 Synthesis of MeO-PEG-FITC-cisPt-Gem-MSN

For the synthesis of MeO-PEG-FITC-cisPt-Gem-MSN, FITC-cisPt-Gem-MSN (25 mg) was dispersed in 15 mL ethanol in a 50 mL round-bottom flask covered with aluminum foil. To this solution, 0.67 mL of the activated MeO-PEG-NH₂ solution was added and the solution was allowed to reflux at 60 °C overnight. The solution was then washed with ethanol (3x), redispersed and stored in ethanol.

2.3.12 Synthesis of FA-PEG-FITC-cisPt-Gem-MSN

To synthesize FA-PEG-FITC-cisPt-Gem-MSN, FITC-cisPt-Gem-MSN (25 mg) was dispersed in 15 mL ethanol in a 50 mL round-bottom flask covered with aluminum foil. To this solution, the activated FA-PEG solution (201 μ L) and the activated MeO-PEG solution (469 μ L) was added. The solution was allowed to reflux at 60 °C overnight. The solution was then washed with ethanol (3x), redispersed and stored in ethanol.

2.4 Release Profiles

For the release profile, the drug-loaded MSNs (5.0 mg) were washed in 5 mL PBS (pH 7.4 or pH 5.0) until less than 1% drug leaking is achieved as determined through AAS or UV-Vis spectroscopy. The drug-loaded MSNs were then dispersed in PBS (pH 7.4 or pH 5.0, 10 mL) and added to a dialysis bag (3.5K MWCO, 16 mm). This bag was placed in a 250 mL beaker covered with aluminum foil and filled with PBS (pH 7.4 or pH 5.0, 190 mL). This solution was gently stirred at 37 °C. To replicate the reducing environment inside cancer cells, glutathione (GSH) was used as a reducing agent. GSH was added to the PBS solution until a concentration of 10 mM was established. For this 30.7 mg was added to the dialysis bag (10 mL) and 583.6 mg was added to the beaker (190 mL). At hourly intervals, an aliquot was collected from the beaker for analysis. A control was also run at each pH value. The control contained no GSH, and determined the passive release of the drugs.

2.4.1 Cisplatin Release Profile

For the cisplatin release profile, 50 μ L aliquots were collected at different times and diluted to 1.0 mL with a 0.1 M nitric acid solution. Platinum concentration was then determined through AAS. Results from this release profile can be seen in Figure 10.

2.4.2 Gemcitabine Release Profile

For the gemcitabine release profile, 5 mL aliquots were collected at different times. UV-Vis analysis ($\lambda=270$ nm) was used to analyze the release of gemcitabine. The aliquot was then returned to the beaker to keep the volume constant. Results from this release profile can be seen in Figure 11.

2.5 Cell Growth, Handling and Maintenance

Cells were cultured with RPMI 1640 medium, Dulbecco's phosphate-buffered saline (DPBS), fetal bovine serum (FBS), and penicillin-streptomycin solution were bought from Corning. Pierce™. For cell growth, cell media was made using RPMI 1640, 10% FBS, and 2% Penicillin/Streptomycin solution. Cervical cancer (HeLa) and pancreatic cancer (AsPC-1 and BxPC-3) cells were grown in cell culture flasks (75 cm²) and maintained between passages 1 and 15.

2.6 Cytotoxicity Assay

2.6.1 Drug Cytotoxicity Assay

For determination of drug cytotoxicity, cells were seeded at a concentration of 10^4 cells per mL (HeLa) or 2×10^4 cells per mL (AsPC-1 and BxPC-3) in a 96-well plate. The cells were incubated for 24 h at 37 °C/5% CO₂ and then inoculated different concentrations of drugs or MSN materials (100 μL). After 48 h of incubation, the cells were washed with DPBS and then incubated with 100 μL of fresh cell media for another 24 h. To test the cytotoxicity, the cells were incubated with the MTS assay (Cell Titer® 96, 20μL) for another 3 h at 37 °C/5% CO₂. After that, the 96-well plates placed in a cell plate reader (FC Multiskan) for quantification of cell viability using an absorbance filter

of 450 nm. The outer rows and columns in the 96-well plate were not used for the experiments due to inaccurate readings from the plate reader.

2.6.2 Drug Synergy Determination

For determination of drug synergy, gemcitabine and cisplatin were combined in solution to afford a total concentration between 10 μM and 0.025 μM to test cytotoxicity. Since gemcitabine has been shown to be more potent than cisplatin, gemcitabine was used in lesser amounts. The drugs were combined in the molar ratios as seen in Table 1.

Table 1: Concentration ratio of cisplatin and gemcitabine used for synergy determination.

<u>Cisplatin (mol %)</u>	<u>Gemcitabine (mol %)</u>
50	50
75	25
90	10
95	5
99	1

The combination index (CI) was then calculated for each concentration using the Compusyn software which utilized Equation 1. The software was obtained for free through the parent company's website. As a disclaimer, we are not obliged to advertise this software. It was not used for commercial purposes and we take no responsibility for the properties of the software. The software is able to use the data from the individual drug cytotoxicity assays, as well as the results from the combination cytotoxicity assay in order to calculate the CI of the drug pair.

2.7 Flow Cytometry

A 6-well plate was seeded with 1×10^5 cells per mL with a final volume of 3 mL of cell medium. The cells were incubated for 24 h, following which they were washed with DPBS (3 mL, pH 7.4) and inoculated with MeO-PEG-FITC-cisPt-Gem-MSN and FA-PEG-FITC-cisPt-Gem-MSN ($10 \mu\text{g/mL}$) using folic acid-free media. The cells were incubated for 4 h. After that, the cells were dispersed in 400 μL of RPMI not containing FBS and 200 μL of Trypan blue.

2.8 Confocal Microscopy

A micro cover glass was placed into each well of a 6-well plate and the wells were inoculated with a concentration of 1×10^5 cells per mL with a final volume of 3 mL of cell medium. The cells were incubated for 24 h, following which, they were washed with DPBS (3 mL, pH 7.4). The cells were then inoculated with the mPEG-FITC-cisPt-Gem-MSN and FA-PEG-FITC-cisPt-Gem-MSN (50, 20, 10 $\mu\text{g/mL}$ each) using folic acid-free cell media. The cells were incubated for 4 h, then washed twice with DPBS (3 mL). 2 mL of DPBS was then added to each well and a nucleus stain, 4',6-diamidino-2-phenylindole (DAPI), was added following the recommendation of the manufacturer (2 drops/mL DPBS). The cells were incubated for 15 min in the DAPI solution. Micro slides (25 x 75 mm, 1.0 mm thickness) were prepared by adding a spacer, with 30 μL of cell medium in the center. The micro cover glass was removed from the wells and placed face down on the adhesive spacer. The slides were then analyzed using a differential interference contrast microscopy channel (DIC), a DAPI channel, and a FITC channel.

2.9 Cytotoxicity for FA Functionalized Materials.

For determination of drug cytotoxicity, HeLa cells were seeded at a concentration of 10^4 cells per mL in a 96-well plate. The cells were incubated for 24 h at $37^\circ\text{C}/5\% \text{CO}_2$

and then inoculated using folic acid-free media with differing concentrations between 0.03 μM to 10 μM and between 0.5 μM and 20 μM of gemcitabine and cisplatin normalized MSN materials, respectively (100 μL). After 48 h of incubation, the cells were washed with DPBS and then incubated with 100 μL of fresh cell media for another 24 h. To test the cytotoxicity, the cells were incubated with the MTS assay (Cell Titer® 96, 20 μL) for another 3 h at 37 °C/5% CO₂. After that, the 96-well plates placed in a cell plate reader for quantification of cell viability using an absorbance filter of 450 nm.

CHAPTER 3: RESULTS AND DISCUSSION

3.1. Synthesis and Characterization of Cisplatin Prodrug

The physicochemical and biological properties of platinum(IV) prodrugs differ significantly from those of their platinum(II) counterparts. For example, the saturated, kinetically more inert coordination sphere of platinum(IV) is more resistant to ligand substitution reactions, thus minimizing unwanted side reactions with biomolecules prior to DNA binding. In addition, the two extra ligands provide a means to impart and fine-tune desired biological properties, such as lipophilicity, redox stability, cancer-cell targeting, and improved cellular uptake. Moreover, these ligands also facilitate the attachment to nanoparticles and other carrier systems. Although platinum(IV) complexes can platinate DNA in their oxidized form, the formation of cytotoxic lesions by ligand substitution occurs in a matter of weeks. The reduction of the platinum(IV) center to platinum(II), through the loss of two ligands, is thought to be essential for the anticancer activity of these agents.¹⁶

In this work, the synthesis of the cisplatin prodrug was carried out through a two-step synthetic pathway (Scheme 3). The first step involved the oxidation of cisplatin from Pt(II) to Pt(IV) using an aqueous solution of hydrogen peroxide. The formation of dihydroxycisplatin(IV) was confirmed by IR, the O-H stretching vibration was observed at 3513 cm^{-1} (Figure A1.20). This compound is further reacted with succinic anhydride through a nucleophilic addition that opens the ring to afford cis,cis,trans-

[Pt(NH₃)₂Cl₂(O₂CCH₂CH₂CO₂H)₂] (cisplatin prodrug). The successful synthesis of cisplatin prodrug was confirmed by FTIR, ¹H NMR, ¹³C NMR, and ESI-MS. The FTIR showed the characteristic stretching vibrations for O-H at 3453 cm⁻¹, C-H at 2921 cm⁻¹, and C=O at 1674, 1716 cm⁻¹ (Figure A1.22). Moreover, the ¹H NMR spectrum depicted the chemical shifts for the hydrogens associated to the methylene groups in the carboxylic acid derivative at 2.43 to 2.23 ppm. In a similar way, ¹³C NMR showed the chemical shifts for the carbons associated to the carbonyl for the carboxylic acid and carboxylate groups at 180.1 and 174.3 ppm. Finally, the molecular ion for cisplatin prodrug was also identified in the ESI-MS at 534.6 m/z compared to the calculated value of 534.0 m/z.

3.2. Synthesis and Characterization of Gemcitabine Prodrug, and Redox-Responsive Linker (RRL)

Gemcitabine prodrugs have been reported to have a half-life of over 10 hours, which is much higher than the parent drug of less than an hour under physiological conditions. The gemcitabine prodrug synthesized in this work can be released either under low pH and/or a high reducing environment to release free gemcitabine. This prodrug has even shown to have at least 4 times more efficacy than gemcitabine in an *in vivo* murine model.⁷¹ The linker (RRL), which is designed and synthesized in this work has not been reported in the literature. This linker contains an amide bond that can be cleaved under acidic pH, and a disulfide bond that is broken under highly reducing environments such as those found in cancer cells. These features allow the release of gemcitabine in a target-specific and controlled fashion.

The synthesis of gemcitabine prodrug was carried out through a two-step synthetic approach. The first step of the synthesis involved the addition of S-trityl-3-mercaptopropionic acid to afford an amide bond. The formation of (tritylthio)mercaptogemcitabine was confirmed through the appearance of the C=O stretching vibration at 1722 cm^{-1} (Figure A1.14) and the molecular ion of 593.8 m/z , which corresponds to the observed molecular ion minus the sodium ion. The molecule was further confirmed through the appearance of the chemical shifts in the ^1H NMR spectrum at $\delta\ 7.3\text{-}7.2\text{ ppm}$ corresponding to the hydrogens on the phenyl groups and at $\delta\ 2.4\text{-}2.1\text{ ppm}$ corresponding to the hydrogens on the methylene group (Figure A1.12). The ^{13}C NMR spectrum confirms the synthesis of the product with chemical shifts at 129.3 , 127.5 , and 126.4 ppm , which correspond to the phenyl rings, and shifts at 35.9 and 26.4 ppm , which correspond to the aliphatic chain. This compound was then reacted with TFA to afford the deprotection of the thiol group. The successful synthesis of the gemcitabine prodrug was confirmed by ESI-MS, observing the molecular ion at 351.98 m/z compared to the calculated value of 593.0 m/z (Figure A1.18). Furthermore, the ^1H NMR spectrum corroborated the loss of the phenyl groups, but keeping the corresponding chemical shifts for the gemcitabine and aliphatic chain (Figure A1.16). In a similar way the ^{13}C NMR spectrum verifies the disappearance of the phenyl carbons (Figure A1.17).

The synthesis of the RRL molecule was performed through a multi-step approach. The first step involved the modification of one end of the TEG with tert-butyl acetate through a bimolecular substitution nucleophilic ($\text{S}_{\text{N}}2$) reaction. To afford RRL1, TEG was deprotonated in the presence of NaH to obtain the corresponding alkoxide, which after a $\text{S}_{\text{N}}2$ reaction with tert-butyl bromoacetate afforded RRL1. The monosubstituted

RRL1 linker was purified by chromatography. ESI-MS shows a molecular ion mass at 287.3 m/z corresponding to $[M+Na]^+$. The presence of Na^+ in RRL1 and other RRL derivatives is most likely due to complexation of the cation with the oxygens in the TEG chain, which resembles crown ethers (Figure 6).

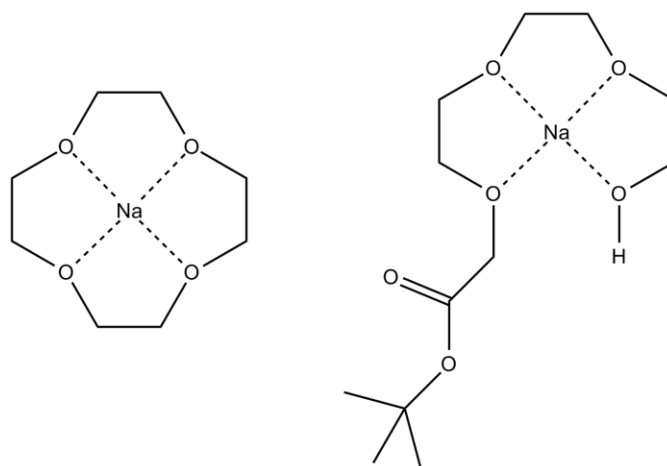


Figure 6: An example of a crown ether (left) and the hypothesized structure for RRL1 (right).

The 1H NMR spectrum depicted the shifts for the hydrogens corresponding to the tert-butyl group as well as the α -carbon (Figure A1.1). RRL1 was further reacted with S-trityl-3-mercaptopropionic acid through a conjugation reaction mediated by EDC to afford RRL2. This molecule was confirmed by 1H and ^{13}C NMR and ESI-MS. 1H NMR confirmed the chemical shifts for the hydrogens corresponding to the phenyl and methylene groups (Figure A1.5). The ^{13}C NMR spectrum verified the molecule with the appearance of the phenyl rings at chemical shifts between 144.8 and 126.8 ppm (Figure A1.6). Moreover, the molecular ion of 616.8 m/z was found by ESI-MS corresponding to $[M+Na]^+$ (Figure A1.8). RRL3 was obtained by deprotecting the carboxylic acid and thiol groups in the presence of TFA. RRL3 was not purified due to the fast oxidation to form dimers under the conditions used to separate the product. RRL3 was reacted with

dipyridyl disulfide to obtain RRL4 through a disulfide exchange reaction. The ^1H NMR spectrum of RRL4 showed the loss of the phenyl and tert-butyl peaks and the appearance of the pyridine peaks (Figure A1.7). ^{13}C NMR analysis identified the product with the chemical shift of the pyridine carbons between 145.6 and 116.0 ppm (Figure A1.8). This compound was confirmed through ESI-MS with the molecular ion of at 405 m/z and 428 m/z which corresponds to $[\text{M}]^+$ and $[\text{M}+\text{Na}]^+$, respectively (Figure A1.10). Finally, the O-H stretching vibration was observed via FTIR at 3124 cm^{-1} , corroborating the deprotection of the tert-butyl group.

3.3. Synthesis and Characterization of NH_2 -PEG-FA, NH_2 -PEG-MeO

Polyethylene glycol (PEG) has been widely used to improve the circulation time of drug delivery systems in *in vivo* settings by preventing the interaction of opsonin proteins with nanoparticles.⁸¹

The synthesis of NH_2 -PEG-FA was carried out through a three-step synthetic pathway. In the first step, the PEG (2K) was activated and reacted with sodium azide to obtain the corresponding diazido-PEG. The successful synthesis of this polymer was confirmed by FTIR with the stretching vibration of the azide at 2100 cm^{-1} (Figure A3.3). The product was also analyzed by ^1H NMR, showing the shift of the hydrogens close to the azide group to 3.35 ppm and the hydrogens from the polymer at 3.7 ppm (Figure A3.1). The ^{13}C NMR spectrum confirmed the carbon chemical shift next to the azide to be 37.6 ppm as opposed to the carbons corresponding to the main chain of the polymer at 70.4 ppm (Figure A3.2). The next step for the synthesis of NH_2 -PEG-FA involved a Staudinger reaction to convert the azide to amine groups through the addition of triphenylphosphine.⁷⁴ Diamino-PEG was obtained by this reaction and confirmed using

FTIR, which showed the disappearance of the stretching vibration for the azide group (Figure A3.6). ^1H NMR and ^{13}C NMR also confirmed the successful synthesis of diamino-PEG. The ^1H NMR spectrum afforded the chemical shift of the hydrogens closest to the amine to 3.1 ppm (Figure A3.4). The carbons closest to the amine were shifted to 36.4 ppm, as confirmed by ^{13}C NMR (Figure A3.5). The next synthetic step was the preparation of NHS-FA; however, this step was not characterized and the crude product was used for the next step. Finally, one end of the diamino-PEG molecule was modified, forming a folic acid derivative. Dialysis in nanopure water was run on the crude product and monitored using ^1H NMR, comparing the ratio of folic acid integration to the PEG repeating unit integration, to verify the purity of the mono-substituted polymer. ^1H NMR shifts also confirmed the presence of folic acid in addition to the PEG peaks (Figure A3.7). The ^1H NMR afforded shifts corresponding to the folic acid moiety in the phenyl region. ^{13}C NMR also verified the addition of phenyl groups, which further confirmed the product. This was confirmed through FTIR with C=C stretching appearing at 1607 cm^{-1} (Figure A3.9).

Similar to $\text{NH}_2\text{-PEG-FA}$, the synthesis of $\text{NH}_2\text{-PEG-MeO}$ was carried out through a two-step synthetic pathway involving the synthesis of the azide-PEG-MeO derivative followed by the Staudinger reaction. The azide-PEG-MeO polymer was confirmed through FTIR (Figure A3.12) with the appearance of stretching vibration of the azide group at 2135 cm^{-1} . The polymer was further confirmed through ^1H NMR and ^{13}C NMR (Figures A3.10 and A3.11, respectively) with the hydrogen shift on the most terminal carbon nearest to the azide group at 3.1 ppm and a carbon shift at 57.9 ppm. The successful synthesis of $\text{NH}_2\text{-PEG-MeO}$ was confirmed using FTIR (Figure A3.15)

through the disappearance of the azide group and the N-H stretching vibration at 3411 cm^{-1} . $\text{NH}_2\text{-PEG-MeO}$ was also verified by ^1H NMR and ^{13}C NMR (Figures A3.13 and A3.14, respectively) with the chemical shift of the hydrogens on the carbon adjacent to the amine group at 3.1 ppm and a carbon shift at 57.8 ppm.

3.4 Characterization of MSN Materials

MSNs are used as drug delivery systems due to the numerous structural and physicochemical advantages that they offer to improve the delivery of drugs to cancer tissues.³⁹ Both hydrophobic and hydrophilic drugs can be loaded, either through a chemical bond or by diffusion. MSNs can also be easily functionalized to improve their blood circulation time inside of the body or to attach imaging, therapeutic, and/or targeting agents.^{46,51}

3.4.1 Synthesis and Characterization of AP-MSNs

In this work, the synthesis of AP-MSNs was carried out by a surfactant templated approach where TEOS and APTES were used as silane precursors. The nanoparticles were washed twice with an acidic solution in methanol to remove the CTAB surfactant. The structural characterization of AP-MSNs was carried out by nitrogen sorption isotherms and analyzed through the BET and BJH methods. BET and BJH were used to calculate surface area, pore volume, and pore diameter of the MSNs. The nanoparticles were also characterized by using DLS and ζ -potential to determine the hydrodynamic diameter and surface charge, respectively.

The size of AP-MSNs were 155 ± 33 nm in diameter as determined by SEM ($n=20$). The organic content of the AP-MSNs was confirmed by TGA; there was little to no CTAB remaining, yet the aminopropyl groups were present (Figure A2.5). ζ -potential

analysis showed the presence of amine groups in the surface of MSNs based on the value of the surface charge, $+27.9 \pm 4.9$ mV. DLS measurements revealed a hydrodynamic diameter of 318 nm in water, which can be attributed to the agglomeration of particles in the solvent (Figure A2.4). The nitrogen sorption isotherms demonstrated a surface area of $1030 \text{ m}^2/\text{g}$ and a pore volume of $1.65 \text{ cm}^3/\text{g}$ which corroborates the removal of CTAB from the channels of MSNs (Figure A2.2).

3.4.2 Synthesis and Characterization of cisPt-MSNs

The cisplatin prodrug was loaded onto the MSNs using conjugation chemistry mediated by EDC as a coupling agent. This reaction involves the activation of the carboxylic acid groups to react with the free amine groups present on the surface of the MSN material. The successful fabrication of cisPt-MSNs was confirmed through DLS, change in ζ -potential, as well as the decrease in surface area and pore volume. The hydrodynamic diameter of the cisPt-MSNs in water was measured to be 1980 nm. Furthermore, with the addition of the cisplatin prodrug, the ζ -potential of the nanoparticle decreased from $+27.9 \pm 4.9$ mV to $+6.9 \pm 4.3$ mV. This can be attributed to the decrease of amine groups and the increase of carboxylate groups from the cisPt prodrug. BET analysis of the surface area decreased from $1030 \text{ m}^2/\text{g}$ to $680 \text{ m}^2/\text{g}$ and the pore volume decreased from $1.65 \text{ cm}^3/\text{g}$ to $1.15 \text{ cm}^3/\text{g}$. In addition, an increase in organic content was observed from 4.6% to 10.4%. With the inclusion of inorganic platinum, loading of cisplatin to the MSN as determined by TGA was calculated at 9.1 wt%. Atomic absorption spectroscopy (AAS) was also used to determine cisplatin loading through the analysis of the supernatants collected after washing the reaction mixture. AAS

determined the amount of cisplatin loading to the MSN was 9.6 wt%. For comparison of further tests and materials the AAS value was used in this study.

3.4.3 Synthesis and Characterization of RRL-MSNs

In a similar way to the cisplatin prodrug, RRL4 was also chemically attached to the surface of MSNs using conjugation chemistry mediated by EDC as a coupling agent. The loading of RRL4 to the AP-MSNs was determined by TGA; an increase from 4.6% to 11.0% organic content was observed as an indication of the presence of RRL4. The ζ -potential of the MSNs slightly decreased from $+27.9 \pm 4.9$ mV to $+23.6 \pm 4.7$ mV. Furthermore, a decrease in the surface area from $1030 \text{ m}^2/\text{g}$ to $870 \text{ m}^2/\text{g}$ also suggested that RRL4 was indeed attached to the surface of the MSN material.

3.4.4 Synthesis and Characterization of Gem-MSNs

The gemcitabine prodrug was loaded using a thiol-disulfide displacement reaction to remove the thiol activating group, pyridyl disulfide, on the RRL4 molecule. The successful fabrication of Gem-MSNs was confirmed through TGA analysis of organic content, the change in the surface area, and the pore volume. The organic content increased from 11.0% to 22.6%, confirming the addition of gemcitabine prodrug. The decrease in surface area from $870 \text{ m}^2/\text{g}$ to $580 \text{ m}^2/\text{g}$ also corroborates the presence of the gemcitabine prodrug on the surface of the MSN. Lastly, the pore volume, as determined by BJH analysis, decreased from $1.52 \text{ cm}^3/\text{g}$ to $1.25 \text{ cm}^3/\text{g}$. UV-Vis spectroscopy analysis was used to determine gemcitabine loading to the nanoparticle using a wavelength of 270 nm. The loading of gemcitabine to the Gem-MSNs was 17.9 wt%. However, to maintain a control with regard to the synergistic ratio (as explained in Chapter 3.6 below), a batch containing 4.6 wt% gemcitabine was used.

3.4.5 Synthesis and Characterization of cisPt-Gem-MSNs

For the ratiometric loading of the combination of drugs, it was determined that gemcitabine would be loaded in lower quantity than cisplatin due to synergy determination (Chapter 3.6). This was decided for two reasons. The first reason is that gemcitabine is more potent than cisplatin based on the LD₅₀ data collected in Chapter 3.5, therefore, less of it is needed to achieve the same therapeutic effect. Secondly, loading cisplatin first ensures that some of the amine groups are reacted and no longer active, providing a lower rate of gemcitabine loading, to help ensure the desired ratio. For this reasoning, the synthesis began with the cisPt-MSNs described in Chapter 3.4.2. CisPt-MSNs were chemically modified with RRL4 using conjugation chemistry. After the cisPt-MSN material had been functionalized with RRL4, the gemcitabine prodrug was attached to the nanoparticles through the thiol-disulfide exchange reaction. The fabrication of this material was confirmed by an increase in organic content from 10.4% to 13.3%, as determined by TGA analysis. In addition, the surface area of the material decreased from 680 m²/g to 560 m²/g and the pore volume decreased from 1.15 cm³/g to 0.71 cm³/g, which also corroborate the presence of the prodrug. The amount of gemcitabine loaded onto the nanoparticle was determined to be 3.9 wt% as determined by UV-Vis spectroscopy at a wavelength of 270 nm. The chemically attached gemcitabine was loaded in a molar ratio of 71% cisplatin to 29% gemcitabine, which was close to the desired synergistic ratio determined in Chapter 3.6 below.

3.4.6 Synthesis and Characterization of cisPt-GemPas-MSN

As a control experiment, cisPt-MSNs were also modified with free gemcitabine drug through a passive loading approach.

Table 2: Structural properties of MSN materials fabricated in this work. Cisplatin loading =9.6 wt%. Gemcitabine loading = 5.5 wt% (Individual), 3.9 wt% (Combination).

Type	Average Diameter (H ₂ O, nm)	Average Diameter (PBS, nm)	Zeta Potential (PBS, mV)	Organic Content	Surface Area (m ² /g)	Pore Diameter (nm)	Pore Volume (cm ³ /g)
AP-MSN	318	1542	+27.9 ± 4.9	4.6%	1030	4.3	1.65
RRL-MSN	351	908	+23.6 ± 4.7	11.0%	870	4.3	1.52
Gem-MSN	340	903	+24.7 ± 4.0	22.6%	580	4.3	1.25
CisPt-MSN	1980	1020	+6.9 ± 4.3	10.4%	680	4.3	1.15
CisPt-RRL-MSN	235	2150	+4.5 ± 4.3	10.1%	805	4.3	1.28
CisPt-Gem-MSN	175	2016	+0.8 ± 3.9	13.3%	560	4.9	0.71

The loading of gemcitabine to the nanoparticle through passive loading was 5.5 wt% as determined by UV-Vis spectroscopy at a wavelength of 270 nm. The molar ratio for the control sample is 63% cisplatin to 37% gemcitabine.

3.5 Determination of LD₅₀ of cisplatin and Gemcitabine Grugs in Human Cervical Cancer (HeLa) and Pancreatic Cancer (AsPC1 and BxPC-3) Cell Lines

Cisplatin, an alkylating agent, and gemcitabine, a nucleoside analog, both target the DNA of the cancer cell to prevent further growth and replication.⁸² Cisplatin cross

links DNA for inhibition of cell growth and replication. Gemcitabine inhibits RNR as well as mimics deoxycytidine which also inhibits growth and replication. Both drugs are approved by the FDA for multiple cancers and are used widely in clinics.

To determine the LD₅₀, or lethal dosage to achieve 50% cell viability, for cisplatin and gemcitabine *in vitro* a viability assay using Promega Cell Titer™ was performed. Cell Titer is a solution composed of 3-(4,5-dimethylthiazol-2-yl)-5-(3-carboxymethoxyphenyl)-2-(4-sulfophenyl)-2H-tetrazolium (MTS). MTS is bio-reduced by viable cells to produce a formazan product with an absorbance at 490 nm.⁷⁵ The viability of the cells in an experiment can then be determined by comparison to a control. The range at which the cisplatin free drug was tested changed between 1 and 100 μM. The LD₅₀ of cisplatin was around 7 μM in HeLa cells, 6.3 μM in AsPC1 cells, and 4 μM in BxPC-3 cells, which can be seen in Figure 7. Gemcitabine was reported to have an LD₅₀ lower than cisplatin using a similar protocol; therefore, the concentrations 5 nM to 10 μM were chosen.²⁴ The LD₅₀ of gemcitabine was determined to be around 35 nM in HeLa cells, 45 nM in AsPC1 cells, and 1 μM in BxPC-3 cells, as seen in Figure 8. Gemcitabine never reached 100% cytotoxicity, but rather plateaued between 20% and 40% cell viability. This was also seen in the literature, particularly in Hodge's research.²² This may be caused by either rapid inactivation or through nucleoside transporters evacuating the cell due to large concentrations; however, the reason is still unknown.

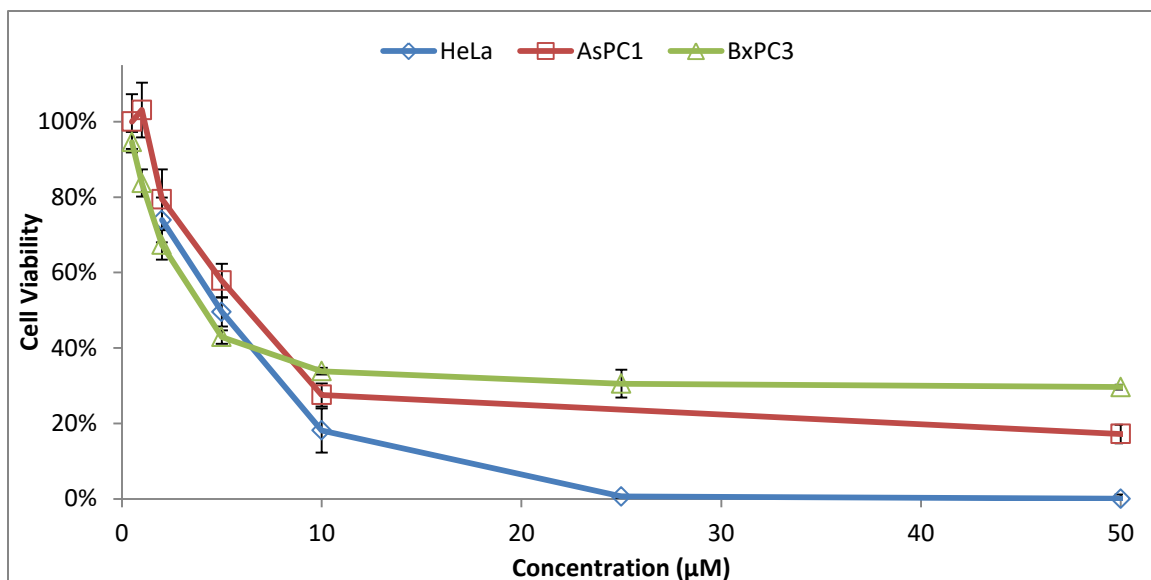


Figure 7: LD₅₀ of Cisplatin in HeLa, AsPC1, and BxPC-3 cancer cells.

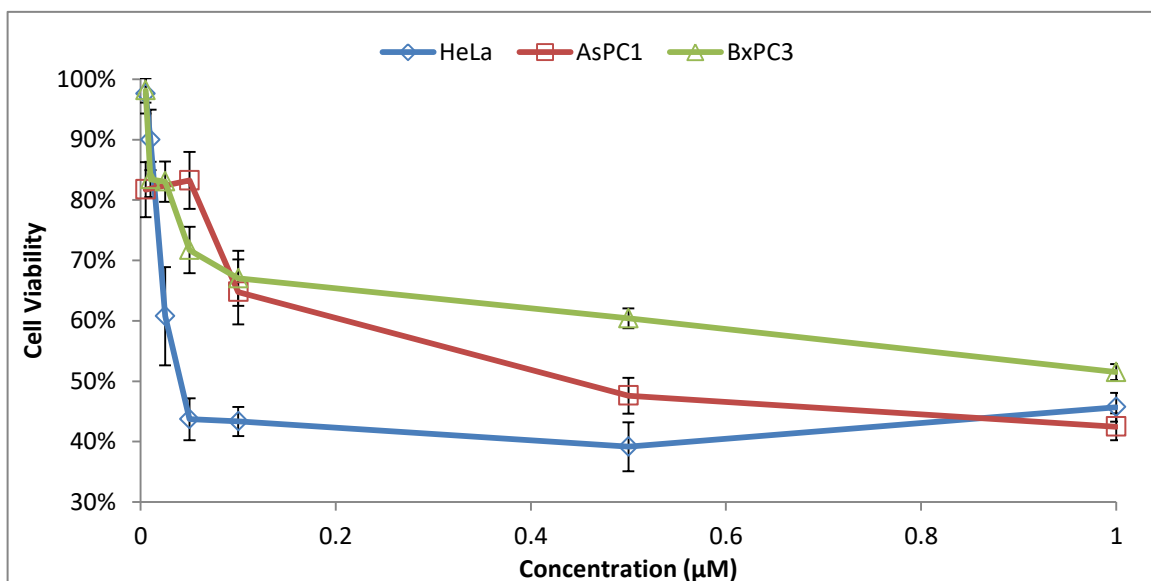


Figure 8: LD₅₀ of Gemcitabine in HeLa, AsPC1, and BxPC-3 cancer cells.

3.6 Therapeutic Combination and Synergy Determination of Cisplatin and Gemcitabine in the HeLa Cell Line

Therapeutic combination is the use of multiple drugs toward the treatment of a disease. The drugs used in this type of treatment can be synergistic in nature. For two or more drugs to be synergistic, they need to function better as a group than the expectation

for the combination treatment. This can be determined by calculating the CI value (Equation 1). If the CI value is less than one, then the drugs are synergistic.

For determination of drug synergy, gemcitabine and cisplatin were combined in solution in the following molar ratios, respectively: 50:50, 25:75, 10:90, 5:95, and 1:99 and the LD₅₀ for each ratio in HeLa cells was determined. The results of these studies were analyzed using the CompuSyn software to assist in the calculation of the CI for synergy determination.⁷⁶ CompuSyn is a tool used to process data from any number of ratios and calculate the CI value at any given point providing ample information to determine synergy. The CI at 50% cell viability can be seen for each ratio in Table 3. Using these values for CI, it can be concluded that all ratios which were tested in this study show synergy.

Table 3: Combination Index of free drugs at 50% cell viability (in ascending order of CI).

Cisplatin (mol%)	Gemcitabine (mol%)	LD ₅₀ (μM, comb.)	CI @ LD ₅₀
99	1	2.3	0.236
75	25	0.6	0.306
90	10	0.3	0.404
95	5	2.0	0.509
50	50	0.1	0.614

3.7 Selection of Loading Ratio of Cisplatin and Gemcitabine to MSN Materials

While the ratio including only 1 mol% gemcitabine demonstrated the strongest synergy, loading such a small amount to the MSNs would be difficult to reproduce and characterize. Therefore, it was determined that the MSN loading would be done with the

next highest synergistic ratio, and so the ratio including 25 mol% gemcitabine was selected.

3.8 Drug Release Profile

A preliminary release profile was performed in water at room temperature. This release profile showed that with the addition of 10 mM GSH as a reducing agent, the drugs were cleaved from the MSN and released into the system.

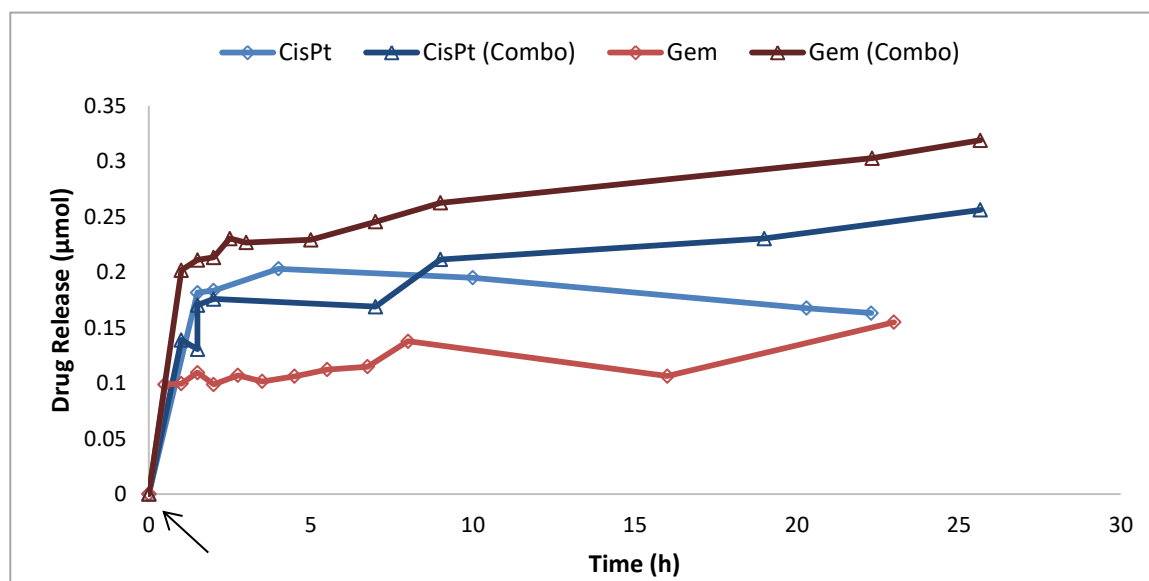


Figure 9: Release Profile of MSN materials in water (GSH added time = 0 h).

The release profiles were run using phosphate buffer solution at two different pHs: 7.4 and 5.0. The first pH mimics physiological conditions and the more acidic pH resembles the environment in late endosomes and lysosomes. Moreover, experiments were also run in the presence or absence of a reducing agent (GSH = 10 mM) to simulate the high reducing environment in the cytosol of cancer cells. Figure 10 shows the results of the release profile of cisplatin from CisPt-MSNs under these conditions. It is clear that in the absence of a reducing agent, there is not a significant release of cisplatin. In this case, pH 5.0 was not evaluated because, as in the case of pH 7.4, no release is expected if

there is not GSH present in the solution. On the contrary, in the presence of GSH, a fast release is observed with a half-time of around 5 h and reaching a plateau about 15 h for both neutral and acidic pH. The amount released after 50 h was almost 18% of the amount loaded, which corresponds to 0.2 μmol of cisplatin per mg of MSNs.

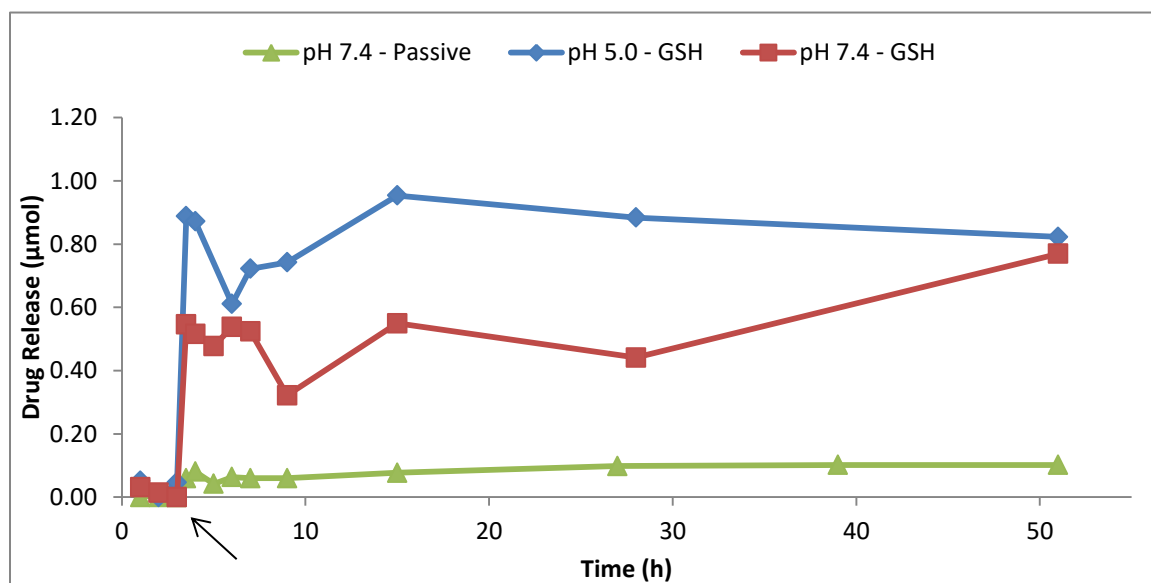


Figure 10: Release Profile of cisplatin from CisPt-MSN (GSH added, time = 3 h).

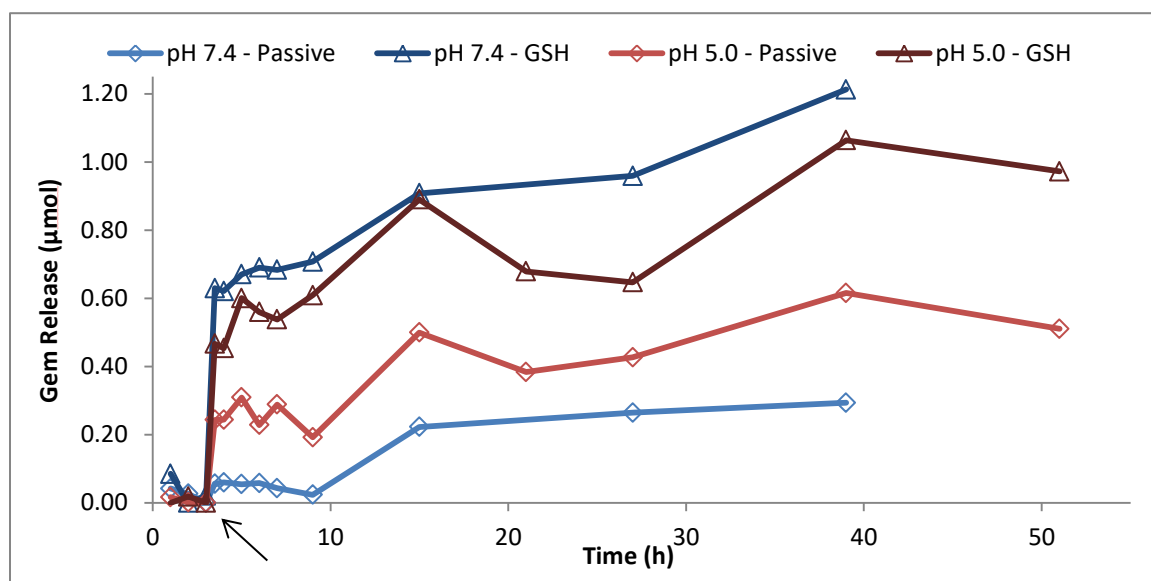


Figure 11: Release Profile of gemcitabine from Gem-MSN (GSH added, time = 3 h).

The release of gemcitabine from Gem-MSNs was also tested under the above mentioned conditions. For this platform, two mechanisms can account for the release of

gemcitabine. The first one is pH-mediated due to the presence of the amide bond. The second mechanism is redox-responsive due to the presence of the disulfide bond in the linker. The release profile in the absence of GSH showed that there is a dependence on the release of gemcitabine due to the pH. Acidic conditions showed higher release than neutral conditions. In this case, the hydrolysis of the amide bond is acid-catalyzed affording higher release of the drug. The half-time for pH 5.0 is 2 h and reached a plateau 12 h after the addition of GSH. In this case only 15% of the amount loaded of gemcitabine was released.

Interestingly, the release of gemcitabine in the presence of GSH showed a fast release, typical of the redox-responsive systems, where the difference in pH did not significantly affect the release kinetics. In this case, the half-time is less than 1 h and the maximum amount released of gemcitabine was 35% of the amount loaded, which corresponds to 0.24 μmol of cisplatin per mg of MSNs.

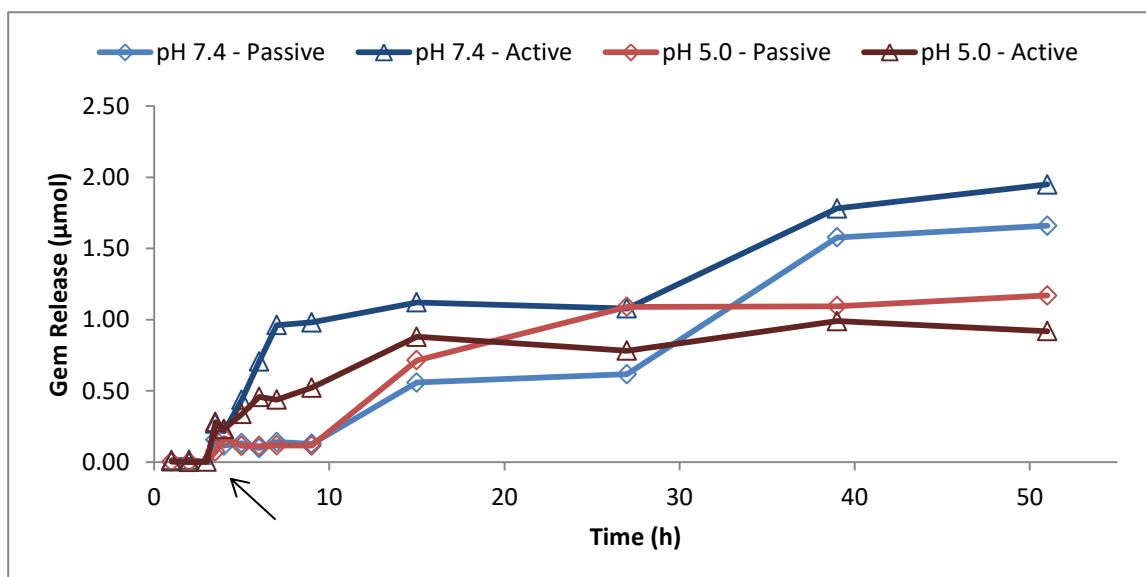


Figure 12: Release Profile of Gem from cisPt-Gem-MSN (GSH added, time = 3 h).

A similar trend can be seen in the gemcitabine release of the combination MSN as compared to the individually loaded nanoparticles.

3.9 *In Vitro* Cytotoxicity of MSN-Based Combination Therapy

The drug-loaded MSNs were tested *in vitro* across three different cell lines to determine efficacy of treatment and cytotoxicity of the materials. The drug-loaded MSNs were added so that either the amount of gemcitabine or the amount of cisplatin was normalized across all samples. This allowed for a fair comparison across all samples. The results of the cytotoxicity of MSN materials in HeLa cells are shown in Figures 13 and 14.

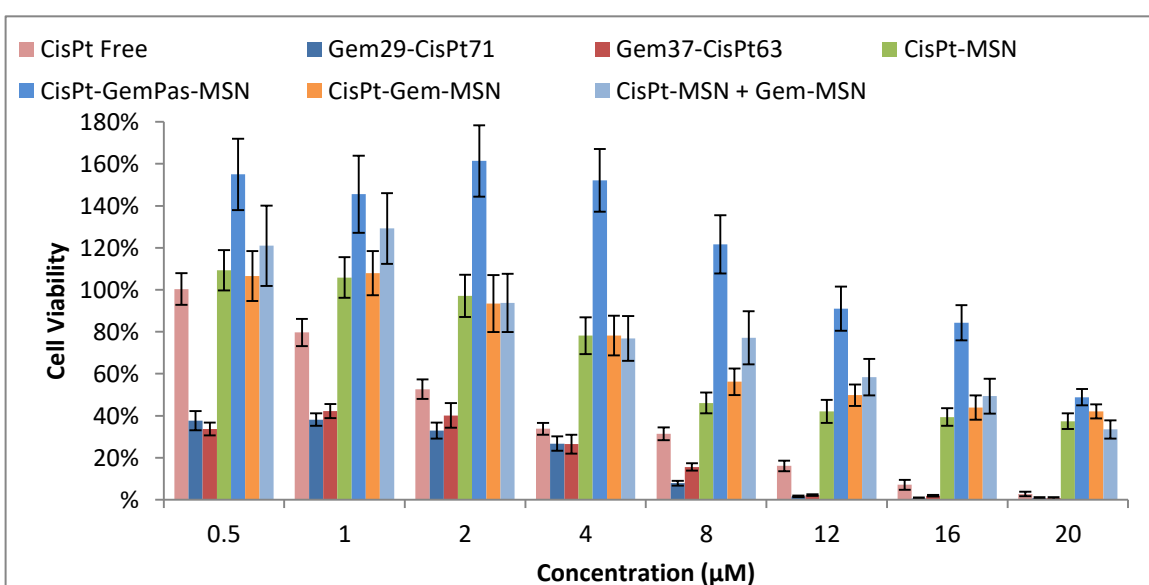


Figure 13: Cisplatin normalized cytotoxicity assay of MSN materials in HeLa cells.

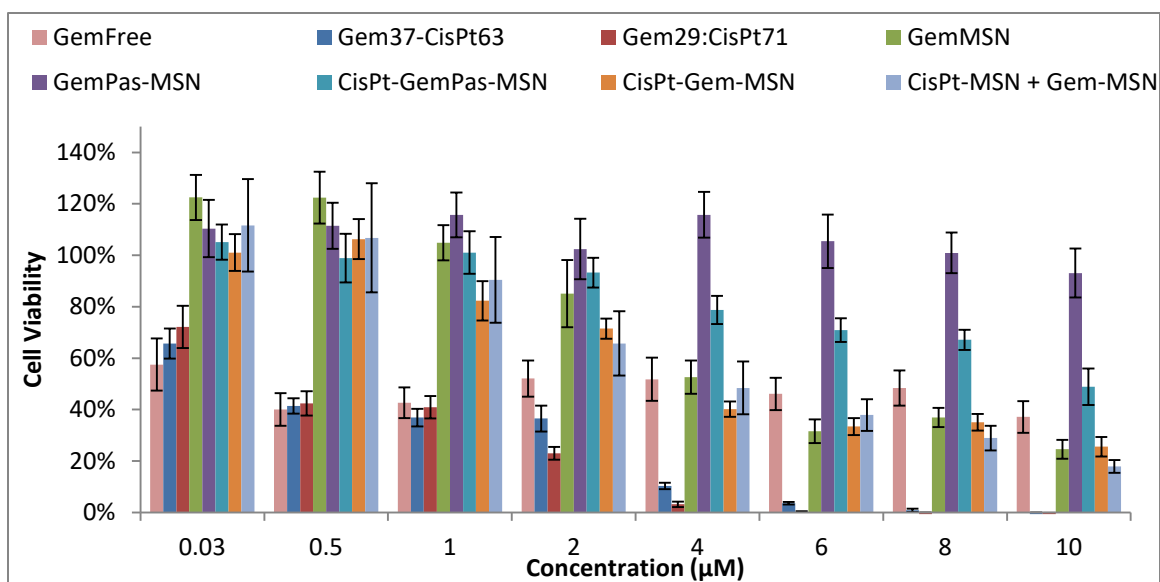


Figure 14: Gemcitabine normalized cytotoxicity assay of MSN materials in HeLa cells.

From the cytotoxicity data, it can be seen that in all cases, the combination of free drug was more effective than the individual drug, in particular, regarding to the ability of the gemcitabine to achieve 100% cell death. Different to the plateau that forms with the free drug alone. For both cases it is also apparent that the individually loaded MSN, mixture of individually loaded MSNs, and the combination (chemically loaded) MSN achieved the highest toxicity of the MSN materials. The passively loaded MSNs did not achieve as high toxicity as their chemically loaded counterparts. While, the MSN materials did not outperform the free drugs in cytotoxicity, the data still provides a trend.

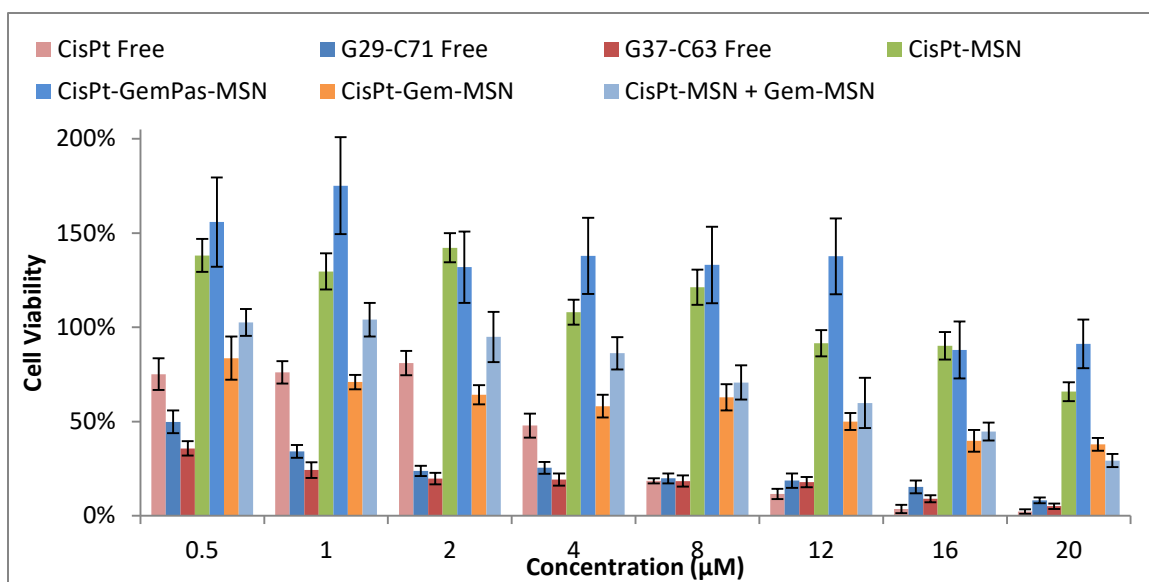


Figure 15: Cisplatin normalized cytotoxicity assay of MSN materials in AsPC1 cells.

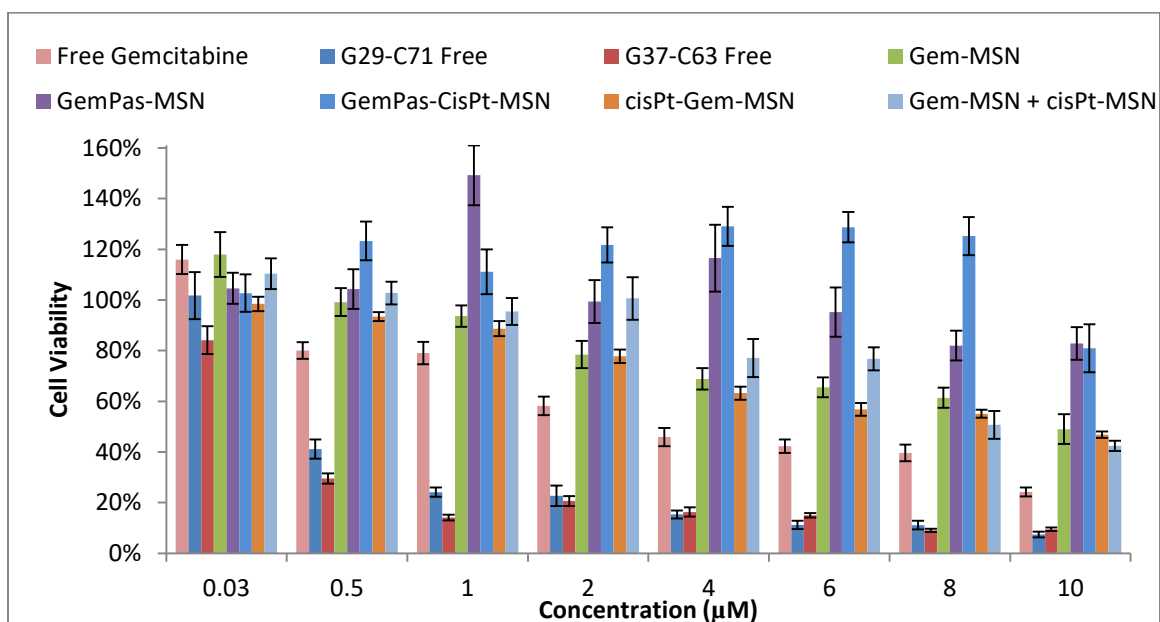


Figure 16: Gemcitabine normalized cytotoxicity assay of MSN materials in AsPC1 cells.

For the AsPC1 cells the combination of free drug was more effective than the individual drug. Again, the free drug outperformed the nanoparticle at every concentration. However, the mixture of individually loaded MSNs achieved a higher cytotoxicity than both of these MSNs. Once again, the passively loaded materials did not show high levels of cytotoxicity.

The effect of the drug loaded MSNs on AsPC-1 cells did not seem to demonstrate the same level of efficacy of treatment. For the cisplatin normalized trials, the combination MSN as well as the mixture of individually loaded MSNs showed similar results to the HeLa cells. However, for the remaining samples as well as the gemcitabine normalized samples, the efficacy was far less. It may also be that pancreatic cancer does not simply uptake as many nanoparticles or perhaps, the cellular uptake is slower or more stringent than HeLa cells. To confirm this, the BxPC-3 cell line was tested.

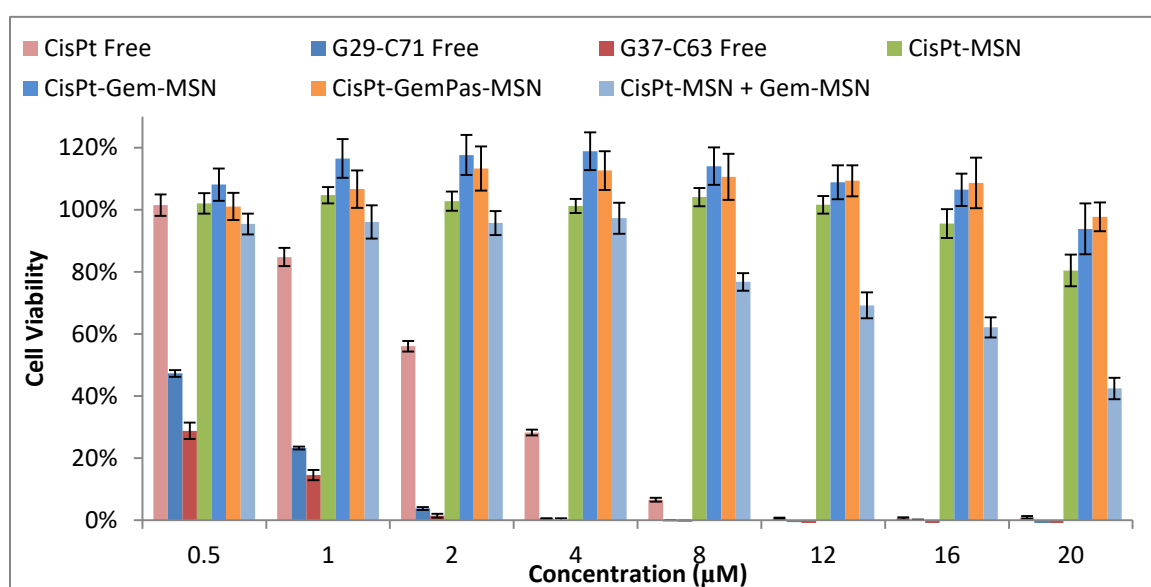


Figure 17: Cisplatin normalized cytotoxicity assay of MSN materials in BxPC-3 cells.

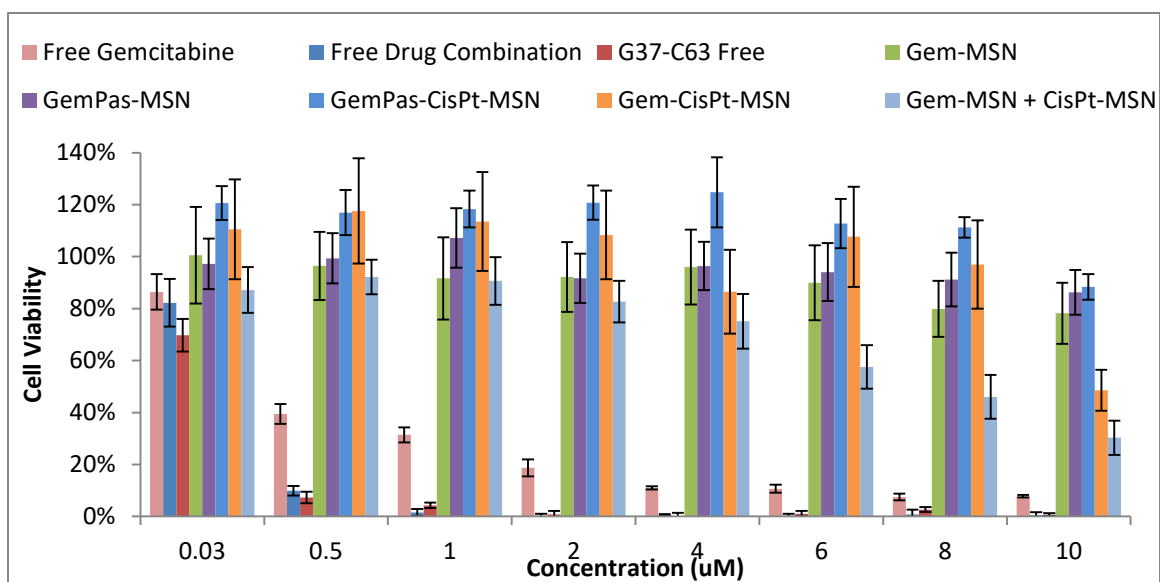


Figure 18: Gemcitabine normalized cytotoxicity assay of MSN materials in BxPC-3 cells.

In this instance, the free drug and the combination of free drug performed very well. However, with the exception of the individually loaded mixture of MSNs, the MSN materials did not demonstrate much cytotoxicity at all. At higher concentrations in the gemcitabine normalized trial, the combination MSN started to show some cytotoxicity. Compared to the free drug, the MSNs are using roughly 10 times the concentration of drug to achieve the same effect.

The BxPC-3 cell line demonstrated less efficiency than the previous cell line. The cisplatin normalized assay showed relatively no toxicity except for the physical mixture of individually loaded nanoparticles. The gemcitabine normalized model showed higher toxicity, with the physical mixture yet again outperforming the dual-drug loaded MSN.

In each of the three tested cell lines, the MSN materials never outperformed the free drug. We hypothesize that this is occurring because of the release mechanism of the MSN. In the release profiles explained earlier, it was observed that of the drug loaded onto the nanoparticle, at no point was all of it released. Release of the drugs occurred between 30 and 50% the maximum, or the initial amount loaded. While it is certain that

we are delivering the free drug at the desired concentration, it is still relatively uncertain at what concentration the drugs loaded onto the MSN are being delivered at. Perhaps the MSNs are getting trapped in the lysosome and/or expelled from the cell before they can deliver their payload.⁷⁷

3.10 Targeting Moiety of FA-Functionalized MSNs

Cancer cells overexpress specific biomarkers that can be used to target them. Folate receptors have been shown to be overexpressed on many cancer cell lines, including HeLa cells.⁷⁸ In this part of the project we decorated the surface of the MSNs with FA-PEG to target HeLa cells and increase the internalization of nanoparticles.

3.11 Flow Cytometry of FA-Functionalized Drug-Loaded MSNs

HeLa cells were incubated for 4 hours in the presence of PEG and FA-functionalized drug-loaded MSNs. Flow cytometry was used to determine the amount of nanoparticles internalized by HeLa cells. The samples were washed several times to ensure that any nanoparticles on the surface of the cell was washed off, leaving only internalized nanoparticles. The data collected shows that FA-functionalized MSNs (57.3% uptake) were taken up more readily than the MeO-PEG MSN (1.3% uptake) control. This data confirms that the folic acid targeting moiety can increase the amount of material taken up by cells overexpressing folate receptors.

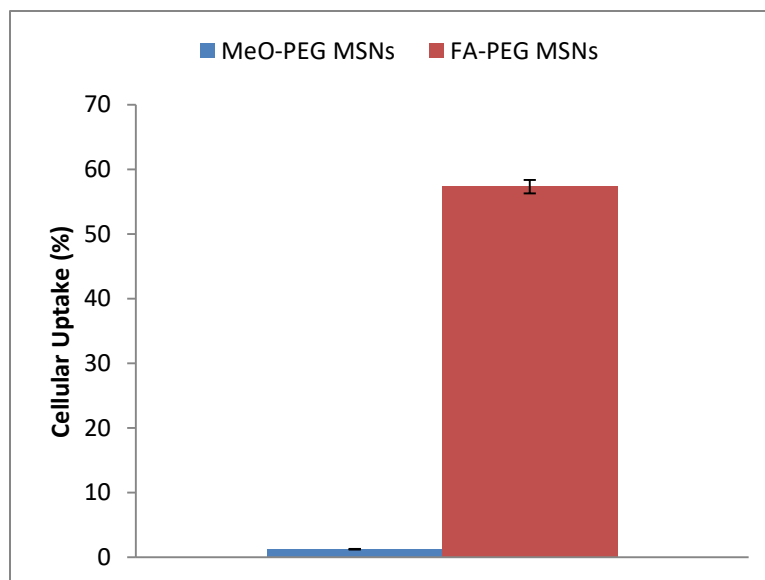


Figure 19: Flow cytometry of FA-PEG drug-loaded MSNs in HeLa cells.

3.12 Confocal Microscopy

Confocal microscopy was used to corroborate the targeting abilities of FA-PEG MSNs. HeLa cells were incubated for 4 h using three different concentrations (50, 20, and 10 $\mu\text{g/mL}$). After that, the microscope slides were prepared for confocal imaging. The results confirmed the higher uptake of FA-PEG MSNs by HeLa cells as was determined by flow cytometry.

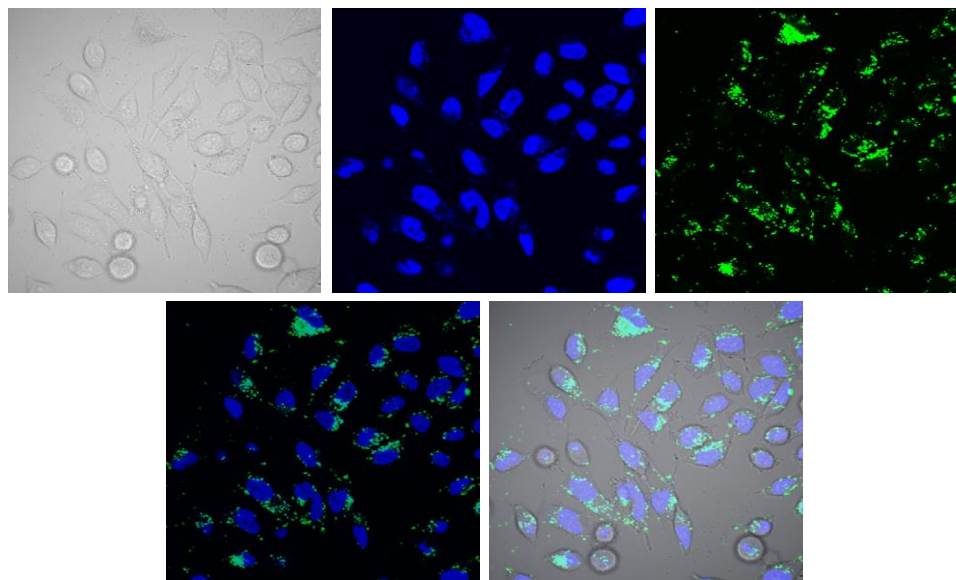


Figure 20: Confocal microscopy of HeLa cells inoculated with 50 $\mu\text{g}/\text{mL}$ FA-PEG-FITC-cisPt-Gem-MSNs. From left to right (top) DIC HeLa cells, DAPI nucleus stain, FITC fluorescence, (bottom) overlay of DAPI and FITC channels, and overlay of DIC, DAPI, and FITC channels.

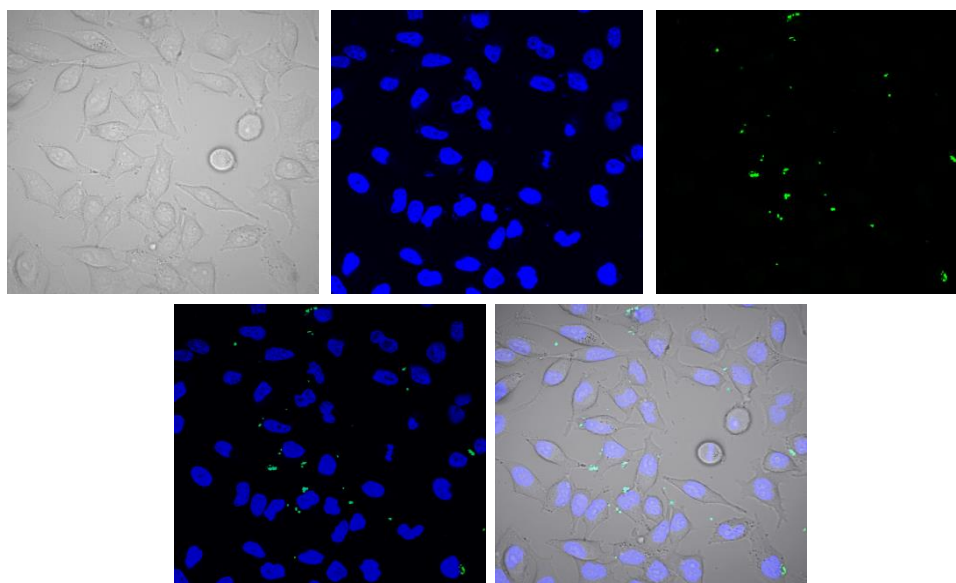


Figure 21: Confocal microscopy of HeLa cells inoculated with 50 $\mu\text{g}/\text{mL}$ MeO-PEG-FITC-cisPt-Gem-MSNs. From left to right (top) DIC HeLa cells, DAPI nucleus stain, FITC fluorescence, (bottom) overlay of DAPI and FITC channels, and overlay of DIC, DAPI, and FITC channels.

3.13 Cytotoxicity of FA-PEG-MSN materials

The cytotoxicity of FA-PEG-MSNs and MeO-PEG-MSNs was carried out in HeLa cells. The MeO-PEG-MSNs showed no significant decrease in the viability of the HeLa cells neither for the cisplatin nor the gemcitabine normalized experiments. On the contrary, FA-PEG-MSNs reduced the cell viability dramatically. In the case of the cisplatin normalized experiment the reduction was about 60%, but still lower than the cisplatin drug by itself. However, the gemcitabine normalized data showed that the FA-PEG-MSNs have a higher cytotoxicity than the parent drug.

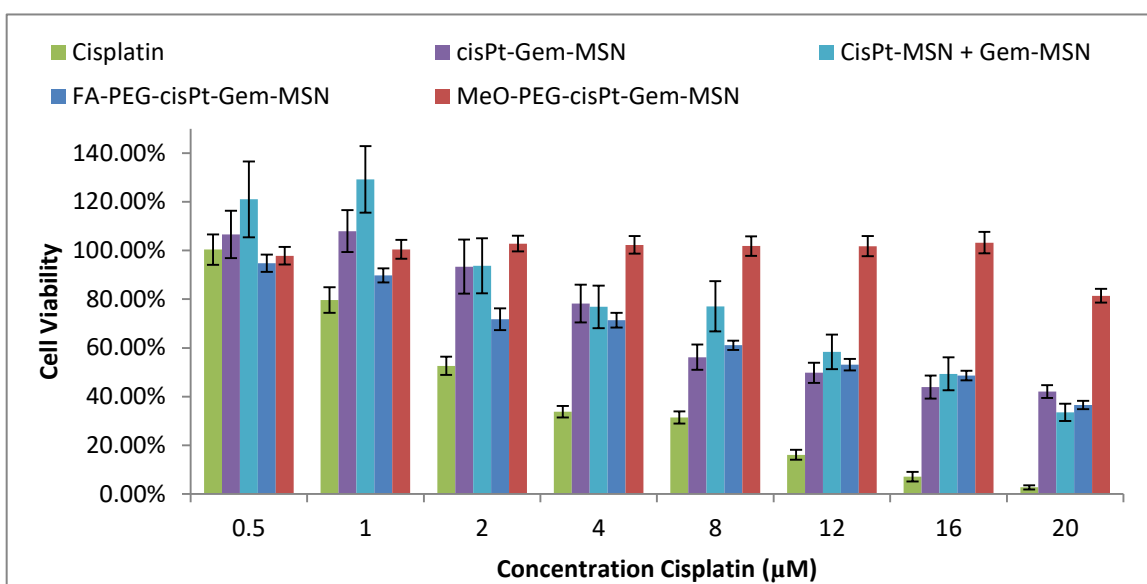


Figure 22: Gemcitabine normalized cytotoxicity assay of MSN materials in HeLa cells.

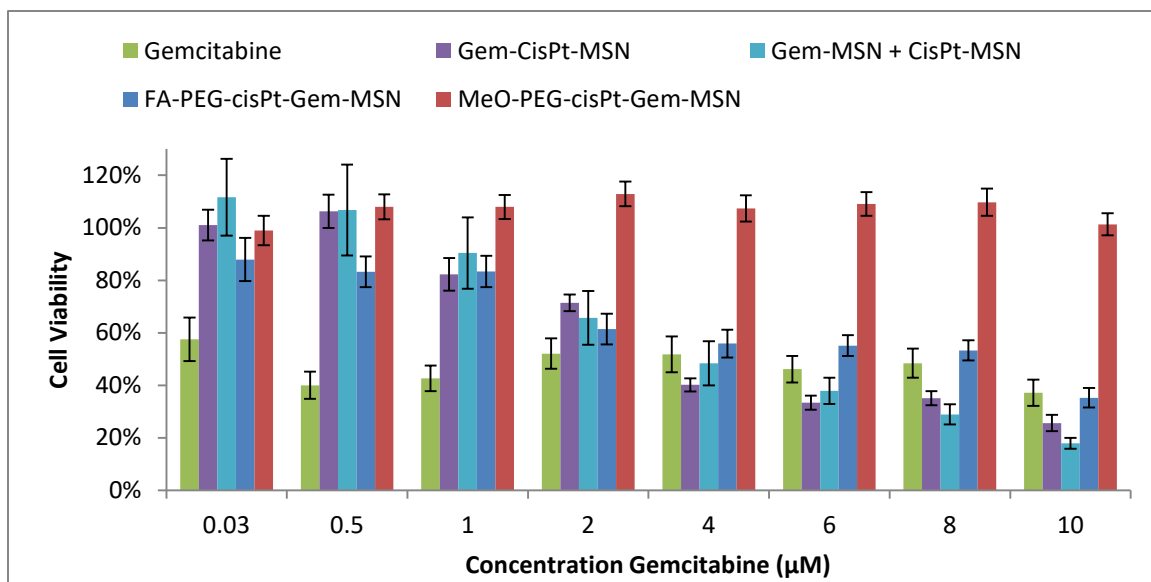


Figure 23: Cisplatin normalized cytotoxicity assay of MSN materials in HeLa cells.

CHAPTER 4: CONCLUSIONS AND FUTURE WORK

With the translation of a number of drug delivery platforms to the clinic, the need for smarter, more precise and controlled drug release is critical. The limitations of current drug delivery systems show that the drug molecule is susceptible to diffuse out from the nanocarrier as soon as is encapsulated. To enhance the therapeutic potential of toxic chemotherapies, it is critical to be able to transport the drug and release it only at the site of disease in a spatiotemporal fashion. Therefore, the development of target-specific, stimuli-responsive drug delivery systems are important to further improve drug performance, patient compliance and therapeutic efficacy.⁸⁰ In this work, we developed a target-specific, stimuli-responsive drug delivery system based on mesoporous silica nanoparticles. The MSN-based platform carries two FDA approved anticancer drugs, cisplatin and gemcitabine, chemically attached to the nanomaterial through stimuli-responsive linkers. In addition, the MSN nanocarrier was further functionalized with polyethylene glycol and folic acid molecules to enhance its targeting ability. The overall goal of this thesis was to design, synthesize, characterize the target-specific stimuli-responsive MSN drug delivery system and evaluate its performance *in vitro*. To reach the main goal of the project, five specific goals were pursued: **1)** Synthesis and characterization of the stimuli-responsive linker, gemcitabine and cisplatin prodrugs; **2)** Synthesis and characterization of MSN materials; **3)** Evaluate the *in vitro* synergy for different ratios of cisplatin and gemcitabine drugs; **4)** Test the *in vitro* cytotoxicity of

MSN materials; and **5)** Determine the targeting ability and therapeutic effect of the folic acid functionalized MSN platform.

The synthesis of gemcitabine and cisplatin prodrugs was carried out through multistep approaches (Schemes 2 and 3). The products obtained in each step of the protocol were characterized by different analytical techniques including FTIR, ^1H and ^{13}C NMR, and ESI-MS. The successful synthesis of the prodrugs was confirmed by the analytical results and further corroborated by data previously reported in the literature.^{16,71} In this work, a novel stimuli-responsive linker (RRL) was used to chemically attached gemcitabine prodrug to the surface of MSNs. This RRL linker can be cleaved by low pH and high reducing environment to release the parent drug, gemcitabine. RRL was also synthesized by a multistep synthetic approach (Scheme 1). The successful synthesis of the RRL was confirmed by a wide variety of analytical techniques including FTIR, ^1H and ^{13}C NMR spectroscopies, and ESI-MS.

Mesoporous silica nanoparticles were used as the drug delivery system in this project. MSN materials were synthesized using the surfactant-templated co-condensation approach. Post-functionalization techniques were used to further modify the surface of MSNs with prodrugs, RRL, chromophores, PEG and/or folic acid to afford the desired MSN materials. The structural properties of these materials were fully characterized by DLS, ζ -potential, TGA, SEM and TEM. In general, these MSN materials showed a high surface area, with a large pore size and volume. High loadings of cisplatin (~9.0% wt.) and gemcitabine (~18.0% wt.) in MSNs were achieved according to AAS and UV-vis spectrometry, respectively. In addition, for the combined MSN platform, the amount of

cisplatin and gemcitabine drugs was tuned to 9.6:3.9% wt., which correspond to a molar ratio of 71:29.

The LD₅₀ of cisplatin and gemcitabine was determined using the MTS assay for different cancer cells, cervical (HeLa) and pancreatic (AsPC1 and BxPC3). Gemcitabine showed a much higher cytotoxic effect than cisplatin under our experimental conditions. The difference is up to two orders of magnitude; the range of the LD₅₀ for gemcitabine and cisplatin is 35-45 nM and 6-7 μM, respectively in HeLa and AsPC1 cell lines. *In vitro* cytotoxicity experiments with HeLa cells showed that, by combining both drugs, synergy can be achieved based on the results obtained from the combination index parameter, which was calculated using CompuSyn software. Combination of cisplatin and gemcitabine in molar ratios of 99:1 or 75:25 showed the highest combination index.

The release profile in solution of cisplatin and gemcitabine demonstrated, in general, that the release of these drugs is mainly triggered by a highly reducing environment. After the addition of glutathione as reducing agent, a fast release was observed in the first hour accounting for almost 60% of the total amount released. The MSN platform can deliver almost 50% of the amount of drugs loaded after 40 hours. The delivery of these drugs can also be triggered by pH, but the total amount released is less than 50% of the one released under high reducing environment. The results from these release experiments demonstrate that the MSN platform is indeed redox-responsive.

The toxicity of the MSN materials was tested *in vitro* using cervical (HeLa) and pancreatic (AsPC1 and BxPC3) cancer cell lines. MSNs with a single drug loaded, drugs passively loaded, the combined and the physical mixture were evaluated in these cell lines. In general, the combined platform containing both drugs and the physical mixture

of MSNs with individual drugs performed better. However, none of the materials outperformed the efficacy of the individual drugs.

The MSN material was further modified with PEG and folic acid. The targeting ability of the system toward cells overexpressing folate receptor was demonstrated by both flow cytometry and confocal microscopy in HeLa cells. In addition, the cytotoxicity of FA-target MSN material is much higher than the control nanoparticle modified with PEG.

Future work of this project will focus on testing the intracellular release of drugs to determine the time of events and the influence of the incubation time in the performance of the combined MSN platform. Moreover, the application of this platform toward other cancer cell lines such as breast, lung and colon cancer will be explored.

REFERENCES

1. National Cancer Institute. cancer.gov/publications/dictionaries/. Accessed November 30, 2016.
2. American Cancer Society. cancer.org/cancer/cancercauses/. Accessed November 30, 2016.
3. Croce, Carlo. Molecular Origins of Cancer: Oncogenes and Cancer. *The New England Journal of Medicine*. **2008**. 358(5):502-511.
4. Dudley, A. Tumor Endothelial Cells. *Cold Spring Harbor Perspectives in Medicine*. **2012**. 2(3):a006536. doi: 10.1101/cshperspect.a006536
5. American Cancer Society. cancer.org/. Accessed June 2, 2016.
6. Rabello L.; Silva J.; Azevedo L.; Souza I.; Torres V.; Rosolem M.; et al. Clinical Outcomes and Microbiological Characteristics of Severe Pneumonia in Cancer Patients: A Prospective Cohort Study. *PLoS ONE*. **2015**. 10(3):e0120544.
7. Cancer Council Victoria. cancervic.org.au/. Accessed June 2, 2016.
8. American Cancer Society. cancer.gov/about-cancer/treatment/. Accessed October 1, 2016.
9. Rosenberg, B. Some Biological Effects of Platinum Compounds: New Agents for the Control of Tumours. *Platinum Metals Review*. **1971**. 15(2):42-51.
10. United States Food and Drug Association. accessdata.fda.gov/. Accessed June 4, 2016.
11. American Cancer Society. cancer.gov/about-cancer/treatment/drugs/. Accessed May 26, 2016.

12. Shen, D.; Pouliot, L.; Hall, M.; Gottesman, M. Cisplatin Resistance: A Cellular Self-Defense Mechanism Resulting from Multiple Epigenetic and Genetic Changes. *Pharmacological Reviews*. **2012**. 64(3):706-721.
13. Giaccone, G. Clinical Perspectives on Platinum Resistance. *Drugs*. **2000**. 59(4):9-17.
14. Galluzzi, L.; Senovilla, L.; Vitale, I.; et al. Molecular Mechanisms of Cisplatin Resistance. *Oncogene*. **2012**. 31:1869-1883.
15. Kitagawa, R.; Katsumata, N.; et al. Paclitaxel Plus Carboplatin Versus Paclitaxel Plus Cisplatin in Metastatic or Recurrent Cervical Cancer: The Open-Label Randomized Phase III Trial JCOG0505. *Journal of Clinical Oncology*. **2015**. 33:2129-2135.
16. Shi, Y.; Liu, Shu-An; Kerwood, D.; Goodisman, J.; Dabrowiak, J. Pt(IV) Complexes as Prodrugs for Cisplatin. *Journal of Inorganic Biochemistry*. **2012**. 107:6-14
17. Tobe, M.; Khokhar, A.J. *Clinical Hematology and Oncology*. **1977**. 7:114-137.
18. Cleare, M.J.; Hydes, P.C.; Hepburn, D.R.; Malerbi, B.W. Cisplatin: Current Status and New Developments, in: Prestayko, A.W.; Crooke, S.T.; Carter, S.K. (Eds.). Academic Press, New York, **1980**.
19. Pendyala, L.; Cowens, L.; Madajewicz, S. Platinum Coordination Complexes in Cancer Chemotherapy, in: Hacker, M.P.; Douple, E.B.; Krakoff, I.H. (Eds.). Martinus Nijhoff Publishers, Boston, Massachusetts, **1984**.
20. Pendyala, L.; Cowens, J.W.; Chheda, G.B.; Dutta, S.P.; Creaven, P.J. Identification of *cis*-Dichloro-bis-isopropylamine platinum(II) as a Major Metabolite of Iproplatin in Humans. *Cancer Research*. **1988**. 48:3533-3536.

21. Heinemann, V.; Hertel, L.; Grindey, G.; Plunkett, W. Comparison of the Cellular Pharmacokinetics and Toxicity of 2',2'-Difluorodeoxycytidine and 1- β -D-Arabinofuranosylcytosine. *Cancer Research*. **1988**. 48:4024-4031.
22. National Cancer Institute. cancer.gov/about-cancer/treatment/drugs/fda-gemcitabine-hydrochloride/. Accessed June 4, 2016.
23. Huang, P.; Chubb, S.; Hertel, L.; Grindey, G.; Plunkett, W. Action of 2',2'-Difluorodeoxycytidine on DNA Synthesis. *Cancer Research*. **1991**. 51:6110-6117.
24. Hodge, L.; Taub, M.; Tracy, T. Effect of its Deaminated Metabolite, 2',2'-Difluorodeoxyuridine, on the Transport and Toxicity of Gemcitabine in HeLa Cells. *Biochemical Pharmacology*. **2011**. 81:950-956.
25. Paolino, D.; Fresto, M.; et al. Gemcitabine-loaded PEGylated Unilamellar Liposomes vs GEMZAR®: Biodistribution, Pharmacokinetic Features and *In Vivo* Antitumor Activity. *Journal of Controlled Release*. **2010**. 144:144-150.
26. Poon, C.; He, C.; Demin, L.; Lu, K.; Lin, W. Self-Assembled Nanoscale Coordination Polymers Carrying Oxaliplatin and Gemcitabine for Synergistic Combination Therapy of Pancreatic Cancer. *Journal of Controlled Release*. **2015**. 201:90-98.
27. Meng, H.; Zhao, Y.; Nel, A. Two-Wave Nanotherapy to Target the Stroma and Optimize Gemcitabine delivery to a Human Pancreatic Cancer Model in Mice. *ACS Nano*. **2013**. 7(11):10048-10065.
28. Cerqueira, N.; Ramas, M.; et al. Understanding Ribonucleotide Reductase Inactivation by Gemcitabine. *Chemistry – A European Journal*. **2007**. 13:8507-8515
29. Miao, L.; Guo, S.; Zhang, J.; Kim, W.; Huang, L. Nanoparticles with Precise Ratiometric Co-Loading and Co-Delivery of Gemcitabine Monophosphate and

- Cisplatin for Treatment of Bladder Cancer. *Advanced Functional Materials*. **2014**. 24:6601-6611.
30. Ma, L.; Kohli, M.; Smith, A. Nanoparticles for Combination Drug Therapy. *ACS Nano*. **2013**. 7(11):9518-9525.
31. Komarova, N.; Boland RC. Cancer: Calculated treatment. *Nature*. **2013**. 499:291-292
32. Breiting, H. Drug Synergy – Mechanisms and Methods of Analysis. *Toxicity and Drug Testing*. **2012**. InTech. Prof. Bill Acree (Eds.).
33. Maase, H.; Hanen, S.; Roberts. J.; et al. Gemcitabine and Cisplatin Versus Methotrexate, Vinblastine, Doxorubicin, and Cisplatin in Advanced or Metastatic Bladder Cancer: Results of a Large, Randomized, Multinational, Multicenter, Phase III Study. *Journal of Clinical Oncology*. **2000**. 17(17):3068-3077.
34. Lee, J.; Nan, A. Combination Drug Delivery Approaches in Metastatic Breast Cancer. *Journal of Drug Delivery*. **2012**. 2012:1-17.
35. Ontario Institute for Cancer Research. <http://oicr.on.ca/>. Accessed November 21, 2015.
36. Sun, T.; et al. Engineered Nanoparticles for Drug Delivery in Cancer Therapy. *Angewandte Chemie*. **2014**. 53(46):12320-12364.
37. Kumari, A.; Yadav, S.; Yadav, S. Biodegradable Polymeric Nanoparticle Based Drug Delivery Systems. *Colloids and Surfaces B: Biointerfaces*. **2010**. 75(1):1-18.
38. Zhang L.; Gu, FX.; Chan, JM.; et al. Nanoparticles in Medicine: Therapeutic Applications and Developments. *Translational Medicine*. 2008. 83(5):761-769.
39. United States Food and Drug Association. accessdata.fda.gov/. Accessed October 4, 2016.

40. Dendritech. dendritech.com/pamam.html. Accessed November 30, 2016.
41. Madaan, K.; Kumar, S.; Poonia, N.; Lather, V.; Pandita, D. Dendrimers in drug delivery and targeting: Drug-dendrimer interactions and toxicity issues. *Journal of Pharmacy & BioAllied Sciences*. **2014**. 6(3):139-150.
42. Nie, Z.; Petukhova, A.; Kumacheva, E. Properties and emerging applications of self-assembled structures made from inorganic nanoparticles. *Nature Nanotechnology*. **2010**. 5:15-25.
43. United States Food and Drug Association. <http://www.fda.gov/ohrms/dockets/>. Accessed October 1, 2016.
44. Ma, X.; Tao, H.; Yang, K.; Feng, L.; et al. A functionalized graphene oxide-iron oxide nanocomposite for magnetically targeted drug delivery, photothermal therapy, and magnetic resonance imaging. *Nano Research*. **2012**. 5(3):199-212.
45. Taylor, KML.; Kim, JS.; Reiter, WJ.; An H.; Lin, W.; Lin, W. Mesoporous Silica Nanospheres as Highly Efficient MRI Contrast Agents. *Journal of the American Chemical Society*. **2008**. 130(7):2154-2155.
46. Vallet-Regi, M.; Rámila, A.; del Real, R.P.; Pérez-Pariente, J. A New Property of MCM-41: Drug Delivery System. *Chemistry of Materials*. **2001**. 13(2):308-311.
47. Beck, J.; Vartuli, J.; et al. A New Family of Mesoporous Molecular Sieves Prepared with Liquid Crystal Templates. *Journal of the American Chemical Society*. **1992**. 114(27):10834-10843.
48. Beck, JS.; Vartuli, JC.; Roth, WJ.; et al. A New Family of Mesoporous Molecular Sieves Prepared with Liquid Crystal Templates. *Journal of the American Chemical Society*. **1992**. 114(27):10834-10843

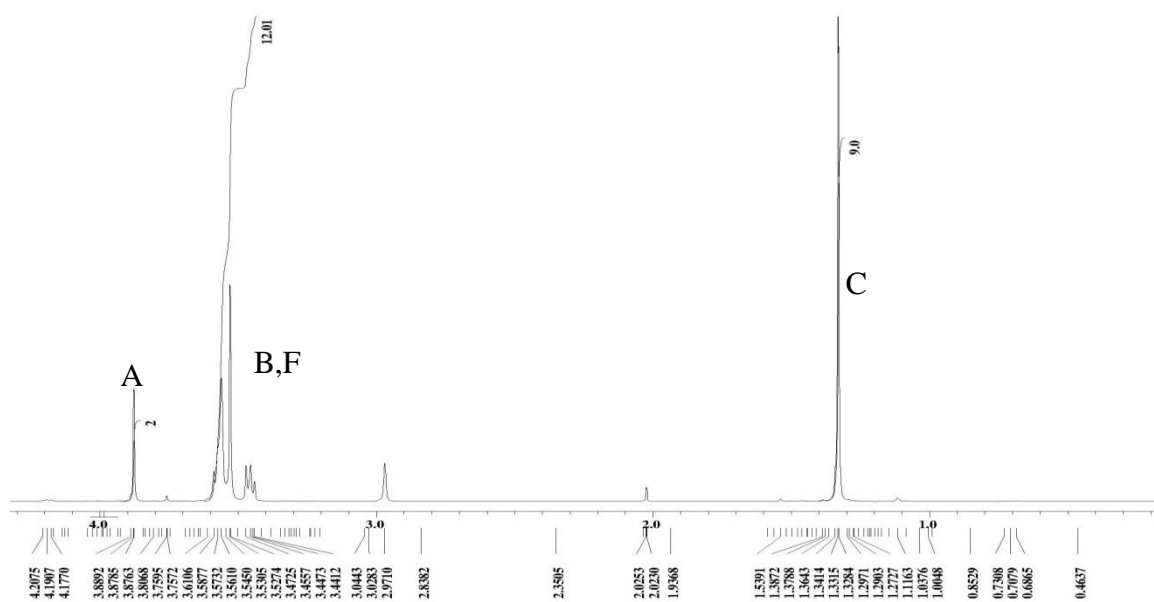
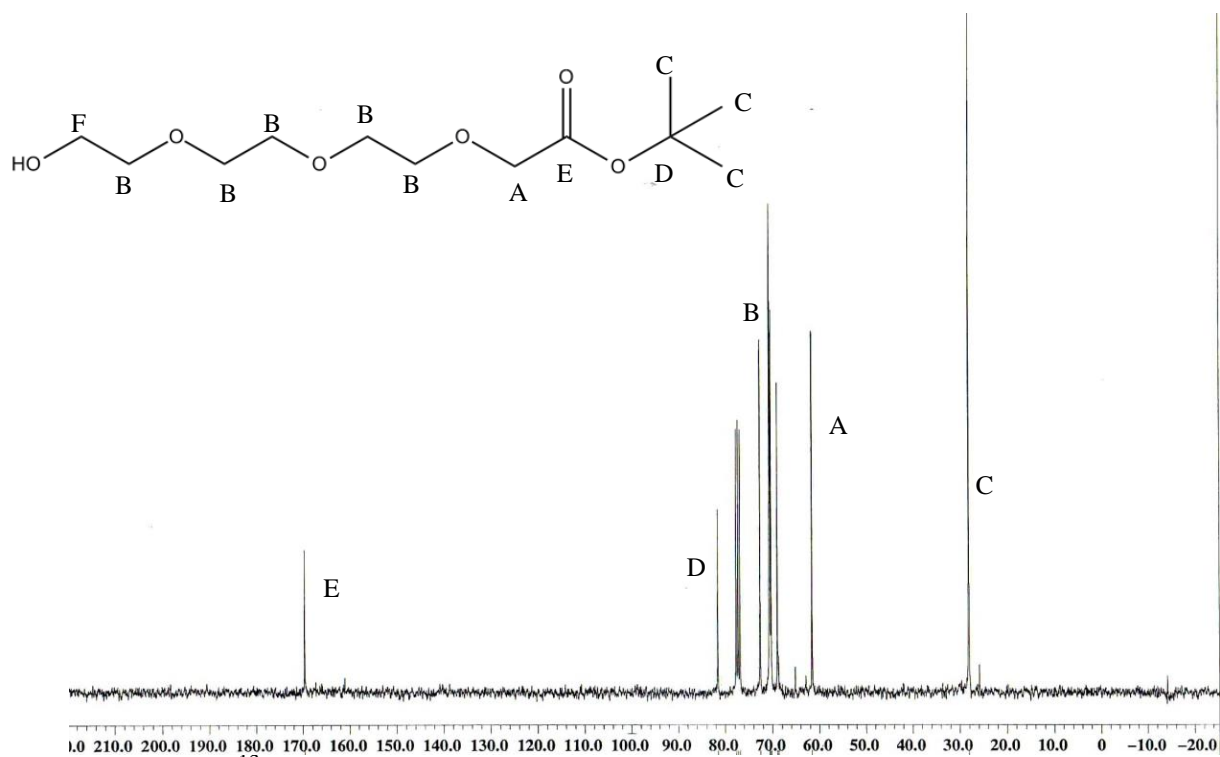
49. Goyal, PS.; Dasannacharya, BA.; Kelkar, VK.; et al. Shapes and sizes of micelles in CTAB solutions. *Physica B: Condensed Matter*. **1991**. 174(1):196-199.
50. Yi, Z.; Dumeé, L.; Garvey, C.; et al. A New Insight into Growth Mechanism and Kinetics of Mesoporous Silica Nanoparticles by in Situ Small Angle X-ray Scattering. *Langmuir*. **2015**. 31(30):8478-8487.
51. Luo, Guo-Feng, et al. Multifunctional Enveloped Mesoporous Silica Nanoparticles for Subcellular Co-delivery of Drug and Therapeutic Peptide. *Scientific Reports*. **2014**. 4(6064):1-10.
52. He, Q.; Shi, J. MSN Anti-Cancer Nanomedicines: Chemotherapy Enhancement, Overcoming of Drug Resistance, and Metastasis Inhibition. *Advanced Materials*. **2014**. 26:391-411.
53. Kim, S.; Canilho, N.; Pasc, A. Stimuli-Responsive Nanostructured Silica Matrix Targeting Drug Delivery Applications. *Biological and Pharmaceutical Applications of Nanomaterials*. **2016**. CRC Press. Prokopovich, Polina (Eds.).
54. Verhoef, J.F.; Anchordoquy, T.J. Questioning the Use of PEGylation for Drug Delivery. *Drug Deliv Transl Res*. **2014**. 3(6):499-503
55. Mura, S.; Nicolas, J.; Couvreur, P. Stimuli-responsive nanocarriers for drug delivery. *Nature Materials*. **2013**. 12:991-1003.
56. Tannock, I.; Rotin, D. Acid pH in Tumors and Its Potential for Therapeutic Exploitation. *Cancer Research*. **1989**. 49:4373-4384.
57. Deneke, S.M.; Fanburg, B.L. Regulation of cellular glutathione. *American Journal of Physiology – Lung Cellular and Molecular Physiology*. **1989**. 257(4):L163-L173.

58. Ma Pa, Xiao H.; Li C.; et al. Inorganic Nanocarriers for Platinum Drug Delivery. *Materials Today (Oxford U.K.)*. **2015**. 18(10):554-564.
59. Gu J.; Su S.; Li Y.; He Q.; et al. Surface Modification-Complexation Strategy for Cisplatin Loading in Mesoporous Nanoparticles. *Journal of Physical Chemistry Letters*. **2010**. 1(24):3446-3450.
60. Gu J.; Liu J.; Li Y.; Zhao W.; Shi J. One-Pot Synthesis of Mesoporous Silica Nanocarriers with Tunable Particle Sizes and Pendent Carboxylic Groups for Cisplatin Delivery. *Langmuir*. **2013**. 29(1):403-410.
61. Zhu X.; Gu J.; Li Y.; Zhao W.; Shi J. Magnetic core-mesoporous shell nanocarriers with drug anchorages suspended in mesopore interior for cisplatin delivery. *Microporous Mesoporous Materials*. **2014**. 196:115-121.
62. Ahn B.; Park J.; Singha K.; Park H.; Kim WJ. Mesoporous silica nanoparticle-based cisplatin prodrug delivery and anticancer effect under reductive cellular environment. *Journal of Materials Chemistry B*. **2013**. 1(22):2829-2836.
63. Mohapatra S.; Rout SR.; Narayan R.; Maiti TK. Multifunctional mesoporous hollow silica nanocapsules for targeted co-delivery of cisplatin-pemetrexed and MR imaging. *Dalton Trans*. **2014**. 43(42):15841-15850
64. Munaweera I.; Shi Y.; Koneru B.; et al. Nitric oxide- and cisplatin releasing silica nanoparticles for use against non-small cell lung cancer. *Journal of Inorganic Biochemistry*. **2015**. 153:23-31.
65. Vivero-Escoto JL.; Elnagheeb M. Mesoporous silica nanoparticles loaded with cisplatin and phthalocyanine for combination chemotherapy and photodynamic therapy *in vitro*. *Nanomaterials*. **2015**. 5(4):2302-2316

66. Zhang W.; Shen J.; Su H.; et al. Co-Delivery of Cisplatin Prodrug and Chlorin e6 by Mesoporous Silica Nanoparticles for Chemo-
67. Ahn, B.; Park, J.; Singha, K.; Park, H.; Kim, W. Mesoporous Silica Nanoparticle-Based Cisplatin Prodrug Delivery and Anticancer Effect Under Reductive Cellular Environment. *Journal of Materials Chemistry B*. **2013**. 1:2829-2836.
68. Meng, H.; Wang, M.; Nel, A.; et al. Use of a Lipid-Coated Mesoporous Silica Nanoparticle Platform for Synergistic Gemcitabine and Paclitaxel Delivery to Human Pancreatic Cancer in Mice. *ACS Nano*. **2015**. 9(4):3540-3557.
69. Malfanti, A.; Miletto, I.; Bottinelli, E.; et al. Delivery of Gemcitabine Prodrugs Employing Mesoporous Silica Nanoparticles. *Molecules*. **2016**. 21(4):522.
70. Singh, R.; Whitesides, GM. Thiol-disulfide interchange. *The chemistry of Sulphur-containing functional groups*.**1993**. 633-658. John Wiley & Sons.
71. Dasari, M.; Acharya, AP.; Kim, D.; et al. H-Gemcitabine: A New Gemcitabine Prodrug for Treating Cancer. *Bioconjugate Chemistry*. **2013**. 24(1):4-8
72. Montalbetti, CAGN.; Falque, V. Amide bond formation and peptide coupling. *Tetrahedron*. **2005**. 61:10827-10852.
73. Vega, D. Design, Synthesis and Characterization of Multifunctional Redox-Responsive Porphyrin-Based Polysilsesquioxane Nanomaterials for Photodynamic Therapy. **2015**. *University of North Carolina at Charlotte*.
74. Gololobov, YG.; Kasukhin, LF. Recent Advances in the Staudinger Reaction. *Tetrahedron*. **1992**. 48(8):1353-1406.
75. Promega Corporation. promega.com/. Accessed October 8, 2016.
76. Compusyn, Inc. combosyn.com/. Accessed September 17, 2016

77. Domenech, M.; Marrero-Berrios, I.; Torres-Lugo, M.; Rinaldi, C. Lysosomal Membrane Permeabilization by Targeted Magnetic Nanoparticles in Alternating Magnetic Fields. *ACS Nano*. **2013**. 7(6):5091-5101.
78. Zhou, J.; Wang, J.; Xu, Q.; et al. Folate-chitosan-gemcitabine core-shell nanoparticles targeted to pancreatic cancer. *Chinese Journal of Cancer Research*. **2013**. 25(5):527-535.
79. Fröhlich, E. The role of surface charge in cellular uptake and cytotoxicity of medical nanoparticles. *International Journal of Nanomedicine*. **2012**. 7:5577-5591.
80. Kamaly, N.; Yameen, B.; Wu J.; Farokhzad O.C. Degradable Controlled-Release Polymers and Polymeric Nanoparticles: Mechanisms of Controlling Drug Release. *Chemical Reviews*. **2016**. 116(4):2602-2663.
81. Salmaso, S.; Caliceti, P. Stealth Properties to Improve Therapeutic Efficacy of Drug Nanocarriers. *Journal of Drug Delivery*. **2013**. 2013:1-19.
82. Targeted Cancer Therapies. cancer.gov/about-cancer/treatment/types/. Accessed November 10, 2016.

APPENDIX A: FIGURES

Figure A1.1: ^1H NMR spectrum of RRL1 (CDCl_3).Figure A1.2: ^{13}C NMR spectrum of RRL1 (CDCl_3).

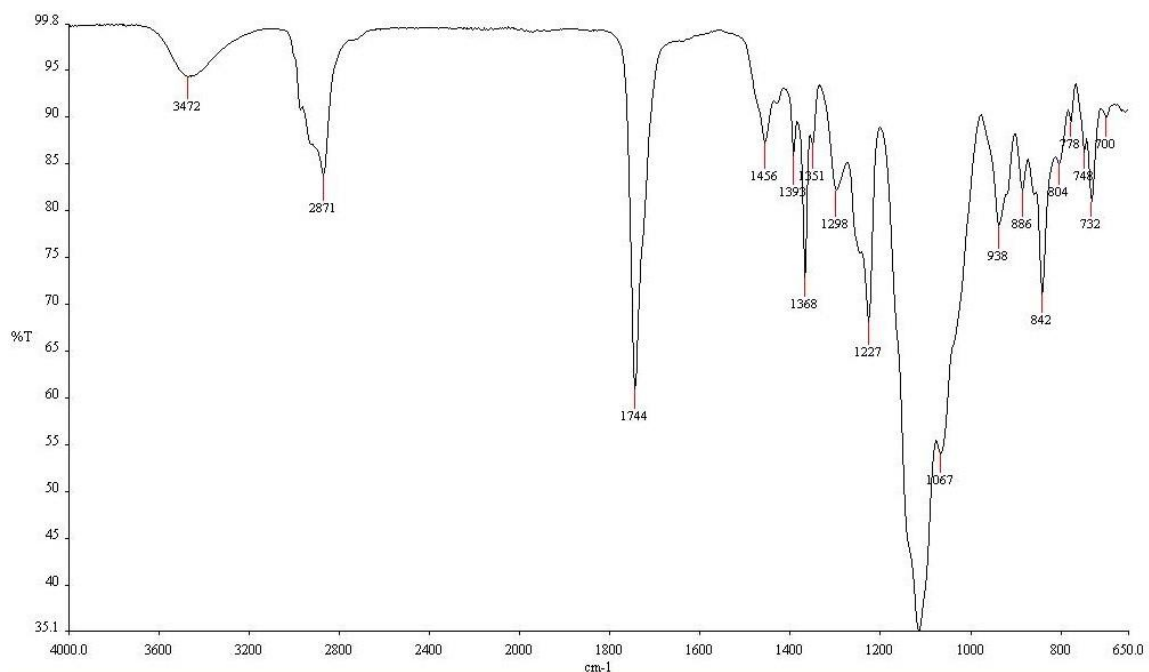


Figure A1.3: FTIR spectrum of RRL1.

Wavenumber (cm ⁻¹)	Functional Group
3472	-O-H
2871	-C-H
1744	-C=O
1227	-C-C
1117	-C-O

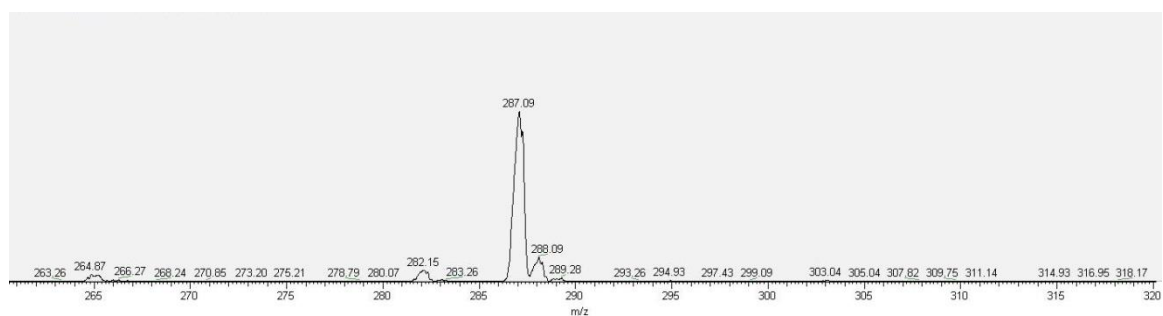


Figure A1.4: ESI mass spectrum of RRL1 (ACN:Water, 50:50 v/v).

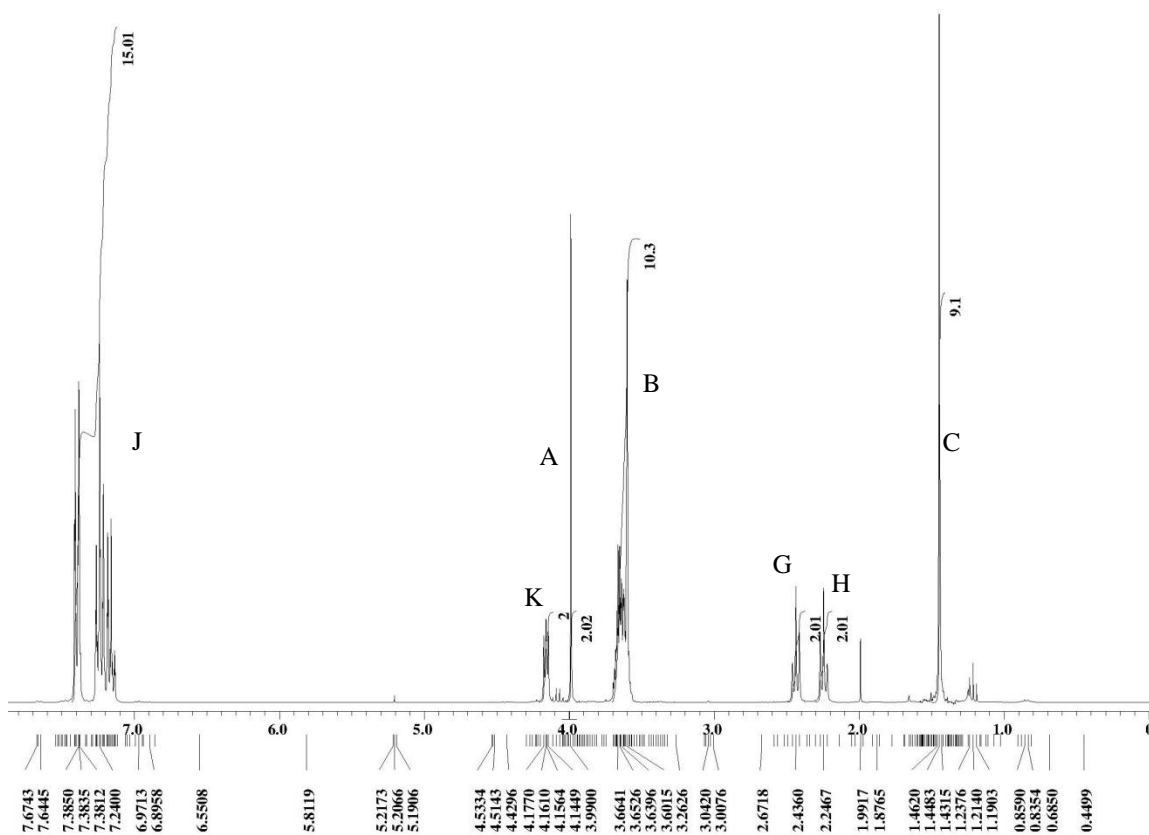


Figure A1.5: ^1H NMR spectrum of RRL2 (CDCl_3).

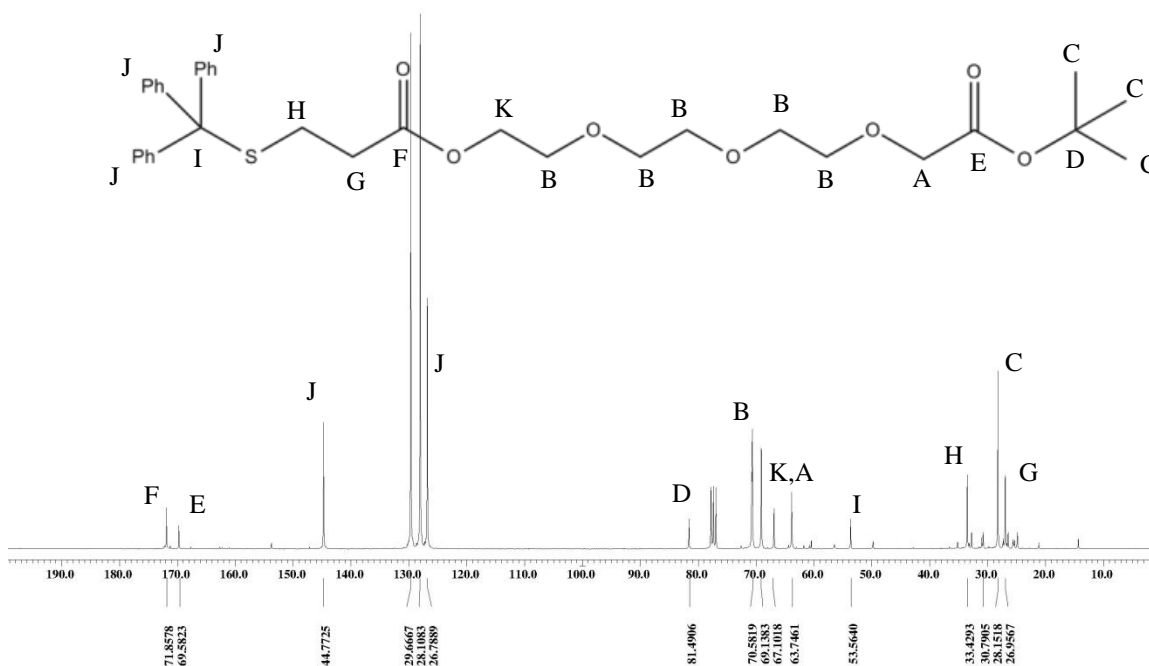


Figure A1.6: ^{13}C NMR spectrum of RRL2 (CDCl_3).

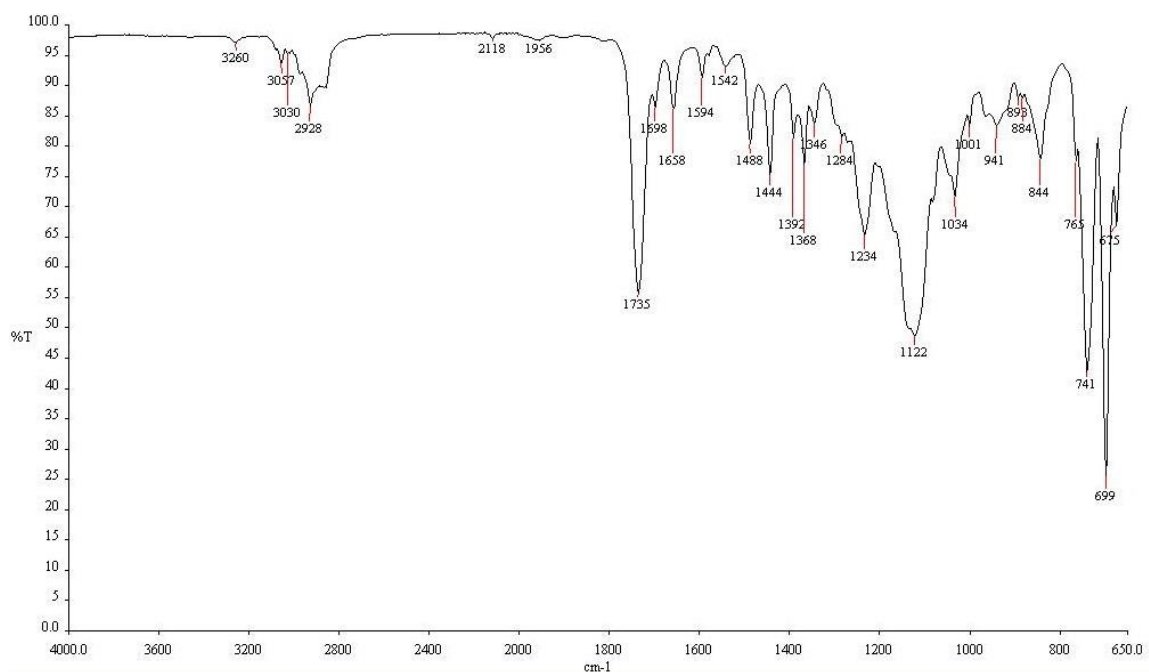


Figure A1.7: FTIR spectrum of RRL2.

Wavenumber (cm ⁻¹)	Functional Group
3057, 3030, 2928	-C-H
1735	-C=O
1594	-C=C
1234	-C-C
1122	-C-O

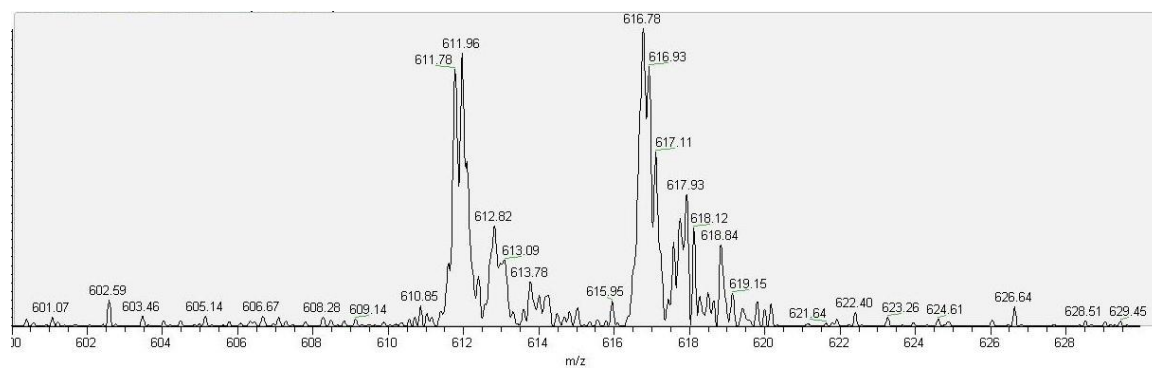


Figure A1.8: ESI mass spectrum of RRL2 (ACN:Water, 50:50 v/v).

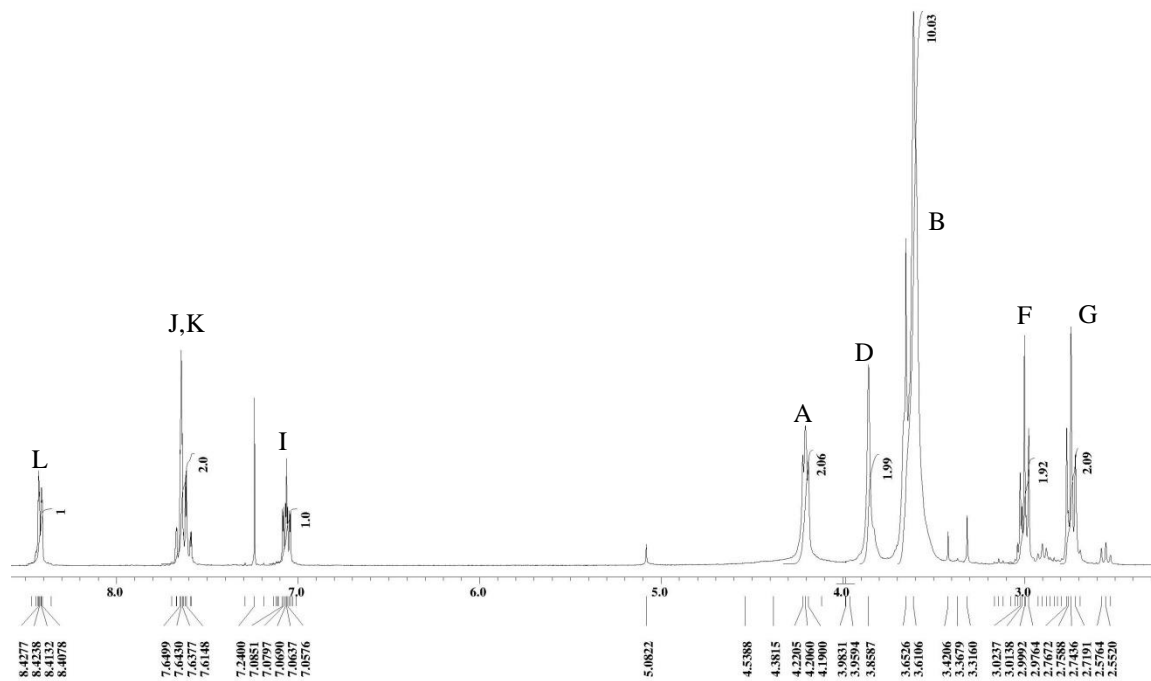


Figure A1.7: ^1H NMR spectrum of RRL4 (CDCl_3).

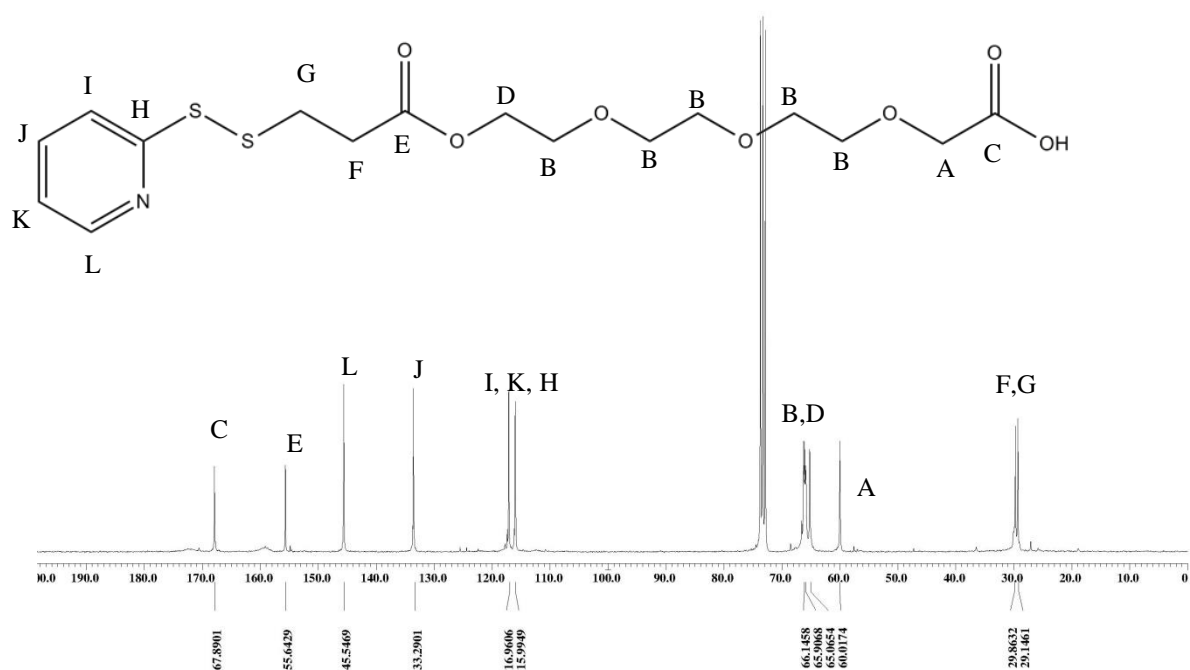


Figure A1.8: ^{13}C NMR spectrum of RRL4 (MeOD-d_4).

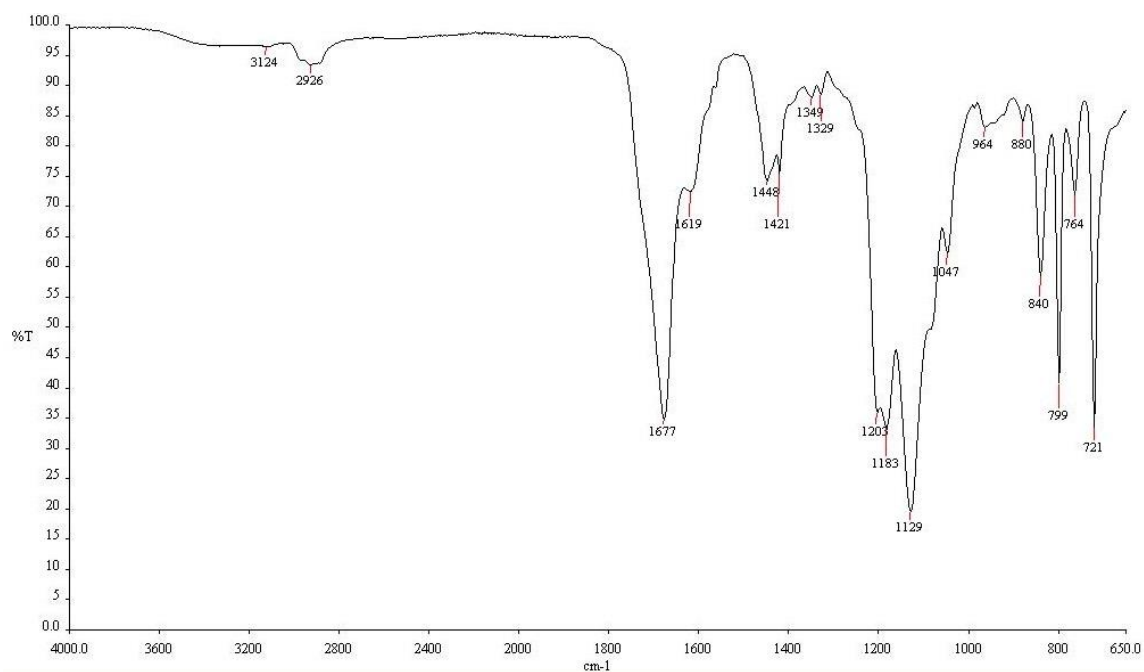


Figure A1.9: FTIR spectrum of RRL4.

Wavenumber (cm ⁻¹)	Functional Group
3124	-O-H
2926	-C-H
1677	-C=O
1619	-C=C, -C=N
1203	-C-C
1129	-C-O

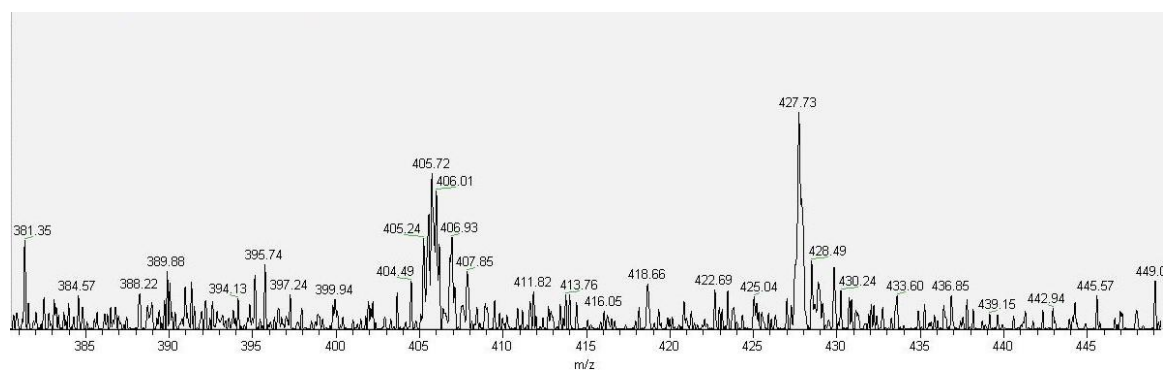


Figure A1.10: ESI mass spectrum of RRL4 (ACN:Water, 50:50 v/v).

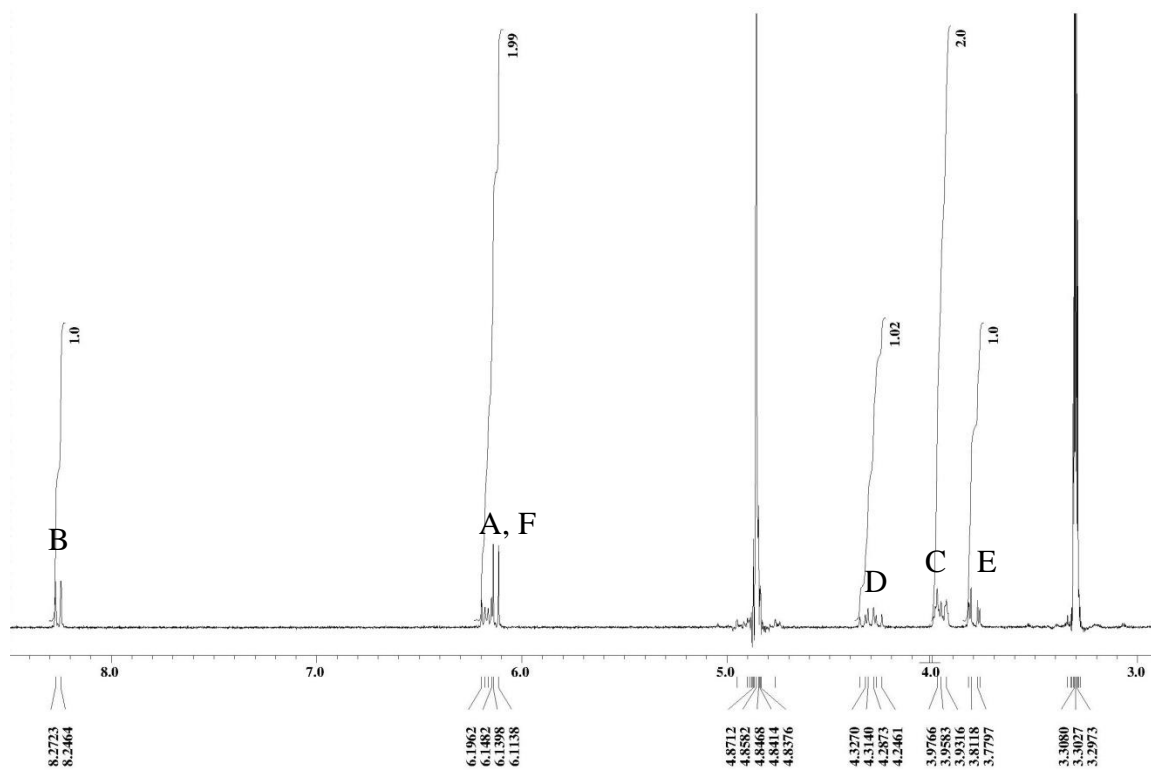
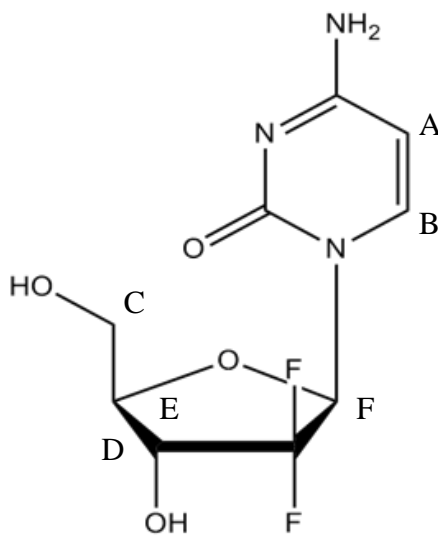


Figure A1.11: ^1H NMR spectrum of Gemcitabine (MeOD-d_4).



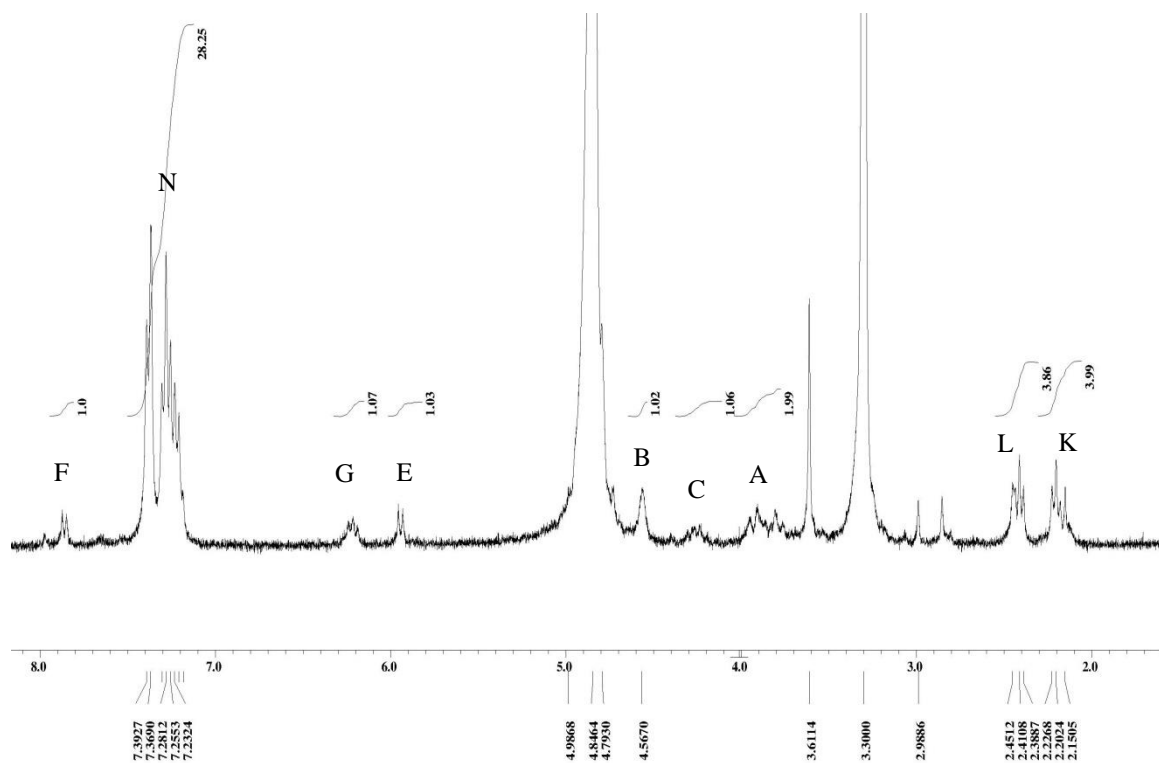


Figure A1.12: ^1H NMR spectrum of (Tritylthio)mercapto-Gemcitabine (MeOD-d_4).

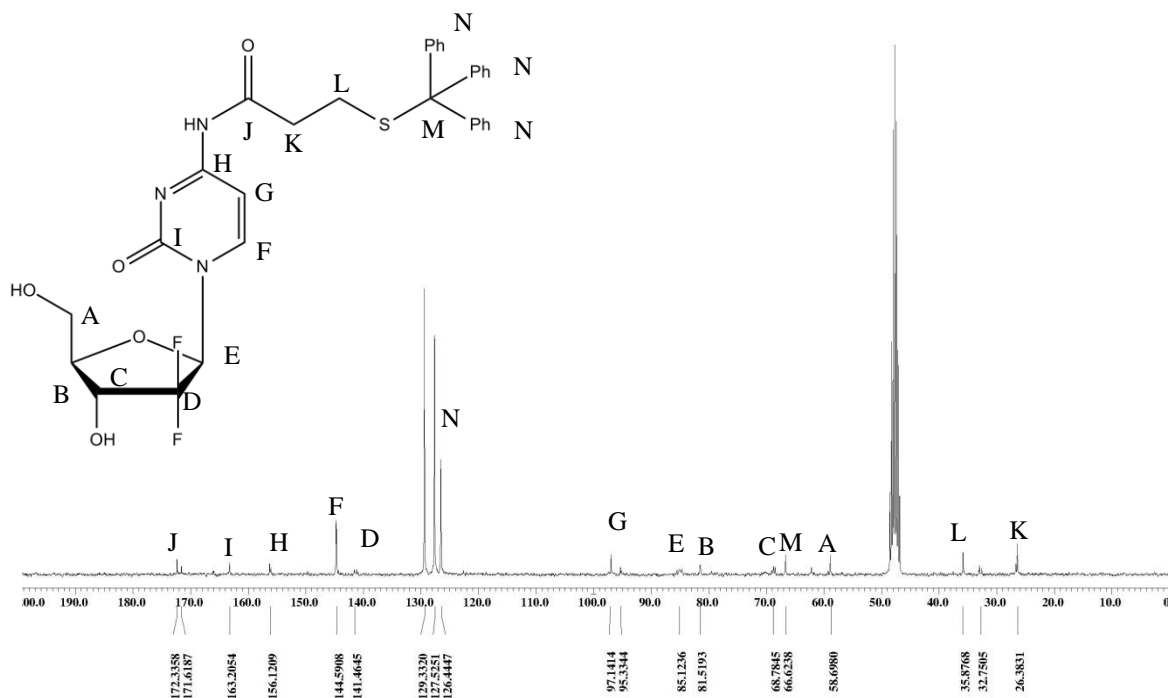


Figure A1.13: ^{13}C NMR spectrum of (Tritylthio)mercapto-Gemcitabine (MeOD-d_4).

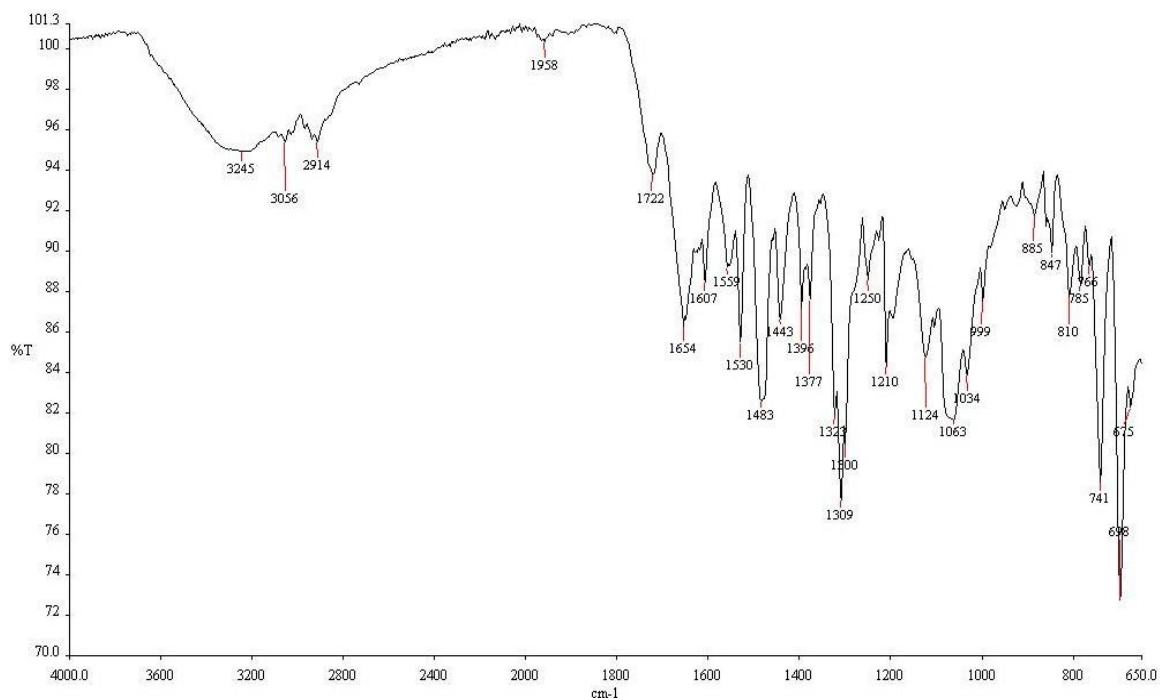


Figure A1.14: FTIR spectrum of (Tritylthio)mercapto-Gemcitabine.

Wavenumber (cm ⁻¹)	Functional Group
3245	-O-H
2914	-C-H
1722	-C=O
1654, 1607	-C=C
1559	-C=N
1210	-C-C
1124	-C-O

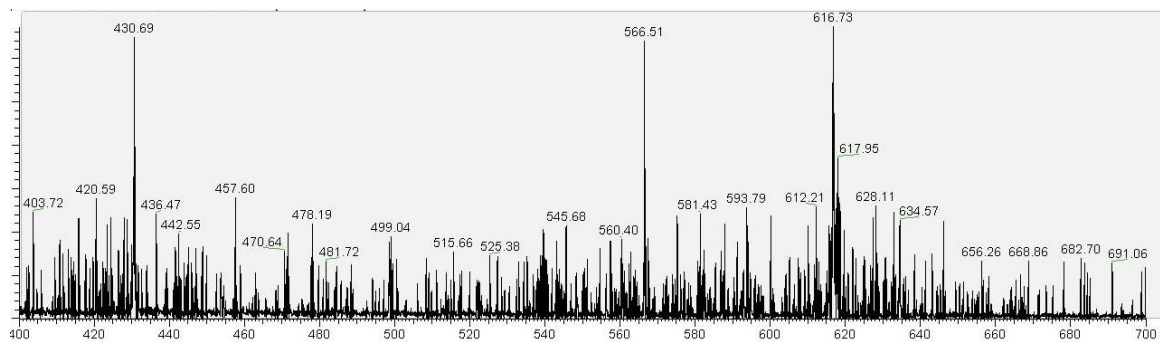


Figure A1.15: ESI mass spectrum of (Tritylthio)mercapto-Gemcitabine (ACN:Water, 50:50 v/v).

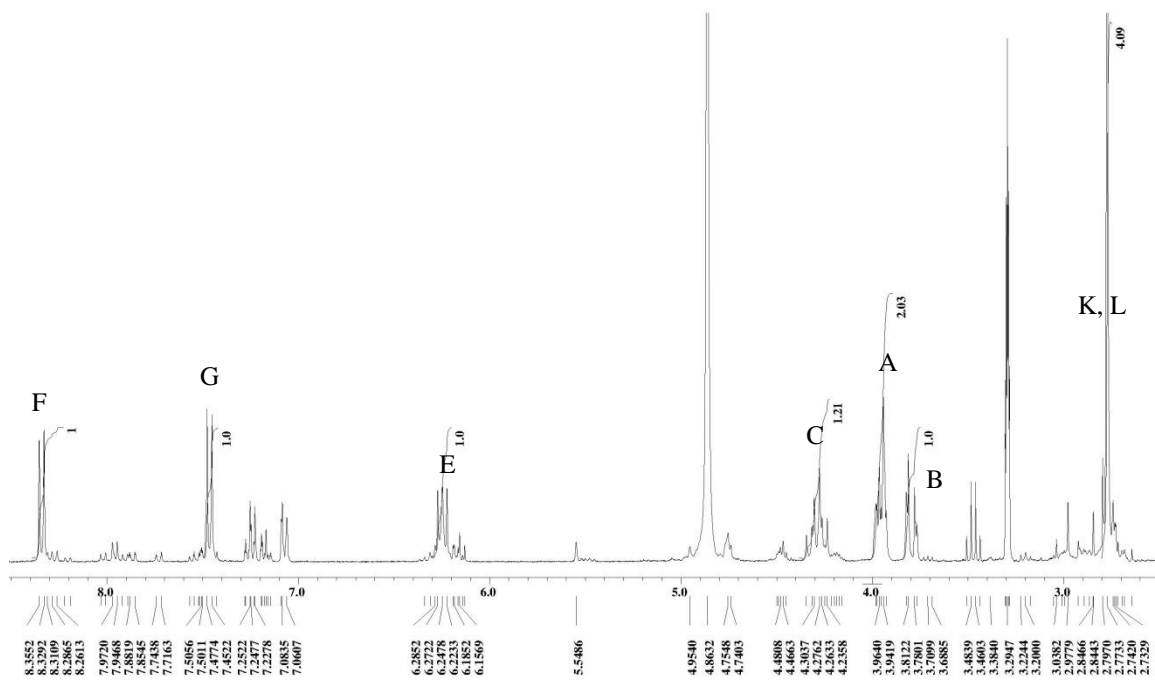


Figure A1.16: ^1H NMR spectrum of Gemcitabine Prodrug (MeOD- d_4).

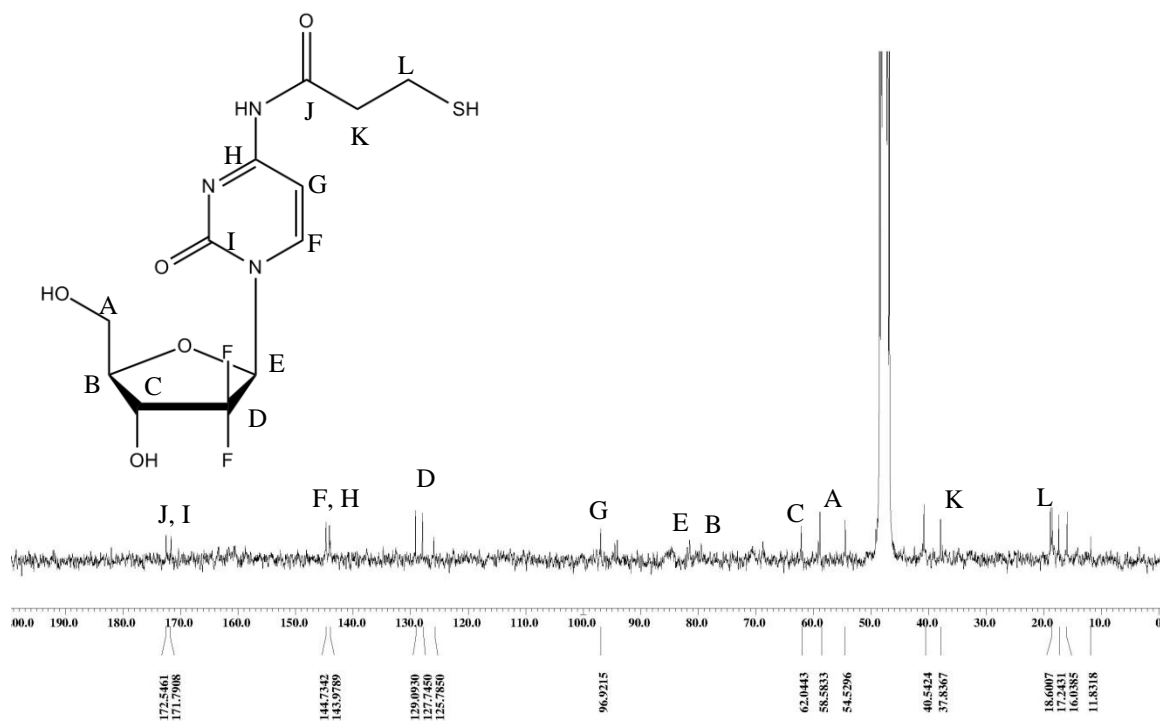


Figure A1.17: ^{13}C NMR spectrum of Gemcitabine Prodrug (MeOD- d_4).

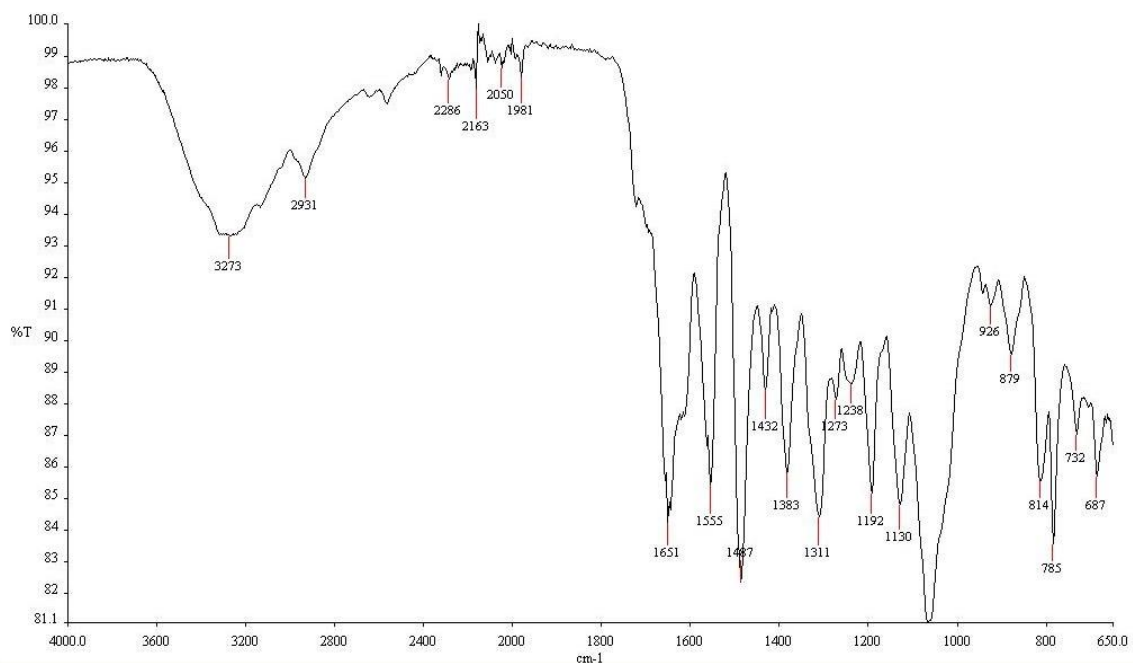


Figure A1.18: FTIR spectrum of Gemcitabine Prodrug.

Wavenumber (cm ⁻¹)	Functional Group
3273	-O-H
2931	-C-H
1716	-C=O
1651, 1609	-C=C
1555	-C=N
1238	-C-C
1130	-C-O

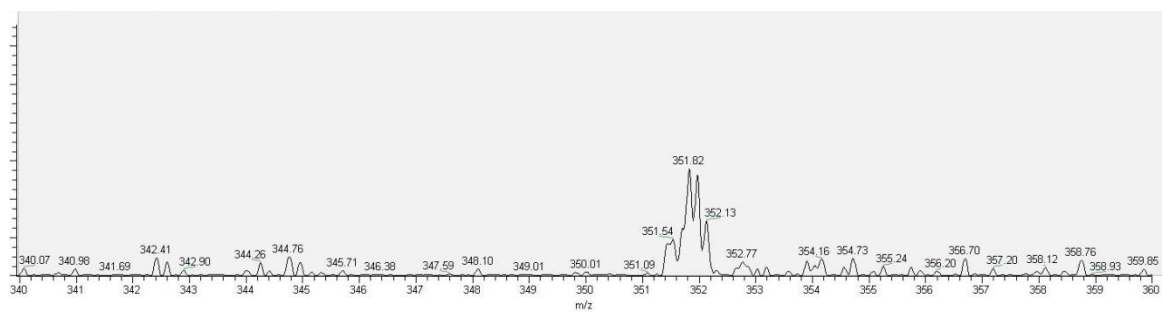


Figure A1.19: ESI mass spectrum of Gemcitabine Prodrug (ACN:Water, 50:50 v/v).

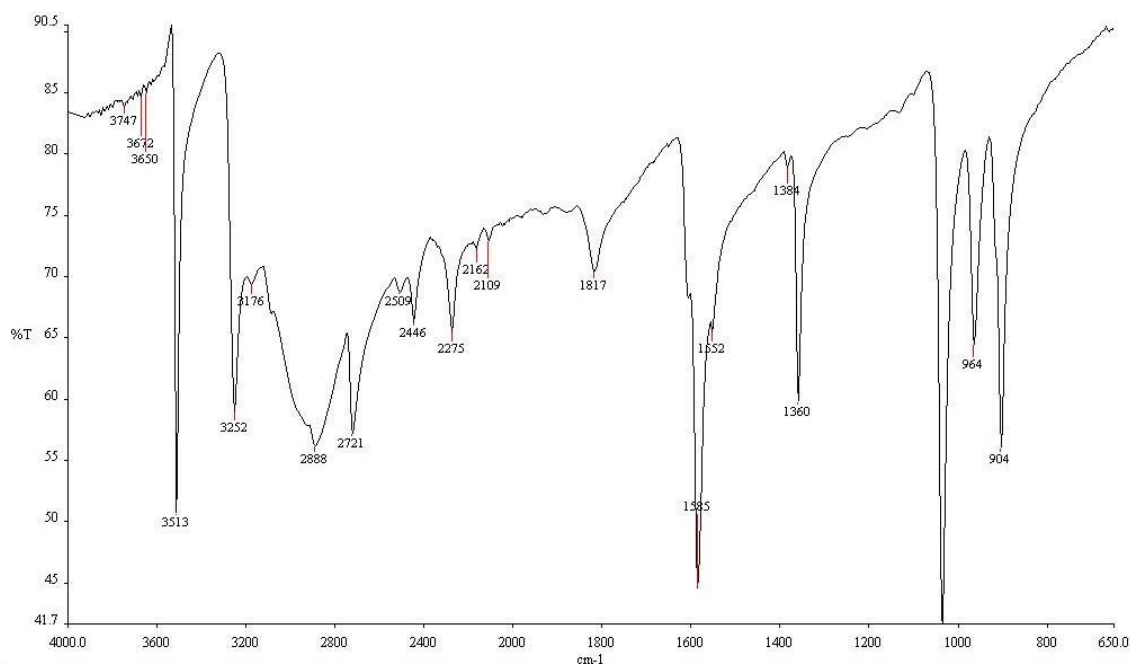


Figure A1.20: FTIR spectrum of Dihydroxycisplatin(IV)

Wavenumber (cm ⁻¹)	Functional Group
3513	-O-H
3252	-N-H

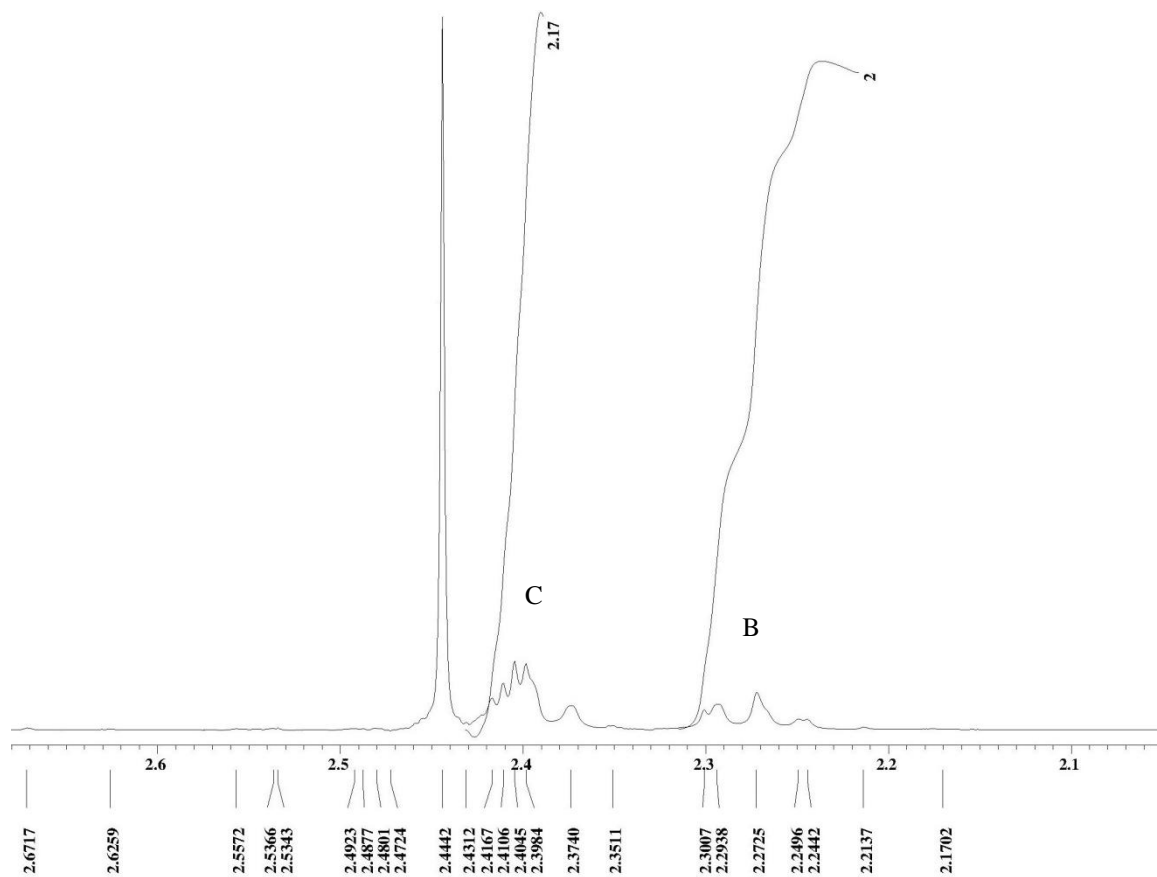


Figure A1.20: ^1H NMR spectrum of Cisplatin Prodrug (DMSO-d_6).

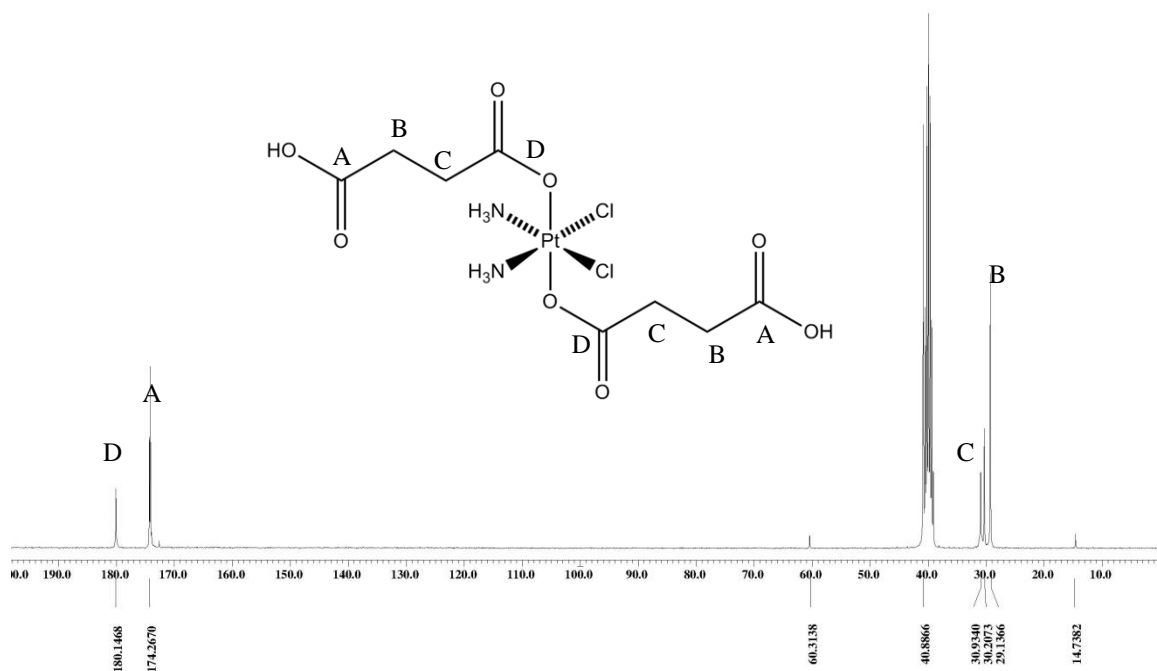


Figure A1.21: ^{13}C NMR spectrum of Cisplatin Prodrug (DMSO-d_6).

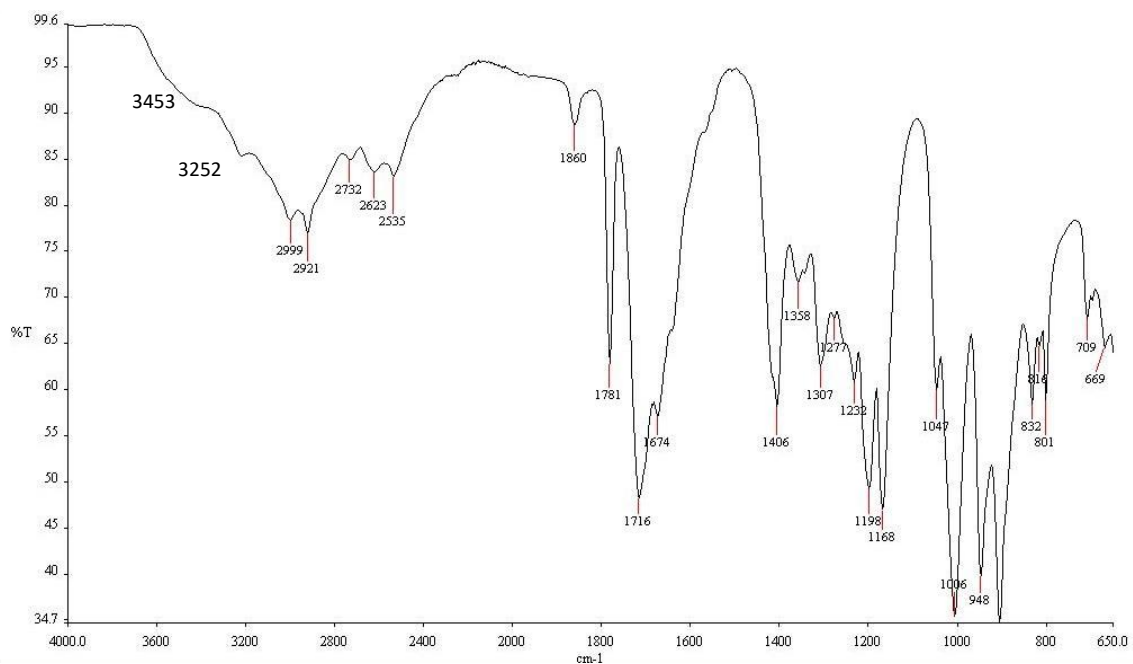


Figure A1.22: FTIR spectrum of Cisplatin Prodrug.

Wavenumber (cm ⁻¹)	Functional Group
3453	-O-H
3252	-N-H
2999, 2981	-C-H
1860, 1781	-C=O
1232	-C-C

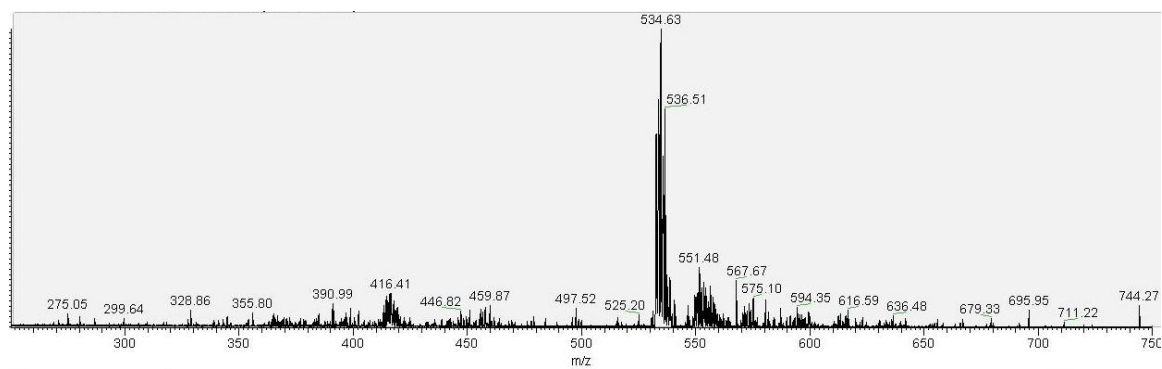


Figure A1.23: ESI mass spectrum of Cisplatin Prodrug (ACN:Water, 50:50 v/v).

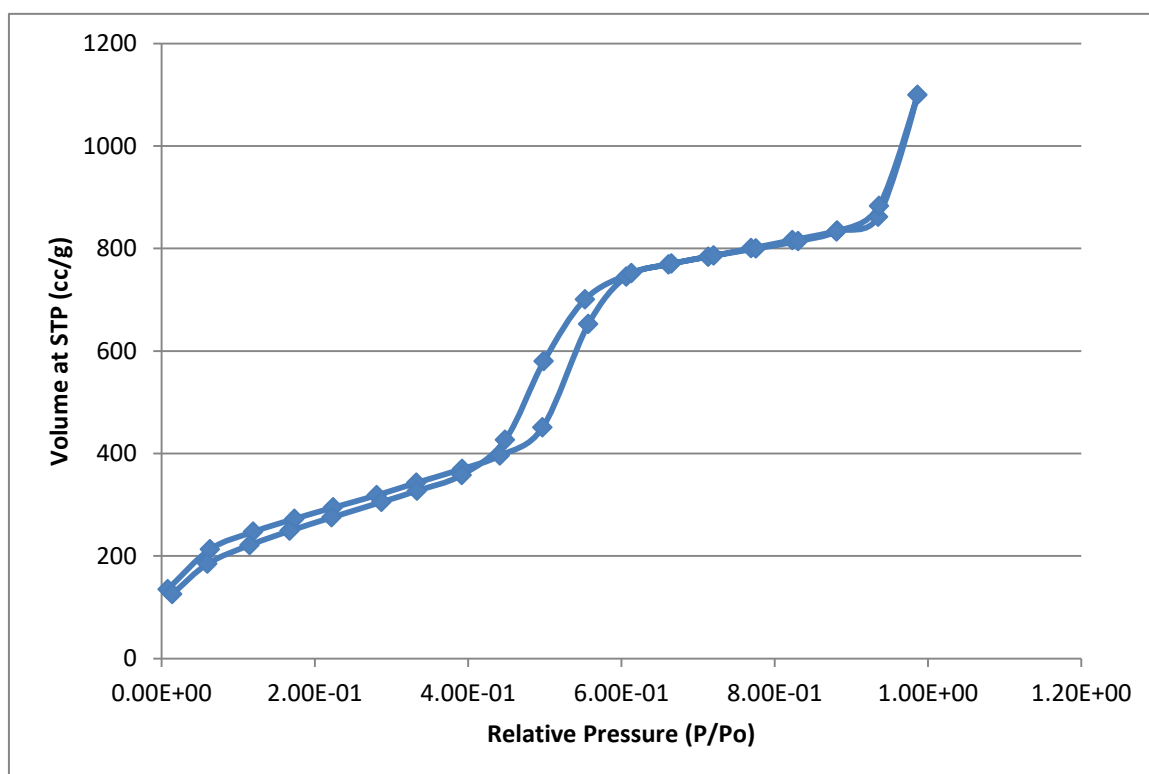
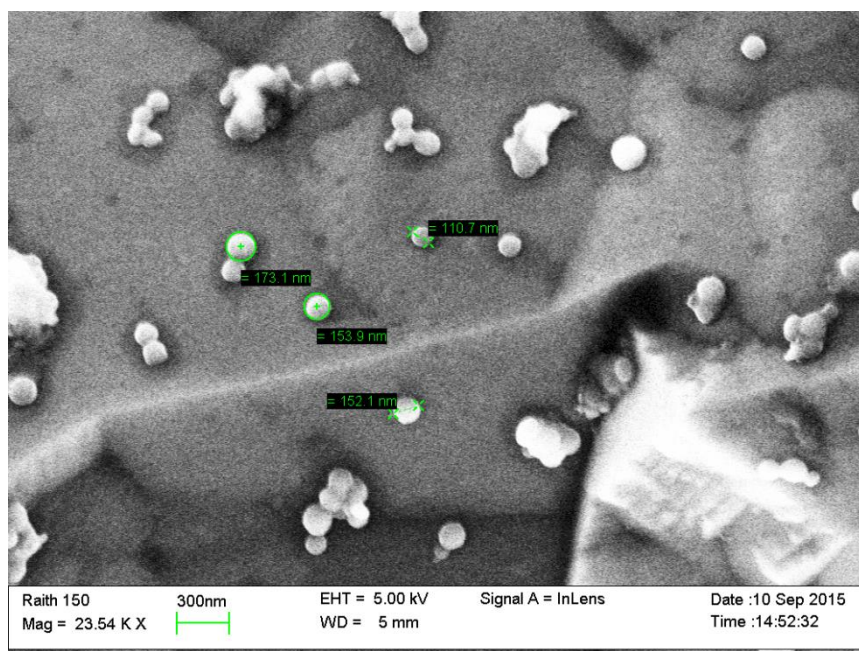


Figure A2.1: SEM image of AP-MSNs.

Figure A2.2: Nitrogen Isotherm Adsorption BET analysis of Surface Area of AP-MSNs.

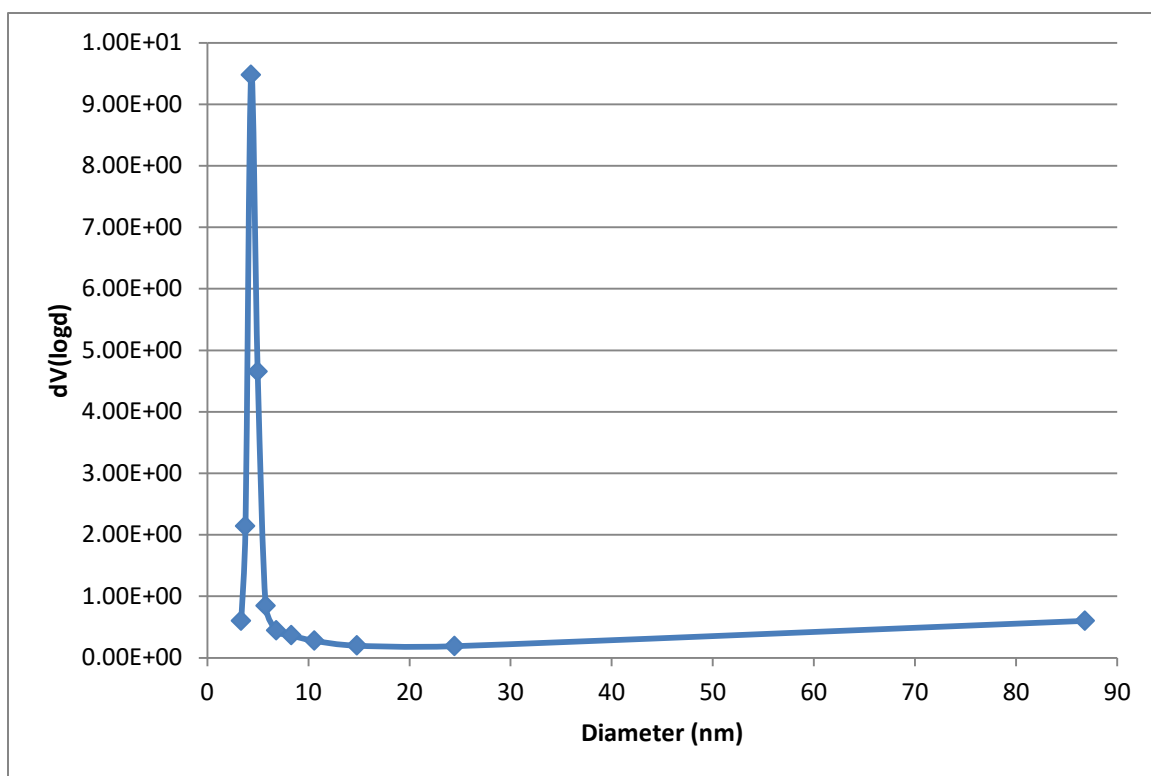


Figure A2.3: Nitrogen Isotherm Adsorption BJH analysis of Pore Volume of AP-MSNs.

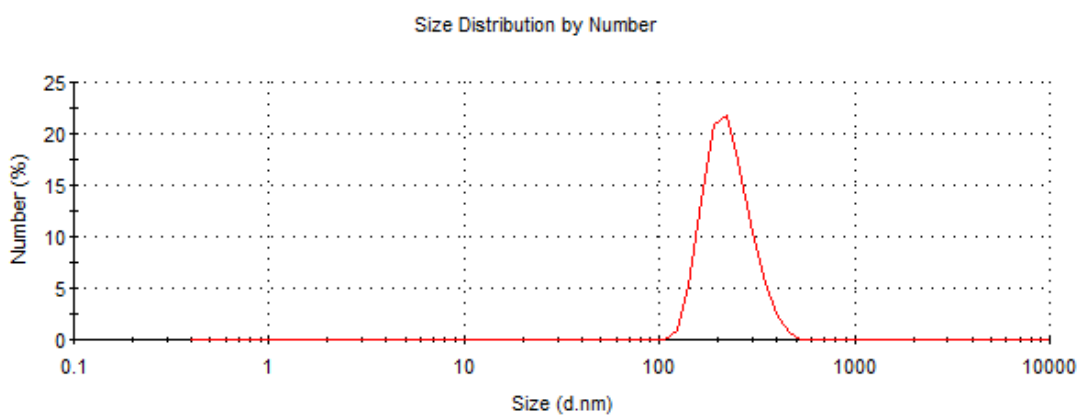


Figure A2.4: DLS hydrodynamic diameter of AP-MSNs in water.

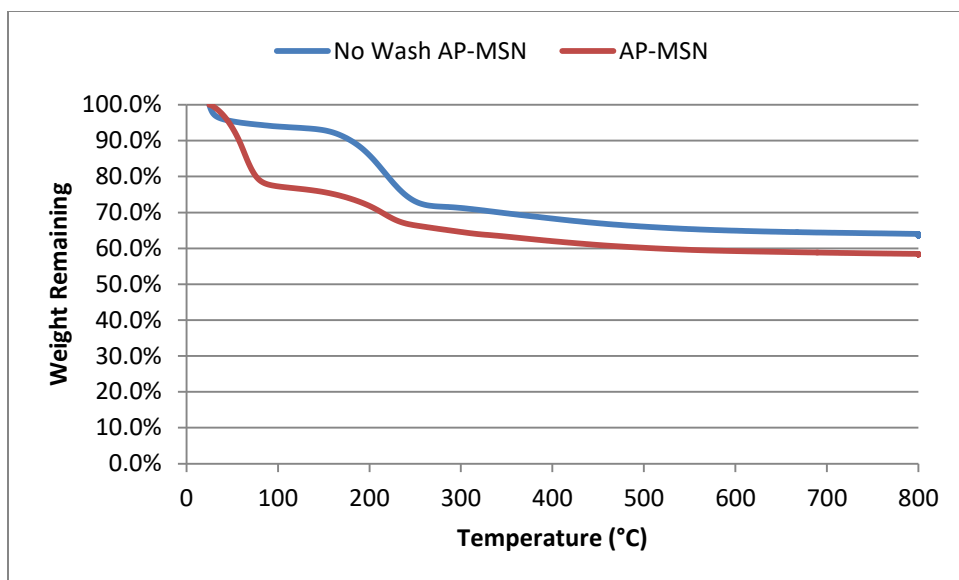


Figure A2.5: TGA analysis of AP-MSN vs non-washed AP-MSN.

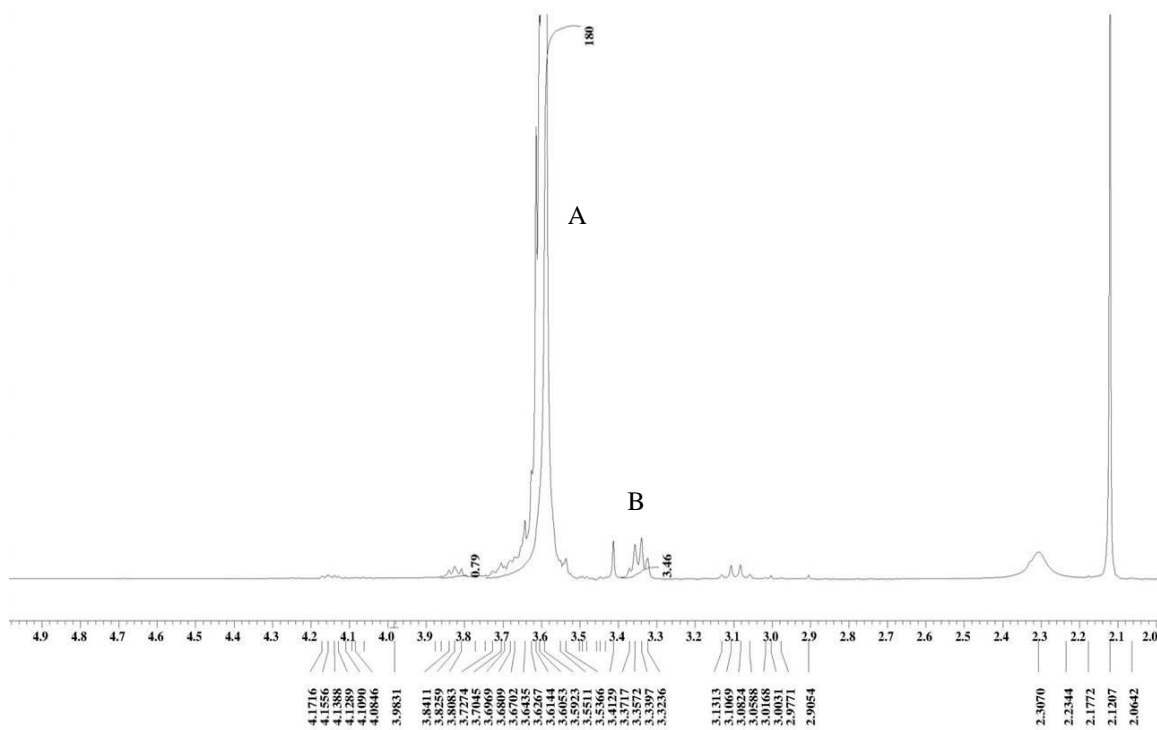


Figure A3.1: ^1H NMR spectrum of Diazido-PEG (CDCl_3).



Figure A3.2: ^{13}C NMR spectrum of Diazido-PEG (CDCl_3).

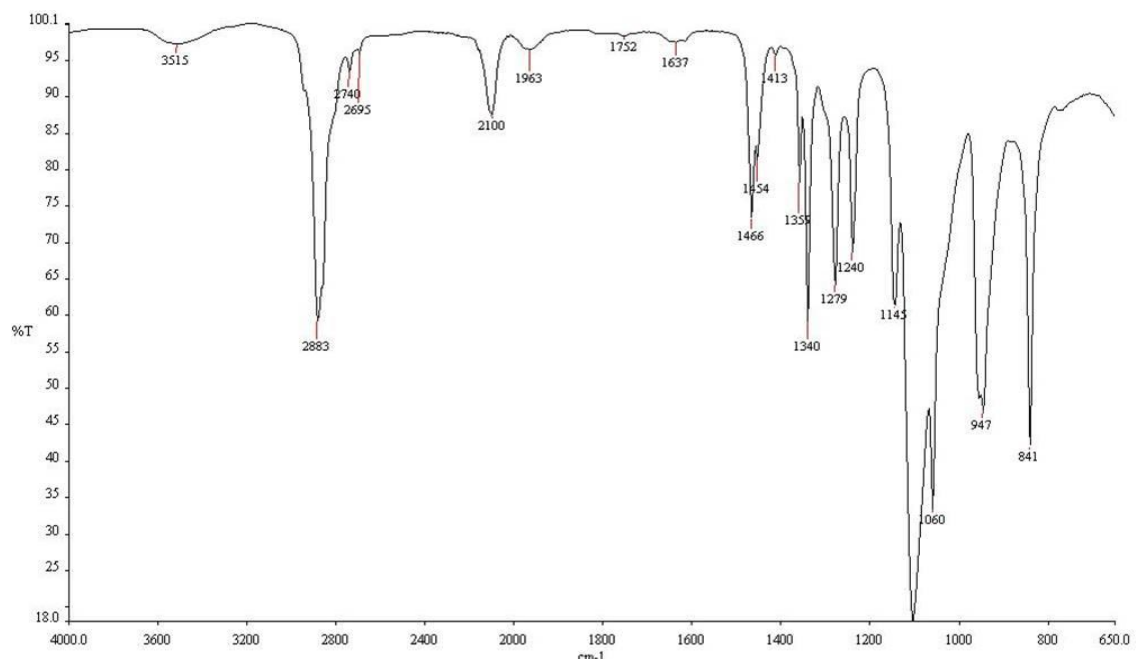


Figure A3.3: FTIR spectrum of Diazido-PEG.

Wavenumber (cm ⁻¹)	Functional Group
2883	-C-H
2100	-N=N
1240	-C-C
1115	-C-O

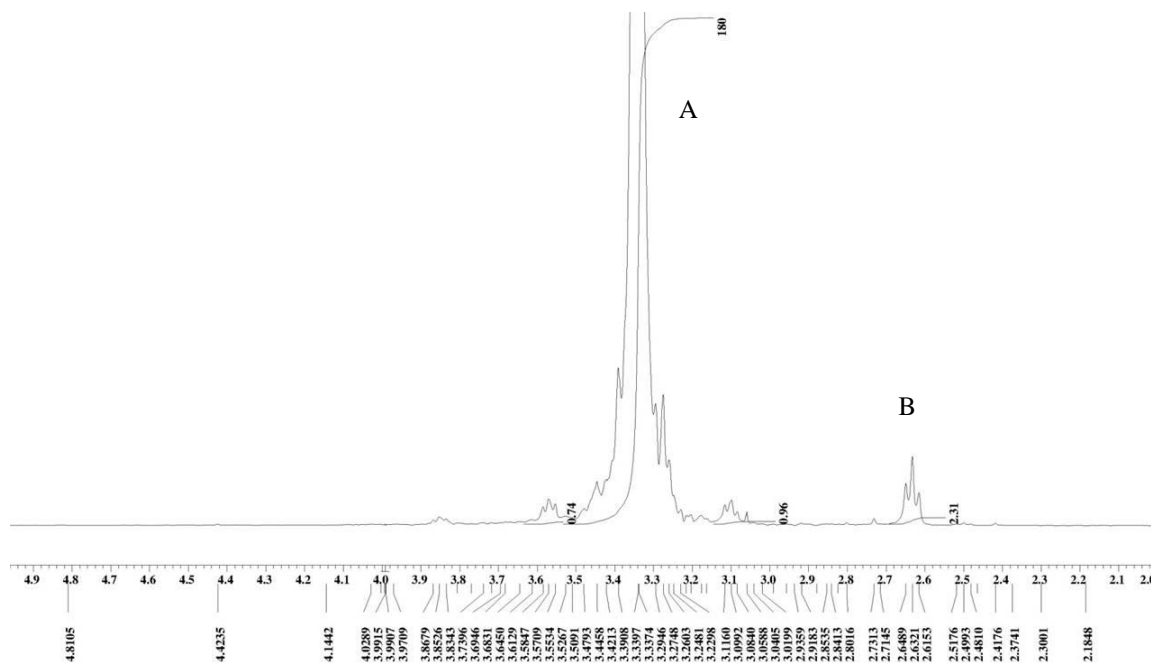


Figure A3.4: ^1H NMR spectrum of Diamino-PEG (CDCl_3).

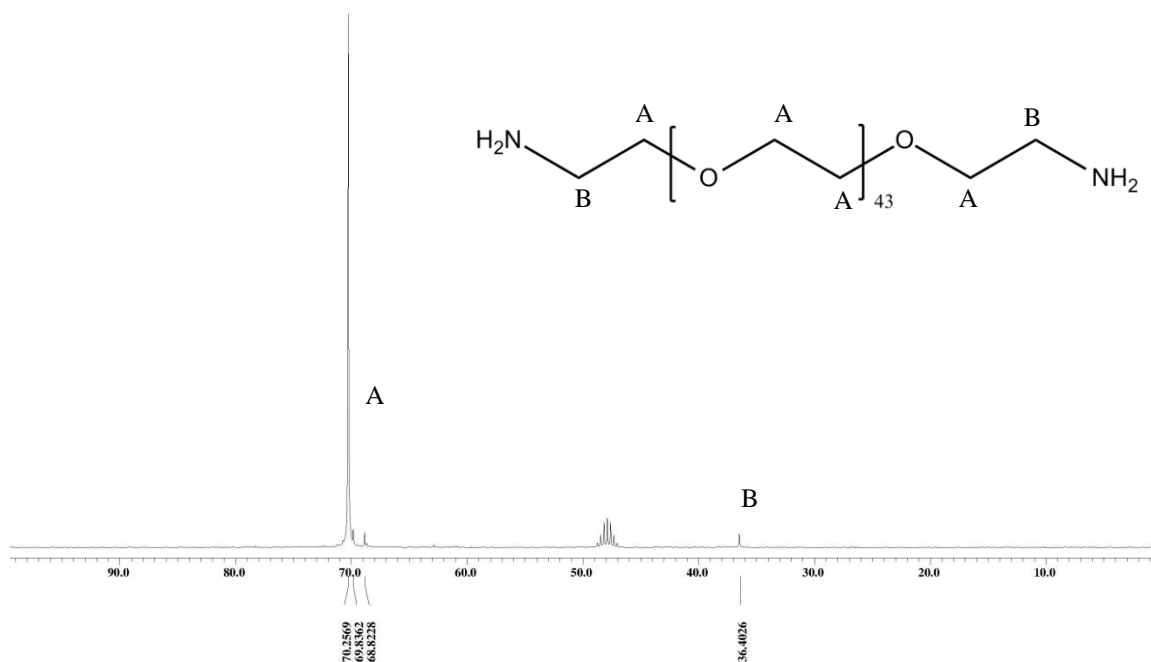


Figure A3.5: ^{13}C NMR spectrum of Diamino-PEG (MeOD-d_4).

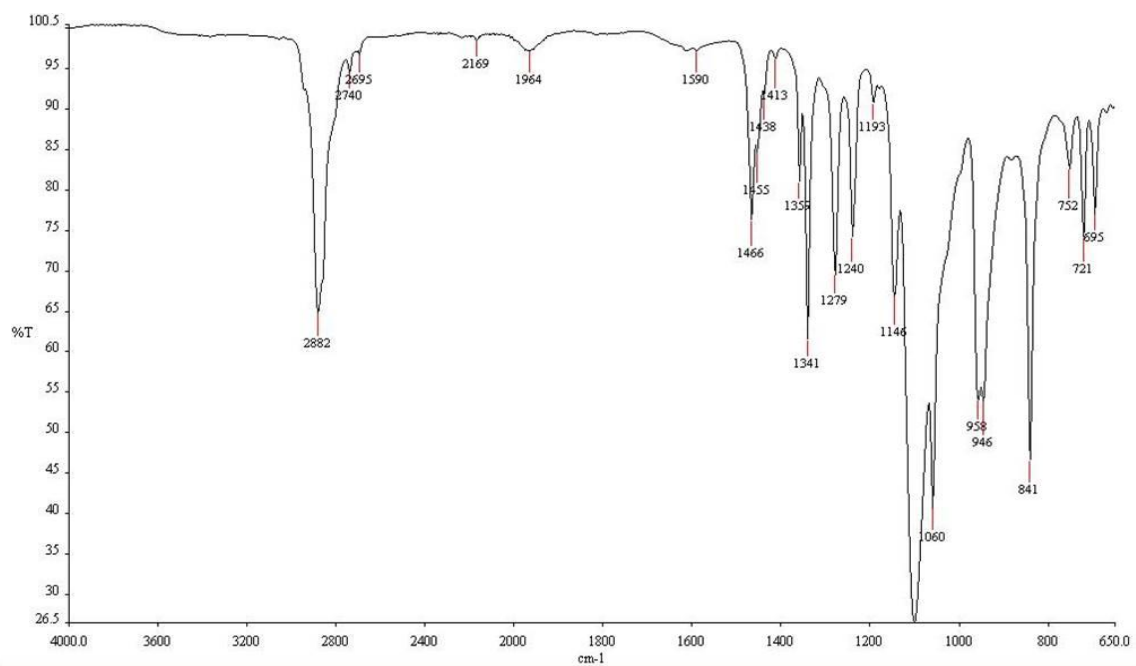


Figure A3.6: FTIR spectrum of Diamino-PEG.

Wavenumber (cm ⁻¹)	Functional Group
2882	-C-H
1240	-C-C
1116	-C-O

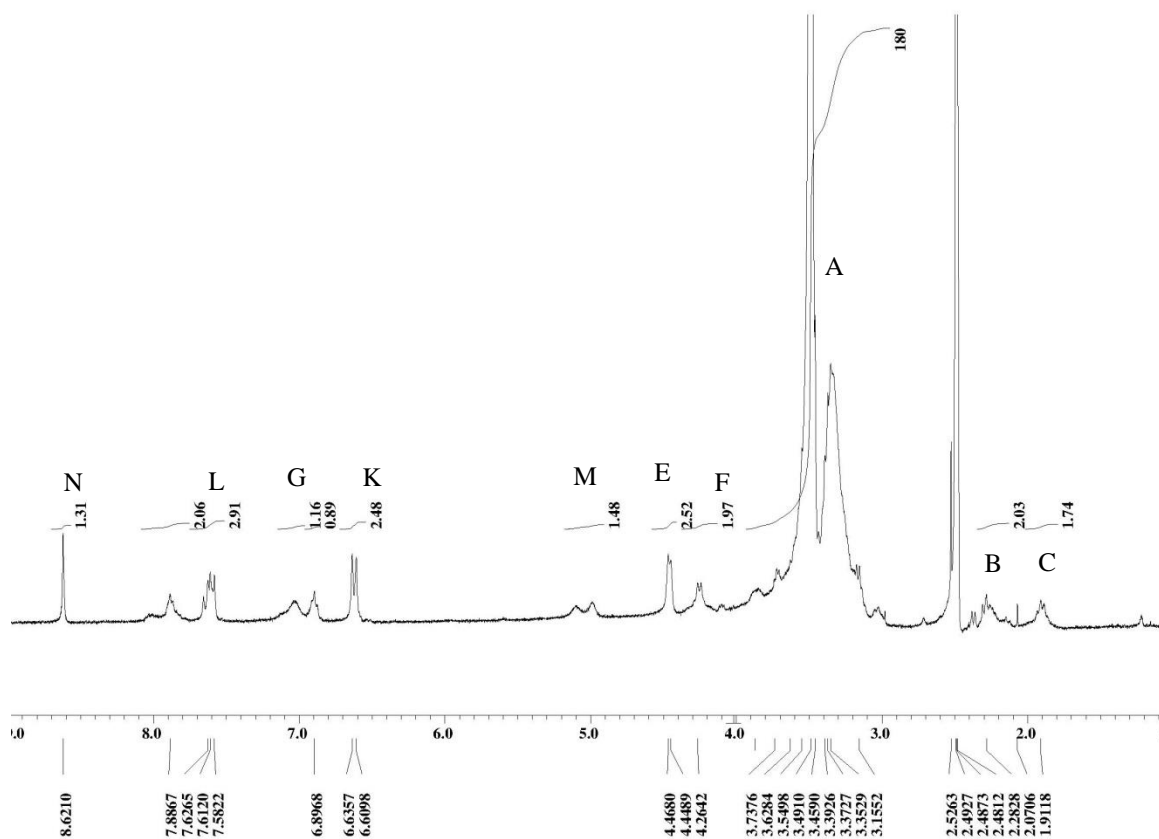


Figure A3.7: ^1H NMR spectrum of $\text{NH}_2\text{-PEG-FA}$ (DMSO-d_6).

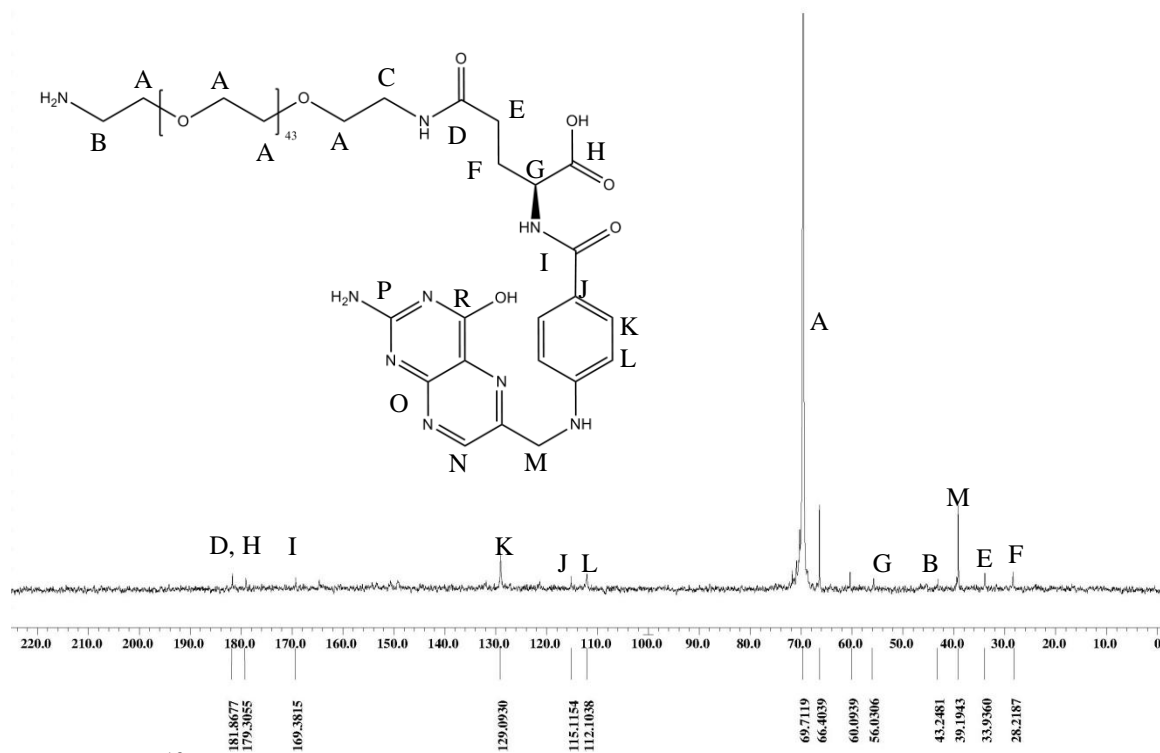


Figure A3.8: ^{13}C NMR spectrum of $\text{NH}_2\text{-PEG-FA}$ (D_2O).

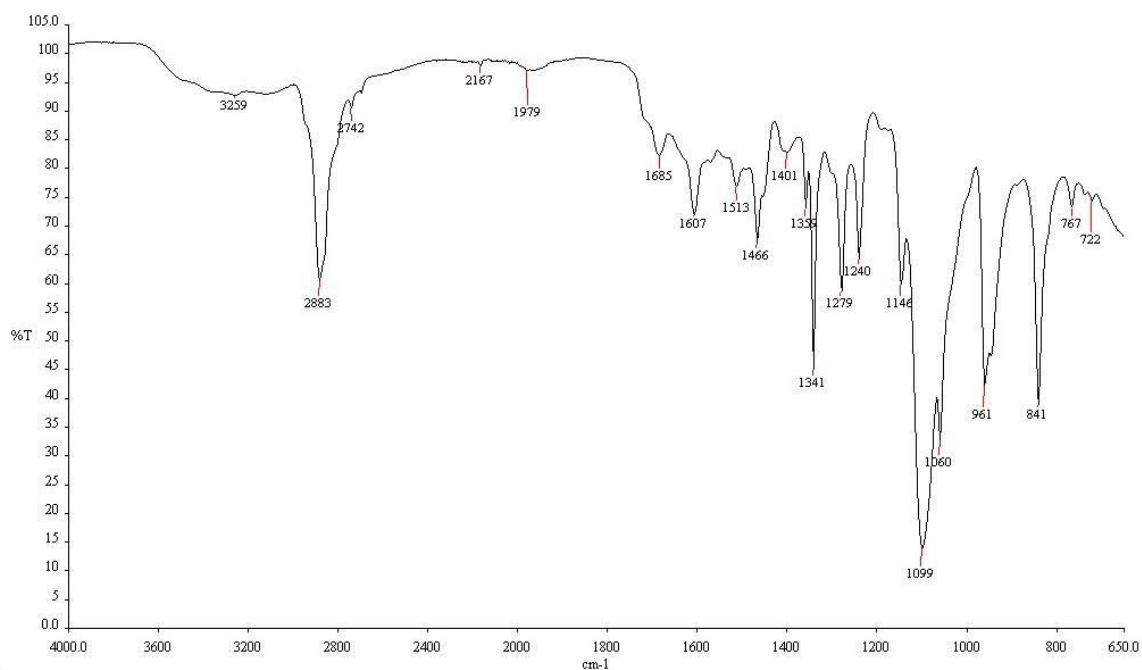


Figure A3.9: FTIR spectrum of NH₂-PEG-FA.

Wavenumber (cm ⁻¹)	Functional Group
3259	-O-H
2883	-C-H
1685	-C=O
1607	-C=C
1513	-C=N
1240	-C-C
1099	-C-O

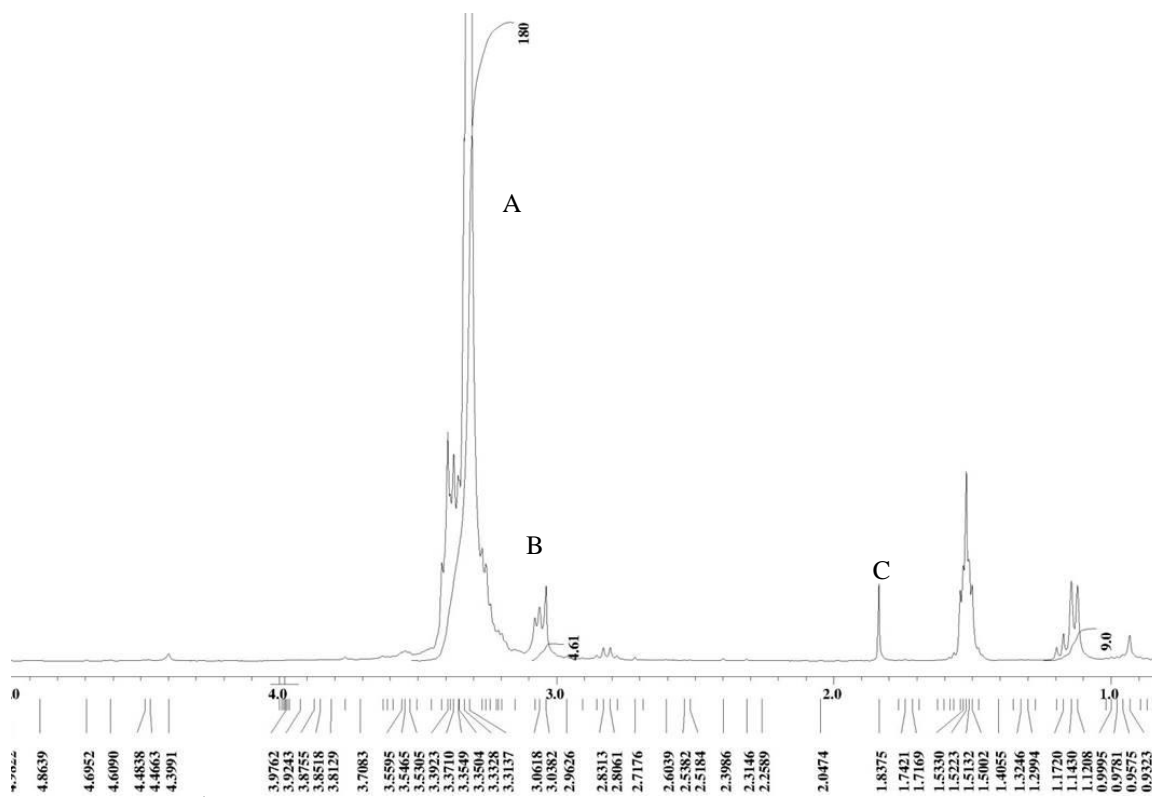


Figure A3.10: ^1H NMR spectrum of Azido-PEG-MeO (CDCl_3).

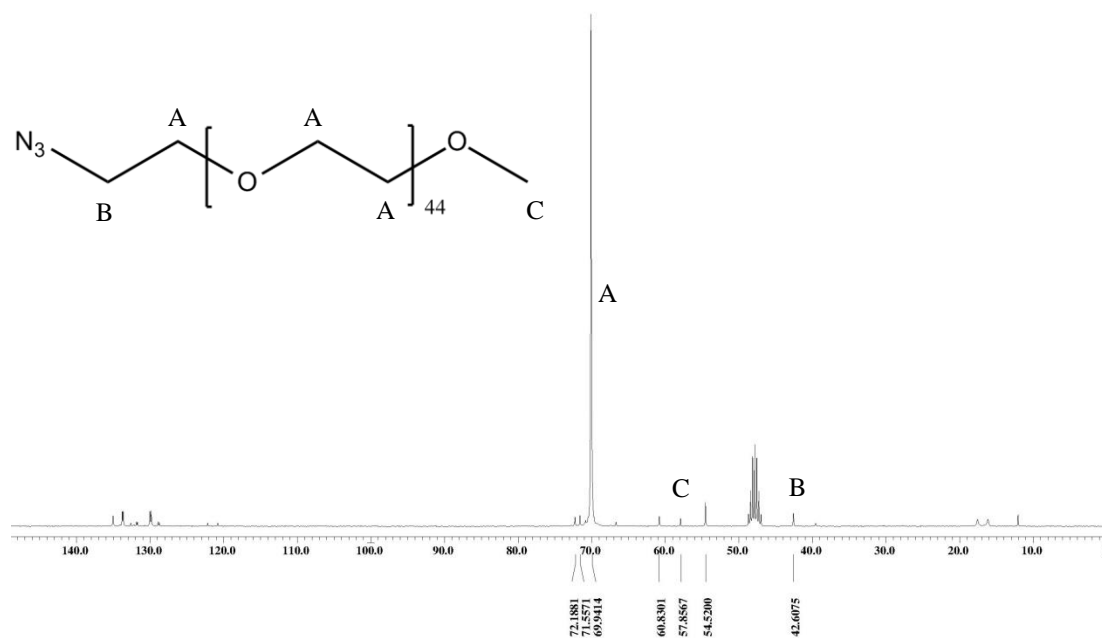


Figure A3.11: ^{13}C NMR spectrum of Azido-PEG-MeO (CDCl_3).

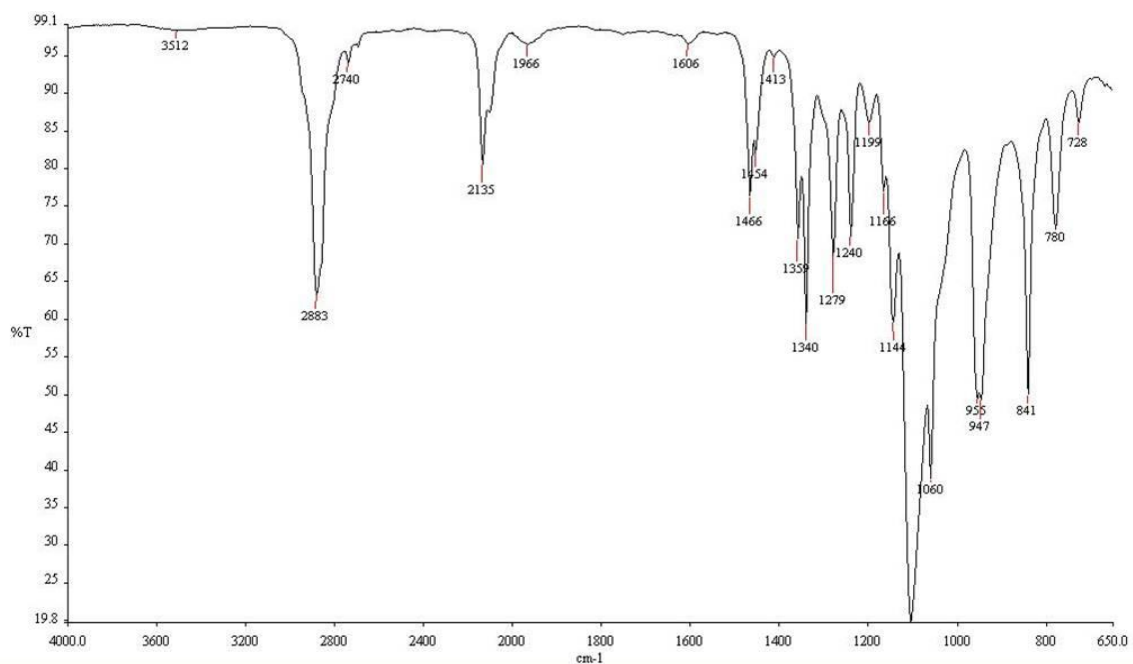


Figure A3.12: FTIR spectrum of Azido-PEG-MeO.

Wavenumber (cm ⁻¹)	Functional Group
2883	-C-H
2135	-N=N
1240	-C-C
1117	-C-O

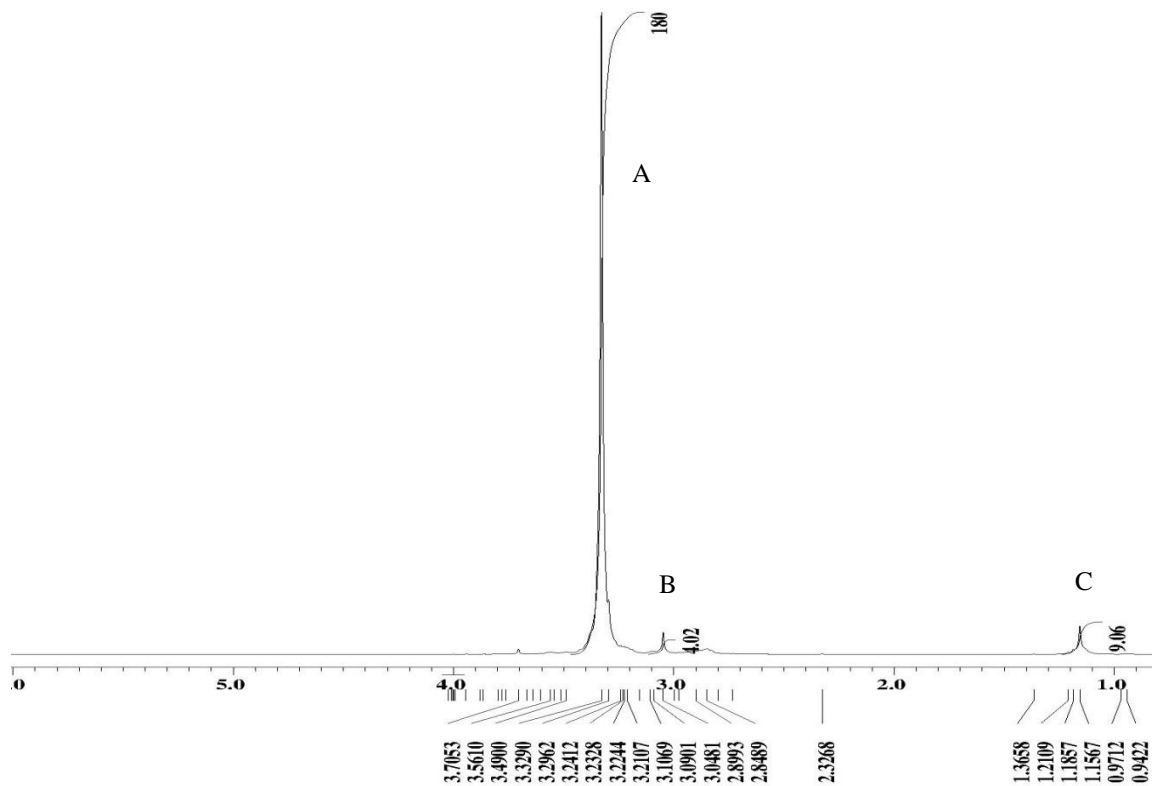


Figure A3.13: ^1H NMR spectrum of $\text{NH}_2\text{-PEG-MeO}$ (CDCl_3).

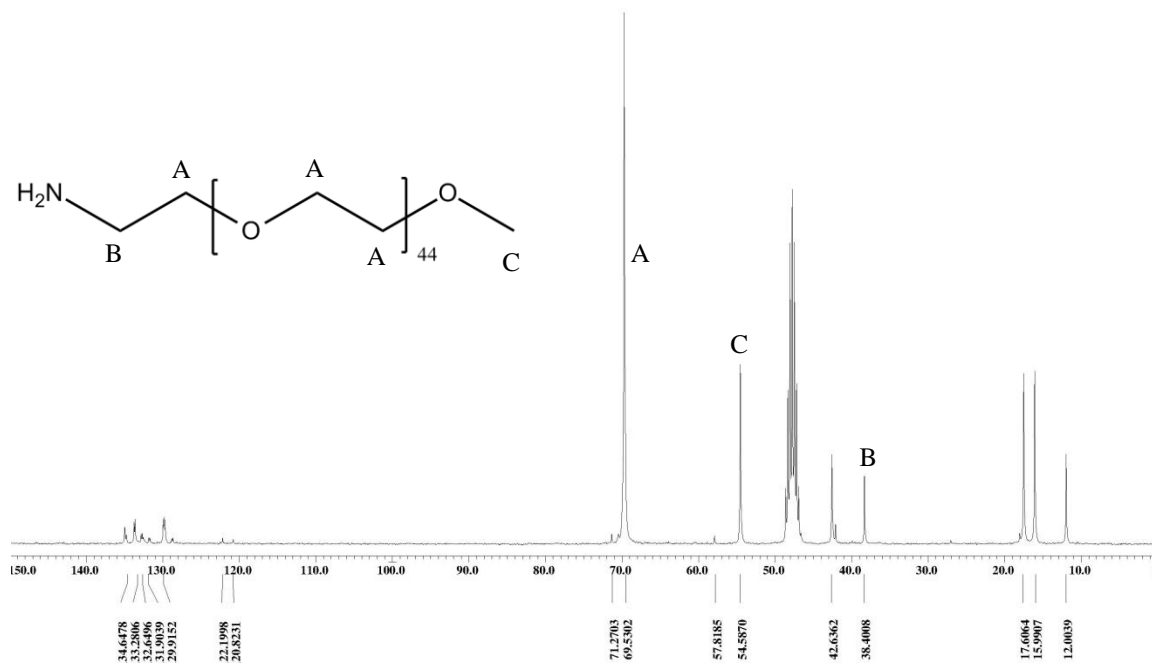


Figure A3.14: ^{13}C NMR spectrum of $\text{NH}_2\text{-PEG-MeO}$ (MeOD-d_4).

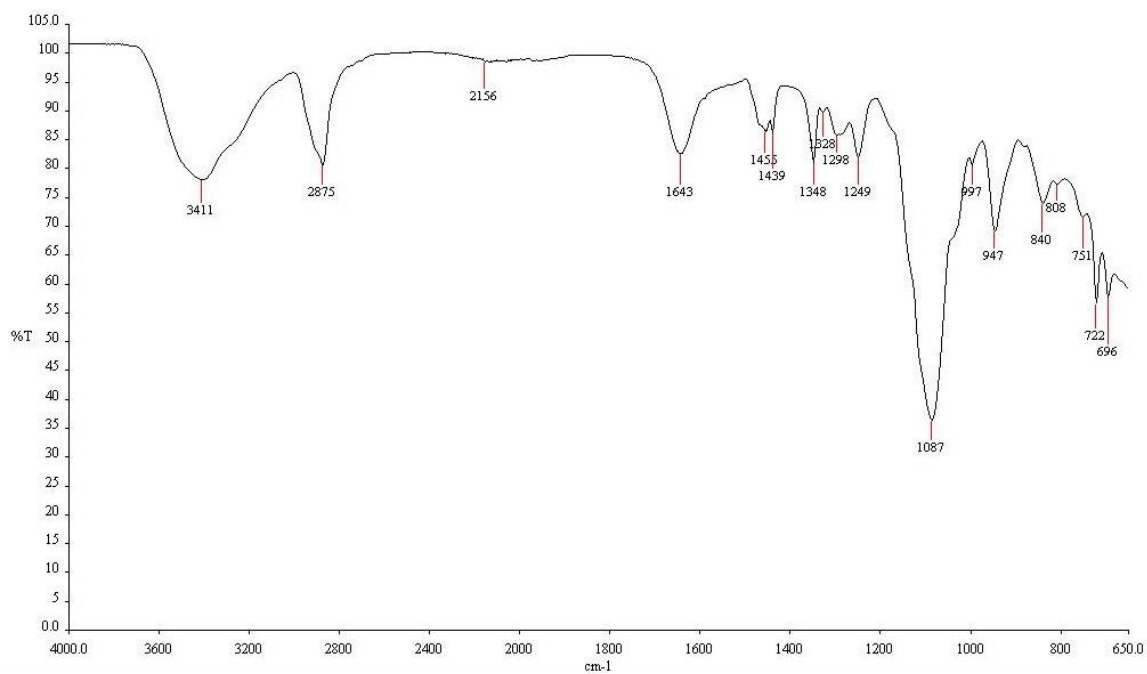


Figure A3.10: FTIR spectrum of NH₂-PEG-MeO.

Wavenumber (cm ⁻¹)	Functional Group
3411	-N-H
2875	-C-H
1249	-C-C
1087	-C-O